

INTER-STAGE AND PERFORMANCE TESTS OF A
TWO-STAGE HIGH-PRESSURE TURBINE

A Thesis

by

KAPIL SHARMA

Submitted to the Office of Graduate Studies of
Texas A&M University
in partial fulfillment of the requirements for the degree of

MASTER OF SCIENCE

May 2011

Major Subject: Mechanical Engineering

INTER-STAGE AND PERFORMANCE TESTS OF A
TWO-STAGE HIGH-PRESSURE TURBINE

A Thesis

by

KAPIL SHARMA

Submitted to the Office of Graduate Studies of
Texas A&M University
in partial fulfillment of the requirements for the degree of

MASTER OF SCIENCE

Approved by:

Chair of Committee,	Taher M. Schobeiri
Committee Members,	Je-Chin Han
	Yassin A. Hassan
Head of Department,	Dennis O'Neal

May 2011

Major Subject: Mechanical Engineering

ABSTRACT

Inter-stage and Performance Tests of a
Two-stage High-pressure Turbine. (May 2011)

Kapil Sharma, B.E., National Institute of Technology Karnataka, India

Chair of Advisory Committee: Dr. Taher M. Schobeiri

The existing 3-stage research turbine at Turbomachinery Performance and Flow Research Laboratory (TPFL) facility, Texas A&M University (TAMU) was replaced with a newly designed and manufactured 2-stage turbine in accordance with the design requirements as per DooSan, DHI. This new design of turbine consisted of bowed stator and rotor blades to study the effect on reduction of secondary flow losses and thus improvement in turbine efficiency if any. The new design also incorporated labyrinth seals on both inner and outer shrouds. Extensive Inter-stage and Performance experiments were carried out on this new turbine. Inter-stage measurements were accomplished by traversing three 5-hole probes radially and circumferentially, using the existing probe traverse system in TPFL. Performance tests were conducted for varying pressure ratio, at fixed rotational speed and for varying rotational speed with fixed pressure ratio and the efficiency was plotted against u/c_0 . Each condition was tested and measured two to three times to check for reproducibility of the data.

The results from inter-stage experiments show that the rotor row loss coefficient is about four times higher than the stator row loss coefficient. This high rotor loss coefficient reduces the total to static efficiency. From the performance tests, the maximum total-to-static efficiency observed was 85.2% located at around $u/c_0 = 0.75$. This relatively low efficiency is in consonance with the inter-stage results (high rotor loss coefficient).

To my family and friends

ACKNOWLEDGMENTS

I take this opportunity to express my deepest gratitude to Dr. M. T. Schobeiri, my advisor, for all the support and guidance he has given me throughout my graduate study and thesis work. His suggestions and constant encouragement helped me a lot. I'm thankful to Dr. J. C. Han and Dr. Y. A. Hassan for being on my advisory committee.

I am extremely grateful to some of my friends from my undergrad days, who have had faith in me and helped me reach this stage, without them this would not have been possible. Special thanks to Mr. Anand Kulkarni for providing all the support I needed to pursue my master's degree in U.S.

I would also like to express my appreciation for the help and support provided by Hicham Chibli and Sharef Abdel-Fattah during the turbine assembly and experimentation. Mr. Eddie Denk has been of great help with his expert suggestions and advice during my stay at Turbolab.

Lastly, I would also like to thank my close friends from Texas A&M, without whom my stay here would have been very bland.

TABLE OF CONTENTS

CHAPTER		Page
I	INTRODUCTION	1
	I.1. Losses in Turbomachinery	1
	I.1.1. Profile or primary losses	2
	I.1.2. Trailing edge thickness losses	2
	I.1.3. Secondary flow losses	3
	I.1.4. Mixing losses (at trailing edge of cooled gas turbine blades)	6
	I.1.5. Exit losses	6
	I.2. Aerodynamic Experimental Research	7
	I.3. Research on Secondary Flow Reduction	11
	I.3.1. Leading edge filleting	11
	I.3.2. End wall contouring	16
II	OBJECTIVES	21
	II.1. Testing and Data Analysis	21
	II.2. Design and 3D Modeling	21
	II.3. Assembly and Instrumentation	22
III	RESEARCH FACILITY	23
	III.1. Existing Facility	23
	III.2. Two-stage Turbine Design for DooSan	29
IV	INSTRUMENTATION	41
	IV.1. Engine Monitoring System	41
	IV.2. Turbine Performance Instrumentation	42
	IV.3. Interstage Traversing System	44
	IV.4. Uncertainty Analysis	50
V	THEORY	52
VI	PERFORMANCE TESTS	57
	VI.1. Testing Procedure	58
	VI.2. Calculations	59
	VI.3. Results	62

CHAPTER	Page
VII INTERSTAGE TESTS	64
VII.1. Testing Procedure	64
VII.2. Calculations	68
VII.3. Results	69
VII.3.1. Line plots	70
VII.3.2. Contour plots	78
VIII CONCLUSION	85
REFERENCES	86
APPENDIX A	90
APPENDIX B	116
APPENDIX C	124
APPENDIX D	130
APPENDIX E	134
APPENDIX F	160
APPENDIX G	165
VITA	166

LIST OF TABLES

TABLE		Page
I	Bill of parts for manufacturing	31
II	Blade geometry and Zweifel coefficients	38
III	Fixed channels for flow parameters	43
IV	Geometry parameters for venturi	44
V	Uncertainty data for the test results	51
VI	Metal angles for stator and rotor blades of DooSan turbine	70
VII	Summary of row and stage performance parameters	74
VIII	Correct sequence of radial movement for probes	127

LIST OF FIGURES

FIGURE	Page
1	Velocity profile showing wakes at downstream of a cascade 3
2	Figure showing evolution of flow pattern over time 4
3	Interpretation of vortex-wake-blade interaction 9
4	Partial Shroud (PS) and Full Shroud (FS) with different labyrinths . 10
5	Partial shroud tested by Porreca, et al. 11
6	Constant radius fillet used by Devenport, et al. 12
7	Endwall bulb configurations tested by Sauer, et al. 13
8	Fillet configurations analyzed by Shih, et al. 14
9	Fillet shape tested by Zess, et al. 16
10	End wall contouring designed by Harvey, et al. 17
11	End wall contouring tested by Hartland, et al. 19
12	End wall contouring tested by Dossena, et al. 20
13	Research turbine at TPFL facility 24
14	Sectional view of the turbine assembly showing details of the heater, torque-meter and the shaft 27
15	Sectional view of the turbine assembly showing the five-hole probe locations 28
16	Cross sectional view of complete assembly 29
17	(a) Complete hub assembly and bearings with (b) 3-D view of stator ring and 3-d views of (c) Rotor blade and (d) Stator blade . . 30

FIGURE	Page
18	Cross sectional view of complete hub assembly, bearings and inner casing 31
19	Cross sectional view of stator and rotor hub assembly showing the seal profiles used 32
20	Stator blade 33
21	Location of outer mounting holes on stator blade 34
22	Details of stator assembly 35
23	Rotor blade 36
24	Details of rotor assembly 37
25	Metal angles, axial chord and chord length at various location of rotor blade 39
26	Metal angles, axial chord and chord length at various location of stator blade 40
27	Interstage traverse grid 45
28	Five-hole probe dimensions in mm 45
29	Definition of pitch and yaw angles w.r.t. probe axes 46
30	Probe coordinate systems 47
31	Probe velocities w.r.t. to machine axis 49
32	$h - s$ diagram for a turbine stage 53
33	Velocity triangle of a typical turbine stage 54
34	Velocity triangle for stator stage of DooSan blade configuration . . . 55
35	Test script code for performance test 58
36	Isentropic total-static efficiency of DooSan two-stage turbine as a function of mass flow 63

FIGURE	Page
37	Isentropic total-static efficiency of DooSan two-stage turbine as a function of u/c_0 63
38	Main screen of data acquisition program, <i>Turbo.vi</i> 65
39	I/O configuration window for data acquisition program 65
40	Temperature configuration window for data acquisition program . . . 66
41	Test configuration window for data acquisition program 67
42	Absolute, relative and meridional flow angles 71
43	Absolute and relative Mach numbers 72
44	Static pressure <i>vs.</i> immersion ratio 73
45	Absolute and relative total pressures 73
46	Absolute axial and meridional velocities 74
47	Stage loss coefficients and efficiencies 75
48	Isentropic stage efficiency <i>vs.</i> immersion ratio 75
49	Absolute and relative flow velocities 76
50	Static temperature and enthalpy 76
51	Absolute and relative total enthalpy 77
52	Contour plots for absolute, relative and meridional flow angle 79
53	Contour plots for absolute and relative Mach number 80
54	Contour plots for static and relative total pressure 81
55	Contour plots for absolute and relative flow velocity 83
56	Contour plots for axial and meridional flow velocity 84
57	Various parts used on 5-hole probes during assembly 107

FIGURE	Page
58	Spacer and hex-nut flush with probe holder and set-screws aligned with probe-tip 108
59	Station-4 probe assembly 108
60	Set-up for station-3 and station-5 probes in probe holder 109
61	Station-3 and station-5 probe assembly 110
62	Steps for sliding station-4 probe assembly into traverse system 111
63	Figure showing station-4 probe tip pointing towards 9 o'clock 111
64	Steps for sliding station-5 probe assembly into traverse system 113
65	Steps for sliding station-3 probe assembly into traverse system 114
66	Icon for SetZero program 117
67	Icon for NetScanner program 117
68	Main window of NetScanner program 118
69	Butterfly and throttle valves for calibration facility 119
70	Icon of TurboProbe program 120
71	Connection window for probe calibration 121
72	Grid configuration window for probe calibration 122
73	Pressure configuration window for probe calibration 122
74	Icon for <i>GenFile</i> program 124
75	Default window of <i>GenFile</i> program 124
76	Radial traverse tab from <i>GenFile</i> program 125
77	Plot showing test-grid generated from <i>GenFile</i> program 126
78	Example plot generated from <i>GenFile</i> program 128

FIGURE	Page
79	Connection map for 5-hole Probes 130
80	Connection map for Rakes (Total Pressure) 131
81	Connection map for Casing-taps (Static Pressure) 132
82	Connection map for Venturi 133
83	Connection map for T-rings 133
84	Plot of all channels from raw data with time history 135
85	Plot showing averages of all channels from raw data 135
86	Input and output windows from Matlab code for weather data 136
87	Oil level indicator for compressor 160
88	Power supply box for dynamometer 161
89	Controller for dynamometer 161
90	Icon for SetZero program 161
91	Variable frequency controller for compressor 162
92	Heater controller 164

NOMENCLATURE

α	absolute velocity flow angle
β	ratio between throat and inlet diameter
β	relative velocity flow angle
Δp_w	pressure difference between venturi inlet and throat in inches of water
\dot{m}	mass flow rate
η	efficiency
γ	adiabatic expansion factor
κ	isentropic exponent
μ	flow viscosity
μ_0	reference flow viscosity
ρ	air density
τ	pressure ratio between throat and inlet pressure
ζ	total pressure loss coefficient
C_d	discharge coefficient
D_i	venturi inlet diameter
D_t	venturi throat diameter
H	specific total enthalpy
h	specific static enthalpy
h_T	specific enthalpy difference for turbine
L_T	turbine output power
M	Mach number
M_T	turbine output torque
N	turbine rotational speed

P_s	static pressure
P_{tr}	relative total pressure
P_t	total pressure
R	specific gas constant
r^*	immersion ratio
Re_t	venturi throat Reynold's number
S	Sutherland constant
T	flow temperature
T_0	reference flow temperature
U	circumferential velocity
u	velocity vector
V	absolute velocity
W	relative velocity
Z	compressibility factor for venturi

CHAPTER I

INTRODUCTION

Almost all electrical power on the Earth is produced with some kind of a turbine. Turbines are rotary engines which extract energy from a working fluid and convert it to work. First successful and self powered gas turbine using both compressor and turbine was built by Aegidius Elling of Norway in 1903. Sir Frank Whittle in England patented a design for a gas turbine for jet propulsion. The first successful use of this engine was in April, 1937. Even though, turbine technology is almost over a century old, there is still lot of scope for improvement. Even to this day, maximum thermodynamic efficiency of some of the best available gas turbines is in the range of 40%. And the ever increasing demand for electricity has been a driving force for researchers across the world to come up with new designs with better efficiency.

I.1. Losses in Turbomachinery

As it is rightly stated by Bradshaw [1], “Of all the fluid-dynamic devices invented by the human race, axial-flow turbomachines are probably the most complicated.” The flow pattern inside a turbine is very complex and is associated with various losses. According to Schobeiri [2] following are the major aerodynamic losses in a turbomachine:

The journal model is ASME Journal of Turbomachinery.

I.1.1. Profile or primary losses

Since working fluids in any turbomachine is viscous, the blades experience shear stresses with no slip condition on pressure and suction surfaces. This viscous flow around the blade surface leads to boundary layer development and the shear stresses cause drag forces that reduce the total pressure downstream of the blade. Schobeiri states that, profile losses are caused by parameters like blade geometry, chord-blade spacing ratio, blade thickness-chord ratio, surface roughness along with Reynolds and Mach number effects. Profile loss coefficient can be expressed by following equation:

$$\zeta_P = (\varepsilon_{optimum})_{single} \left[1 + K \left(\frac{c}{s} \right)_{optimum}^n \right] C_L \left(\frac{c}{s} \right) \frac{1}{\sin(\alpha_\infty)}$$

where,

$(\varepsilon_{optimum})_{single}$ is the optimum drag-lift ratio for a single blade

c is the blade chord length

s is the blade spacing

C_L is the blade lift coefficient

α_∞ is angle of the mean velocity vector

n and K are determined experimentally

I.1.2. Trailing edge thickness losses

As explained earlier, the no-slip condition on suction and pressure surfaces lead to boundary layer development on both sides of blades and since every turbomachine blade has a certain definite thickness at the trailing edge, it leads to spatially periodic wake flow downstream of a cascade as shown in Fig. 1. As per Schobeiri, the total

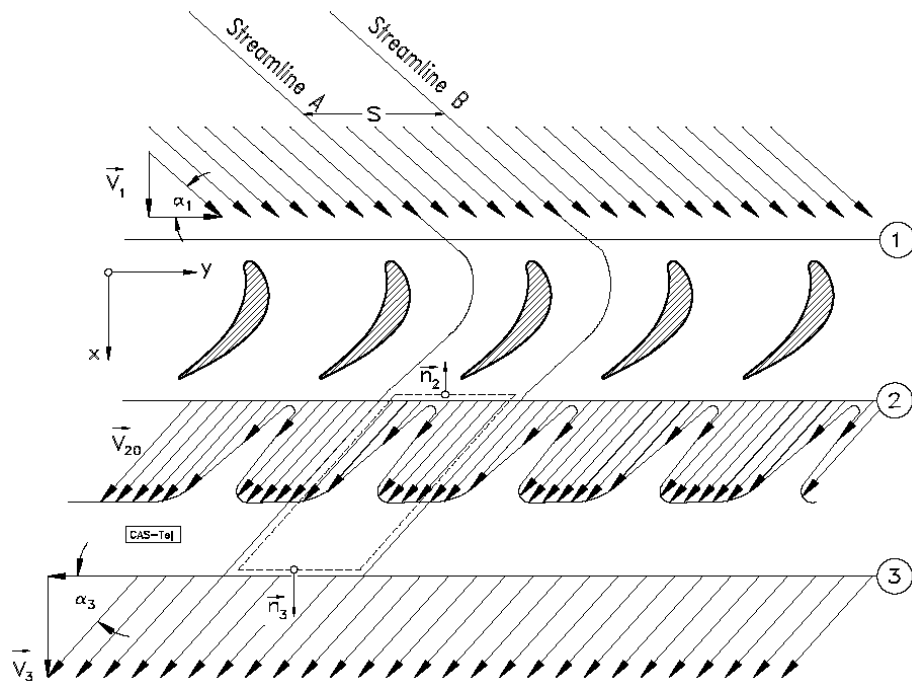


Fig. 1.: Velocity profile showing wakes at downstream of a cascade [2]

pressure losses observed at the exit of a cascade increase with increasing trailing edge thickness.

I.1.3. Secondary flow losses

As per Schobeiri [2], boundary layer development at the hub and tip region of blades due to rotor-hub and casing walls causes secondary flow. Secondary flow in a turbine passage leads to flow separation and vortices, which induce drag forces thus reducing the mainstream total pressure. The cross-flow between the blade pressure and suction surfaces also contributes to the secondary flow.

To help in understanding this complex secondary flow in turbine passage many flow models have been published by various researchers and over the course of time, based on experimental investigations these flow models have evolved and been documented. Fig. 2 shows some of the models of flow pattern as visualized by researchers

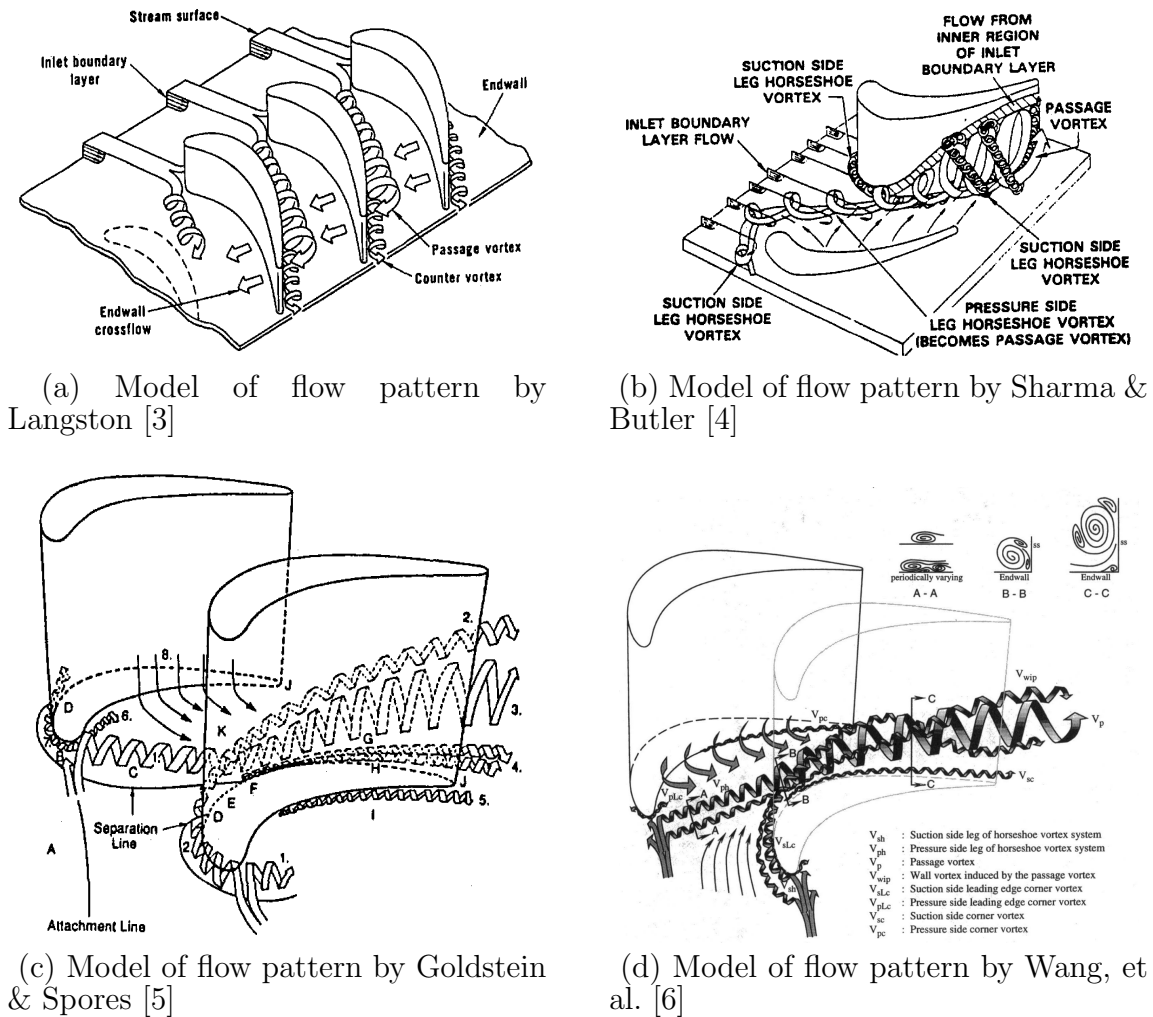


Fig. 2.: Figure showing evolution of flow pattern over time

like Langston [3] in 1980, Sharma and Butler [4] in 1987, Goldstein and Spores [5] in 1988 and Wang, et al. [6] in 1997.

According to Acharya, et al. [7], the flow field near the hub endwall region of the blade passage is dominated by the boundary layer, strong pressure gradients, and cross flow in the pitchwise direction from the pressure side to the suction side. As seen in Fig. 2, flow pattern through a blade passage is a series of complex vortices that are explained below:-

Leading edge horse-shoe vortex: As flow approaches the leading edge stagnation line, static pressure rises across the flow from the endwall. The static pressure increases more in the free-stream region above the boundary layer since the free-stream velocity is higher compared to the velocity in the boundary layer [8]. This pressure gradient in spanwise direction at the leading edge causes a vortex build-up, known as the leading edge horse-shoe.

Passage vortex: The horseshoe vortex developed at the leading splits into two separate legs rotating in opposite direction to each other while moving to suction and pressure side each. Pressure side leg of this horseshoe vortex system is swept towards the suction surface of adjacent blade because of the pressure difference. This resultant vortex formed by the combination of suction side and pressure side leg of horseshoe vortices from two adjacent blades is referred as the passage vortex between them. The direction of rotation of passage vortex is determined by the dominant pressure side leg vortex as it much larger and stronger than suction side leg vortex [7]. Pressure gradients in the blade passage result in the growth of these vortices.

Induced and corner vortices: A small vortex is formed close to the suction wall of the blade due to strong induction of the passage vortex and originates at the same location where the passage vortex starts to form (merging point of the counter-rotating vortex legs). This induced vortex stays above the passage vortex and is driven along with the passage vortex. The small corner vortex induced at the junction of blade leading edge and endwall by the horse-shoe vortex is driven along the pressure side and suction side edge with the two main vortex legs. In Wang, et al. [6], they are identified as the pressure side leading edge vortex and suction side leading edge vortex.

I.1.4. Mixing losses (at trailing edge of cooled gas turbine blades)

One of the ways of increasing the thermal efficiency of gas turbines is by increasing the pressure ratio which leads to higher turbine inlet temperatures, however, the metallurgical properties of the blade materials can limit this. Cooling mass-flow is injected through various slots on the blades to allow for higher inlet temperatures. This additional mass flow affects the flow parameters downstream of the cooled blade and leads to mixing losses. One has to keep a check on these losses in order to make sure the increase in the efficiency of gas turbine with increased inlet temperatures is not affected drastically by these losses. According to Schobeiri [2], the cooling mass flow ratio to actual mass flow along with angle and velocity of cooling mass flow ejection affect the mixing losses. Also, the slot-width ratio for coolant mass flow ejection plays a role in deciding the level of mixing flow losses.

I.1.5. Exit losses

Since, the working fluid leaving the turbine has an exit velocity, the kinetic energy associated with this velocity is referred as the total energy loss. In a multi-stage turbine, the exit velocity of the flow at the last stage decides the exit loss. Exit loss plays a significant role in deciding the stage efficiency for a single stage turbine. According to Schobeiri [2], following equation gives the exit loss coefficient for a stage:

$$Z_E = \frac{1}{2\lambda} \left[\tan^2(\alpha_2) \left(1 - r + \frac{\lambda}{2}\right)^2 + \left(1 - r - \frac{\lambda}{2}\right)^2 \right]$$

where,

λ is stage load coefficient

α_2 is exit flow angle of stator

r is degree of reaction for stage

I.2. Aerodynamic Experimental Research

In 1991, Boletis, et al. [9] investigated 3D flow field through a low aspect ratio, high turning turbine stator preceded by a full stage which according to Boletis simulates the flow conditions of an intermediate stator row in a multistage turbine. Double-headed four-hole probes were utilized to capture the flow parameters. Boletis, et al. concluded that inlet flow angles and total pressure distributions are affected by radial free-stream gradients and rotor secondary and clearance flows, hence the inlet flow conditions to a turbine stator preceded by a full stage are considerably different from those generated in isolated cascades.

In 1993, Arndt [10] tested a low pressure, multistage (five stages), subsonic, moderately high-aspect-ratio turbine to study the unsteady flow phenomena. Hot film probes were utilized for measuring interstage flow parameters at the exit of every rotor blade row. To separate the periodic and random fluctuations in the signals, the unsteady data were ensemble averaged. Arndt found that flow through the low pressure turbine was profoundly effected by the rotor-rotor and stator-rotor interaction. The rotor-rotor interaction cause by the wakes from one rotor blade row on a downstream rotor led to periodic and turbulent velocity fluctuations at exit of every rotor blade row except that of first row. Arndt concludes that stator-rotor interaction strongly influenced overturning and underturning rotor wakes as a result

of secondary flow close to end walls.

In 1997, Schobeiri, et al. [11] developed a large-scale, high-subsonic research facility for simulating the periodic unsteady flow to study the unsteady cascade aerodynamics and heat transfer. The facility was capable to generate up to four different types of inlet conditions with different wake structures and free stream turbulence intensities, however, detailed measurements were carried out along pressure and suction surfaces of one blade out of a total of seven blades for two different inlet wake formations. Calibrated hot-wire was used to capture mean velocities and turbulent fluctuations and the reference upstream flow velocity was monitored using a Prandtl probe, placed upstream of the diffuser. Data was ensemble-averaged with respect to rotational period of wake generator. Schobeiri, et al. concluded that the initially strong acceleration seen in pressure distribution on suction side followed by a continuous mild deceleration significantly influenced unsteady boundary layer and an increase of unsteady parameter, resulted in increase of the momentum deficiency thickness over the entire blade surface.

In 2000, Schobeiri, et al. [12] carried out experimental research on a three stage research turbine to measure the interstage flow field and temperature field for varying rotational speeds. Efficiency measurements were also carried out from 1800-2600 rpm. Five-hole probes with a traversing system, were used for interstage measurements and were replaced by temperature probes for getting the interstage temperature field. The test results for 5600 blade configurations were compared with then existing test results for 9600 blade configuration. It was observed that the 9600 blade configurations had a higher efficiency across all speed ranges. The authors provided significant suggestions to improve the testing, measuring and data analysis procedures at TPFL.

In 2005, Schlienger, et al. [13] studied the interaction of vortex-wake-blade by running experiments on a two stage shrouded axial turbine. It was observed that the

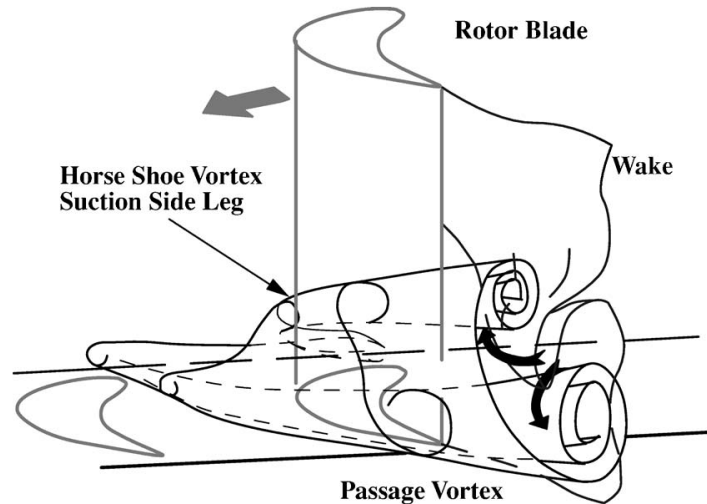


Fig. 3.: Interpretation of vortex-wake-blade interaction [13]

hub passage vortex from rotor and secondary flow field from upstream stator blade row played a major role in the unsteady secondary flow observed at the exit of rotor blade row. Also, Schlienger, et al. concluded that the rotor wake layer rolled-up to form a passage vortex close to the hub. A visual interpretation by Schlinger, et al. showing this mixing of rotor wake with passage vortex is given in Fig. 3.

Also at the same time, Porreca, et al. [14], carried out numerical and experimental study on two different shapes of shroud configurations for similar rotor bladings and tip clearance. However, the labyrinth seal package for the shrouds were different and are shown in Fig. 4. Unsteady flow field was analyzed using numerical simulation, however, the steady flow parameters were captured using miniature five-hole probes along with fast response aerodynamic probe (FRAP). Up to the blade midspan, it was seen that there was strong interaction between cavity flow and blade tip region of rotor blades, this was attributed to the different distinct vortex structures observed in the downstream of second stator exit. For the partial shroud, a strong tip vortex is evident. Porreca, et al. concluded that to achieve optimal performance it is imperative

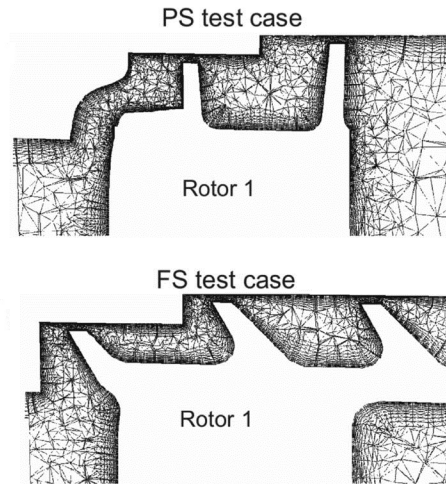


Fig. 4.: Partial Shroud (PS) and Full Shroud (FS) with different labyrinths [14]

to have a well integrated and matched blade-shroud aerodynamic design.

In 2007, Gaetani, et al. carried out an extensive research to study unsteady flow field in a high-pressure turbine with leaned stator and bowed rotor blades. Five-hole probes were used to capture flow field in axial gap between stator and rotor rows. To study the flow field upstream of rotor row, the axial gap between stator and rotor row was increased to 100% of blade chord length. 3D flow field was captured starting from station close to stator trailing edge and further downstream to allow mixing process. Downstream measurements of rotor exit was done with axial gap of 35% and 100% of blade axial chord length. With 35% axial gap, it showed traces of vane hub shed vortex, however for 100% axial gap, all traces of stator vortex structures had vanished downstream of rotor. Stage efficiency levels were higher for the minimum axial gap case.

In 2009, Porreca, et al. [15] studied unsteady interactions of 3D flow introduced by a nonaxisymmetric partial shroud in a two-stage axial turbine. Measurements are carried out using stereoscopic particle image velocimetry (PIV), fast response aerodynamic probe (FRAP) and five-hole probes. The partial shroud geometry tested is

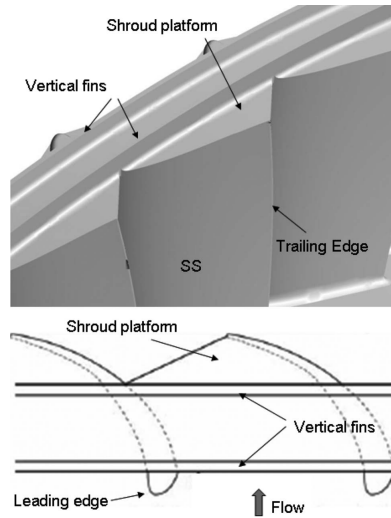


Fig. 5.: Partial shroud tested by Porreca, et al. [15]

shown in Fig. 5. It was observed that downstream of the blade throat, passage vortex grows in strength before passing over the shroud platform. Porreca, et al. concluded that a sudden flow expansion at trailing edge of shroud leads to the formation of a vortex apart from the passage vortex generating a core of local pressure losses that are measured downstream.

I.3. Research on Secondary Flow Reduction

I.3.1. Leading edge filleting

Studies by researchers like Tan, et al. and Harrison [16, 17] have revealed that introduction of bow or lean to a blade cascade can help in reduction of secondary vortices and thus improve efficiency. Depending on a cascade, the blades can be given a positive or a negative bow so as to increase the pressure at hub which helps in opposing secondary flow. Harrison [17] reported that the introduction of bow in a blade improves the flowfield for the subsequent blade rows. Many ongoing research projects across the world focus on improving flowfield and reducing secondary flow

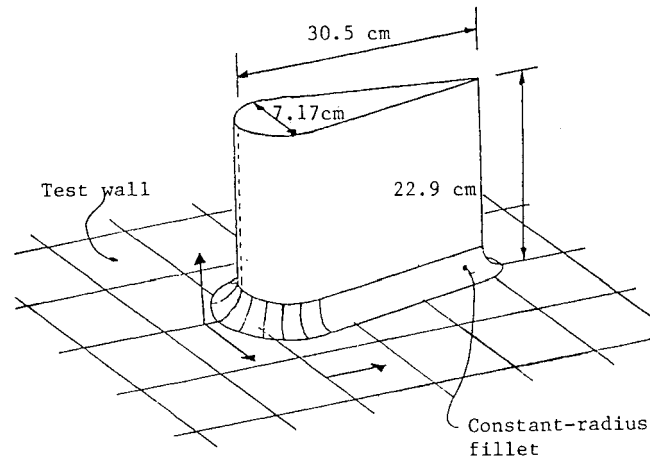


Fig. 6.: Constant radius fillet used by Devenport, et al. [18]

through a turbine passage using nonaxisymmetric endwalls.

Providing a fillet at the leading edges of blades is one of the possible ways of reducing secondary flow losses in a turbine passage. A fillet can help in reducing the pressure gradient at the leading edge which causes the formation horseshoe vortex. A lot of work has been done on optimizing the shape and size of the fillet for a blade configuration.

Devenport, et al. [18], carried out their research with a fillet having constant radius shown in Fig. 6, the fillet went around the entire blade and was tangent to both the blade wall and endwall. Oil-flow visualization technique was used to get a view of the flows produced with and without fillet. Detailed flow measurements were carried out by the help of static pressure ports and hot-wire anemometry. Laser doppler velocimeter was utilized to measure histograms of the streamwise component of velocity in the regions of leading edge separation generated by the wing with fillet. It was concluded by Devenport, et al. that, the constant radius fillet does not prevent leading edge separation or the formation of a horseshoe vortex. However, they reported that this fillet pushed the horseshoe vortex further away from the blade

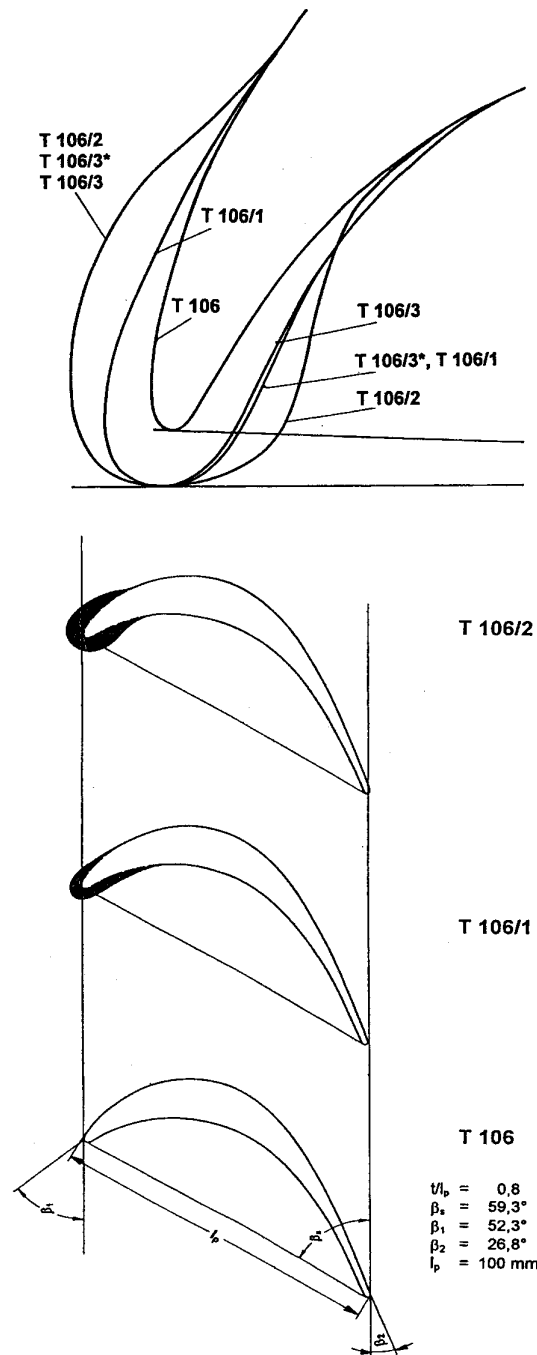


Fig. 7.: Endwall bulb configurations tested by Sauer, et al. [19]

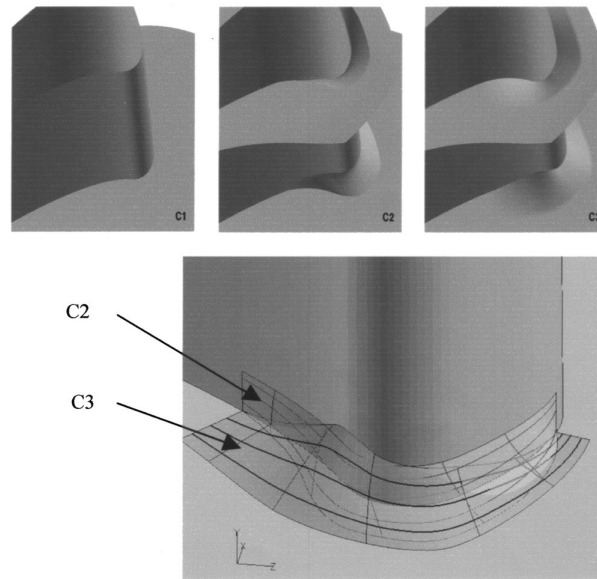


Fig. 8.: Fillet configurations analyzed by Shih, et al. [20]

surface, thus enlarging the effective radius of the nose of the blade. It was observed that the size and shape of the vortex was actually augmented.

Sauer, et al. [19] studied a different type of fillet, one that enhances instead of diminishing horseshoe vortices. They conducted numerical and experimental analysis with three different configurations of leading edge endwall modifications as shown in Fig. 7. They believed that creating a “bulb” effect (increased blade thickness at junction of leading edge and hub) would increase the strength of suction side leg of the horseshoe vortex and hence weaken the passage vortex. According to their findings, one of the configurations with extended profile on the suction side when compared to pressure side proved to reduce endwall losses by almost 50%, apparently because the passage vortex was deformed and moved further away from suction surface by the stronger suction side leg of the horseshoe vortex. Various pitot tubes and 5-hole probes were utilized to study the flowfield. Similar results were obtained by their numerical analysis.

Shih, et al. [20] carried out numerical analysis on three different configurations: *no fillet (baseline)*, *a fillet whose thickness fades on the airfoil*, and *a fillet whose thickness fades on the endwall* as shown in Fig. 8. Maximum height of fillets for both configurations were positioned along the stagnation line on the airfoil. Three inlet swirls were also studied for each fillet configuration: no swirl (baseline) and two linearly varying swirl angle from one endwall to the other (-30° to $+30^\circ$) and ($+30^\circ$ to -30°). It was observed that the difference in stagnation pressure from the nozzle's inlet to its exit were reduced by more than 40% irrespective of the swirl because of the larger stagnation region. In this region, turbulent flow was minimized as a result of lower flow speeds, and thus the pressure losses are lower. According to Shih, et al., the stagnation zone also shifts further downstream on the airfoil surface, to a flatter part of the airfoil creating a thicker boundary layer. Different boundary layer development and smaller gradients, led to decreased aerodynamic losses. Also, surface heat transfer was found to be reduced by as much as 30% on the endwalls. However, with the presence of swirl it was seen that these fillets were less effective in reducing aerodynamic loss and surface heat transfer. Shih, et al. concluded that the size and strength of secondary flows aren't the only factors that influence aerodynamic losses and heat transfer.

Zess, et al. [21] used numerical analysis to study various different fillet shapes before they finally zeroed on to an asymmetric profile having dimensions 1δ high and 2δ long as shown in Fig. 9. From their numerical study, it was seen that this profile chosen for experiments was the most effective at eliminating the horseshoe vortex. This design had a pointed leading edge at the stagnation plane. Unstructured and tetrahedral mesh that were second-order accurate were utilized for numerical calculations. The final grid size for the filleted vane was 1.2 million cells. Turbulence model used was a RNG- $\kappa\varepsilon$ model with non-equilibrium wall functions. To measure the

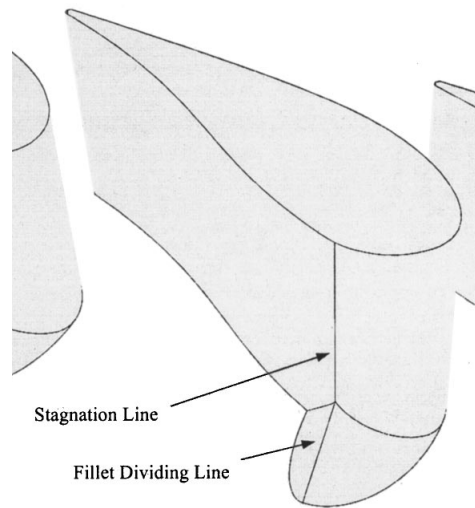


Fig. 9.: Fillet shape tested by Zess, et al. [21]

mean and turbulent flow fields in the vane passage, a two-component, back-scatter, fiber optic Laser Doppler Velocimetry (LDV) system was employed. The numerical results showed that lower levels of turbulent kinetic energy levels indicating reduced strength of leading edge horseshoe vortex. Elimination of the horseshoe vortex and a delay in the development of the passage vortex was confirmed by the results of the flow field measurements on the pressure side of the vane.

I.3.2. End wall contouring

Boletis [22] used an annular turbine nozzle guide vane test rig to study the effect of meridional tip endwall contouring on flow fields around the guide vane. The benefits of this type of contouring are due to the increase of the channel convergence, the decrease of the pressure gradient at the front half of the blade passage, and the positive influence on the spanwise static pressure distribution at the blade trailing edge region. Boletis, compared his test results with previous experiments which had been performed with cylindrical endwalls. A double-head, four-hole pressure probe

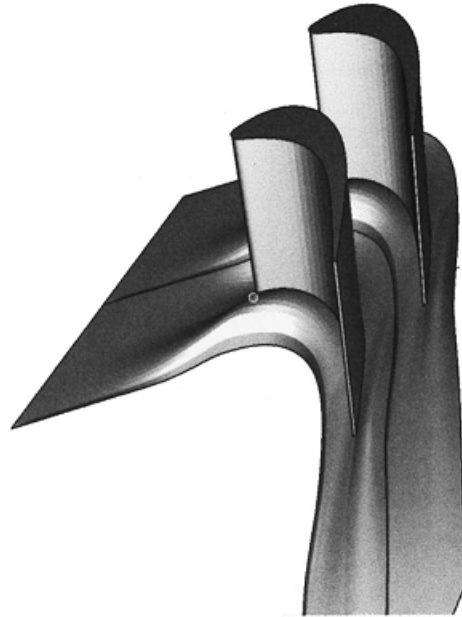


Fig. 10.: End wall contouring designed by Harvey, et al. [23]

along with surface pressure taps were employed for pressure measurements. A cubic function governed the contouring, started upstream of mid-chord and continued to the trailing-edge. Boletis observed a significant decrease in the transverse pressure gradient at the front part, while a low static pressure region is created at the tip endwall suction side corner, which according to him reduces the inward flow of low momentum fluid over the blade suction surface. Also, overall losses observed were considerably reduced compared to cylindrical tip endwall contouring cases studied by other researchers. Boletis also observed a small change in the exit flow angle leading to moderate change in the inlet flow conditions for the following row.

Harvey, et al. [23] designed a nonaxisymmetric end wall for a turbine rotor blade in linear cascade by extending the method of linear design system which is used for forward and inverse design of 3-D turbine aerofoils. The design study focused on controlling the surface static pressures and improving the exit whirl angle distribution (reducing the secondary flow deviations). Ups and downs on the axisymmetric end

wall surface is created by the product of two curves in axial and circumferential directions. A B-spline with six control points was chosen to govern the axial profile of the surface. After optimizing the design, the final profiled end wall shown in Fig. 10 is calculated to reduce secondary flow deviations.

Hartland, et al. [24] undertook extensive experimental study for the end wall contouring designed by Harvey, et al. [23]. Fig. 11 gives an idea of the end wall profile as a contour plot of end wall heights. A five-holed cobra type probe along with several pressure tappings were employed to measure flow parameters. Also, fluorescent dye in diesel oil was used to get the flow visualization on the end walls. The static pressures observed in experimental results agreed with the CFD results carried out by Harvey, et al. [23], in fact showing a greater reduction in pressure difference between suction and pressure side in early part of the passage. Significant reduction in secondary losses was observed due to the end wall modification designed and tested by Harvey, et al. and Hartland, et al. respectively.

Dossena, et al. used a 2-D contoured endwall on a turbine vane linear cascade to performed simulations and experiments. As shown in Fig. 12, the blade span decreases smoothly from h_1 to h_2 from leading to trailing edge respectively. Contraction ratio (h_2/h_1) of 0.70 was used by Dossena, et al. Five-hole probes were used at the downstream of trailing edge for pressure measurements and numerical calculations were used to understand the flow structure within the blade passage. It was observed that a stronger acceleration of flow because of contoured end wall mitigates vortex generation and development. However, variation in exit flow angles was seen in span-wise direction. Also, lower velocities observed in the passage resulted in reduced secondary and profile losses.

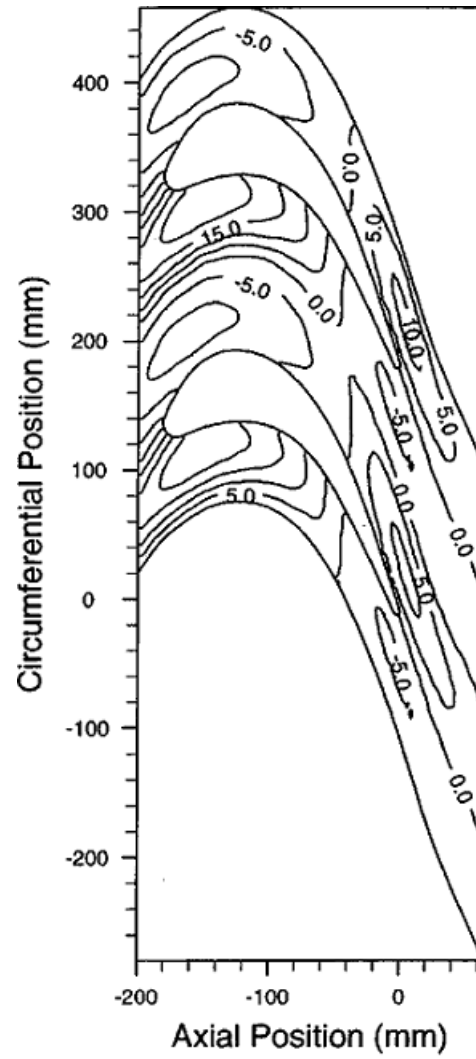


Fig. 11.: End wall contouring tested by Hartland, et al. [24]

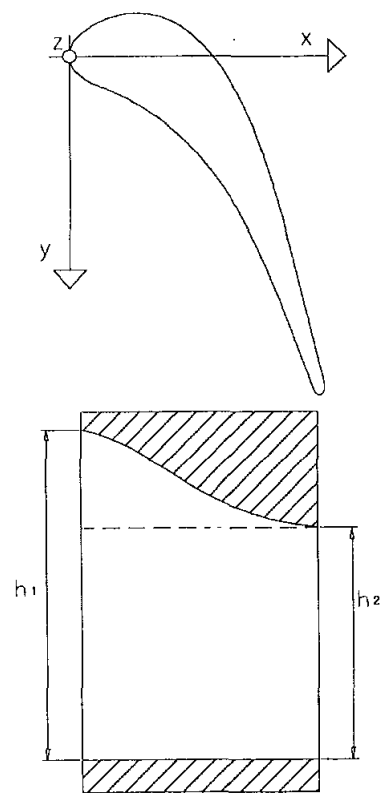


Fig. 12.: End wall contouring tested by Dossena, et al. [25]

CHAPTER II

OBJECTIVES

Following are the objectives for this thesis report:

II.1. Testing and Data Analysis

- Interstage test measurements and data analysis
 - Interstage measurements at design and off-design points
- Performance test measurements and data analysis
 - Varying rotational speeds (1750 RPM - 3000 RPM) at 3 fixed mass flow rates.
 - Varying mass flow rates (2.58 kg/s - 3.84 kg/s) at 3 fixed rotational speeds.
- Develop analytical codes to:
 - Quickly check instrumented channels for discrepancies.
 - Automatically generate input files with ambient conditions for main analysis program.

II.2. Design and 3D Modeling

- Design of a cover with knife edges to cover the window on exiting TPFL top casing.
- 3D modeling of complete TPFL facility

II.3. Assembly and Instrumentation

- Complete assembly of DooSan two-stage turbine into the existing TPFL facility.
- Installation of 7-axes probe traversing system.
- Instrumentation of TPFL facility with total pressure rakes, static pressure taps, pneumatic pressure tubes, five-hole probes and thermocouples.
- Calibration of 3 five-hole probes at respective Mach numbers for station 3, 4 and 5.

CHAPTER III

RESEARCH FACILITY

III.1. Existing Facility

The experimental research turbine facility at Turbomachinery Laboratory, Texas A&M University is a state of the art facility designed and set-up by Schobeiri, et al. [26] to measure flow physics and performance characteristics for different blade configurations of stators and rotors.

A 3D rendered model of the research facility with its various components is shown in Fig. 13. The main components of existing facility are described as below:

Three-stage centrifugal compressor (not shown in Fig. 13) A 300 kW electric motor is used to run this three-stage centrifugal compressor installed outside the test-cell. This compressor operates in suction mode and is controlled by a variable frequency controller. Operating frequency range of 0 to 66 Hz allows to vary pressure and volumetric flow rate of the compressor. The compressor is rated for a maximum pressure difference of 55 kPa and volumetric flow rate of $4 \text{ m}^3/\text{s}$.

Venturi flow meter A venturi flow meter is installed to measure the mass flow through the turbine. Both venturi inlet and throat sections are equipped with four total pressure probes and two thermocouples.

Long pipe with exit diffuser An exit diffuser along with a long pipe serve for a smooth transition between turbine and the venturi flow meter.

Three-stage turbine A versatile turbine section to accommodate three-stages of

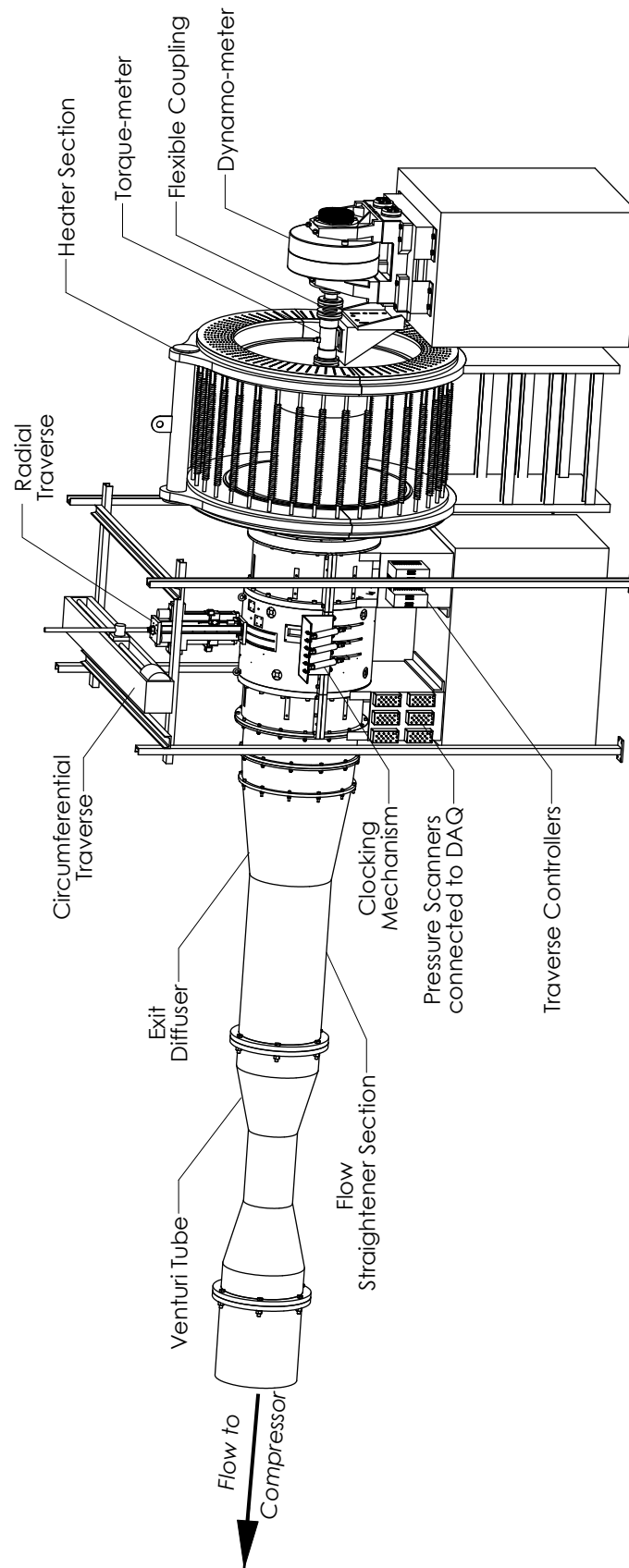


Fig. 13.: Research turbine at TPFL facility [26]

any blade configuration with a maximum and minimum blade outer diameter of 27in and 22in respectively. The turbine section is rated for a maximum speed ranges of 3000 rpm and allows for interstage measurements at stations 3, 4 and 5 using high-response five-hole probes. Three T-rings are provided to seal the probe traversing slots at each of these stations.

Clocking mechanism A clocking mechanism with three pneumatic pistons is devised to clock each of the stators externally and individually without the need to open the turbine.

Probe traverse system The research turbine facility is equipped with a probe traverse system to allow for traversing each of the three five-hole probes in both radial and circumferential direction. Three stepper motors are used for radial traverse of probes to span the blade height and one stepper motor controls circumferential movement of all three probes to span a window of about 18° in order to cover more than one blade during interstage measurements. Additionally, the probe angles can also be controlled through the use of three small stepper motors which can rotate the probes around their respective axes. This enables accurate positioning of the probe measurement head into the direction of flow, and thus minimizing the errors inherent with five hole probe calibration angle range.

Heater The turbine inlet has an integrated heater to maintain turbine exit temperature above dew point to prevent condensation of water from humid air expanding through the turbine during operation. The heater has 162 elements arranged and distributed circumferentially between two aluminum sheets, to create a cross-flow and achieve symmetric temperature along inlet cross-section.

Torque meter This high-precision torque meter used between turbine shaft and flexible coupling is connected to data acquisition computer and acquired torque data is used to calculate the power, losses and efficiency values of turbine. The torque meter is rated for a maximum rotation speed of 8500 rpm and a maximum torque of 677.9 Nm.

Flexible coupling Flexible coupling is used to transmit torque while permitting some radial, axial, and angular misalignment.

Dynamometer An eddy current low inertia dynamometer with maximum power of 150 kW, maximum torque of 500 Nm and maximum rotational speed of 8000 rpm, is used to maintain the rotational speed of the turbine during operation. A rotational speed accuracy of ± 1 rpm and torque accuracy of ± 1.25 Nm is achievable by this dynamometer.

Fig. 14 and Fig. 15 show sectional views of the turbine assembly that highlight the dynamo-meter, torque-meter, heater section, drive shaft, flexible couplings and bearings.

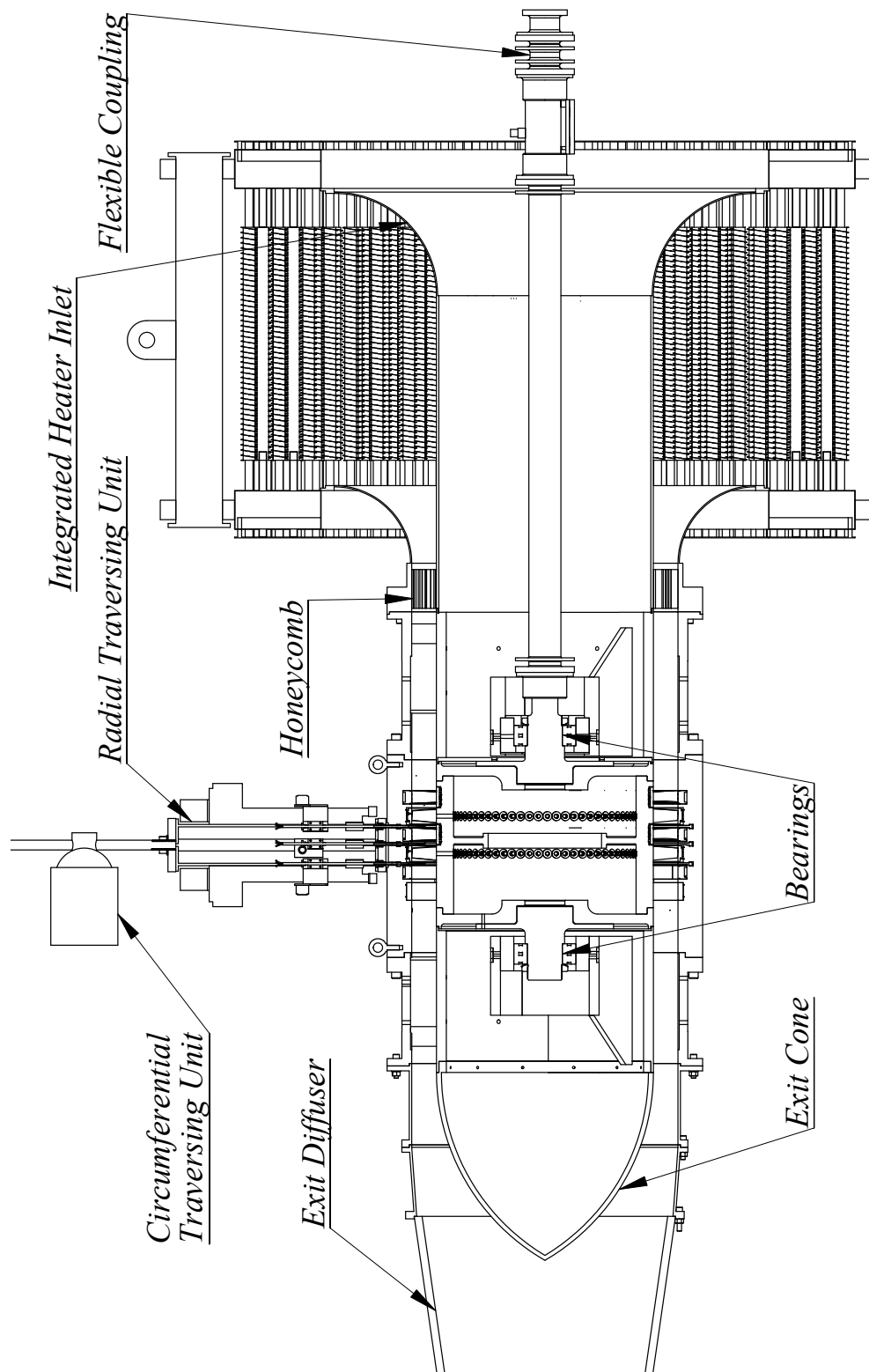


Fig. 14.: Sectional view of the turbine assembly showing details of the heater, torque-meter and the shaft [26]

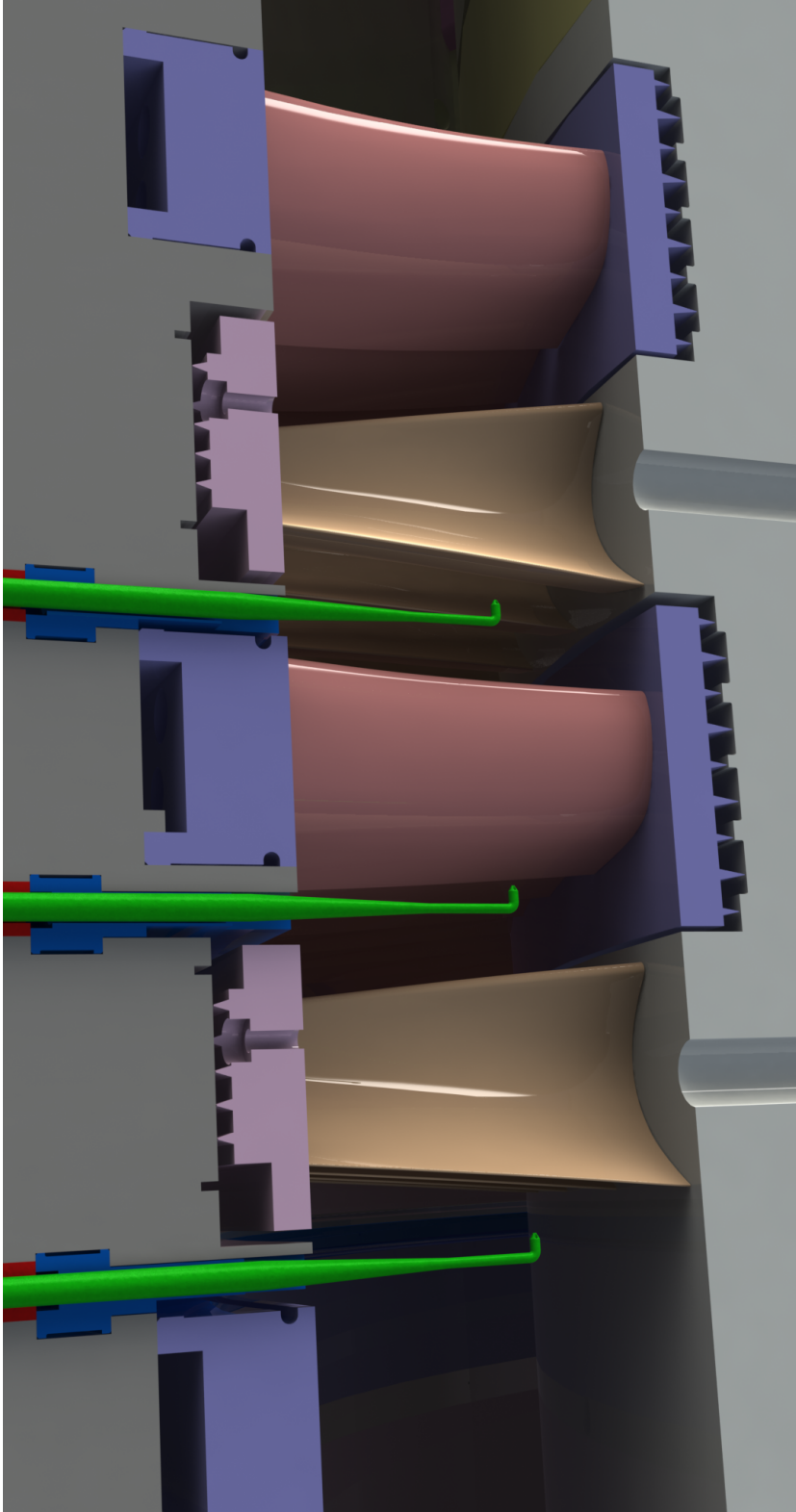


Fig. 15.: Sectional view of the turbine assembly showing the five-hole probe locations [26]

III.2. Two-stage Turbine Design for DooSan

In this chapter the component design drawings of the two-stage high efficiency turbine using the newly designed DooSan blades are presented. Also a detailed bill of materials (BOM) of parts shown in Fig. 16 that were manufactured at the facilities of Sulzer Turbo Services in Houston is presented in Table I.

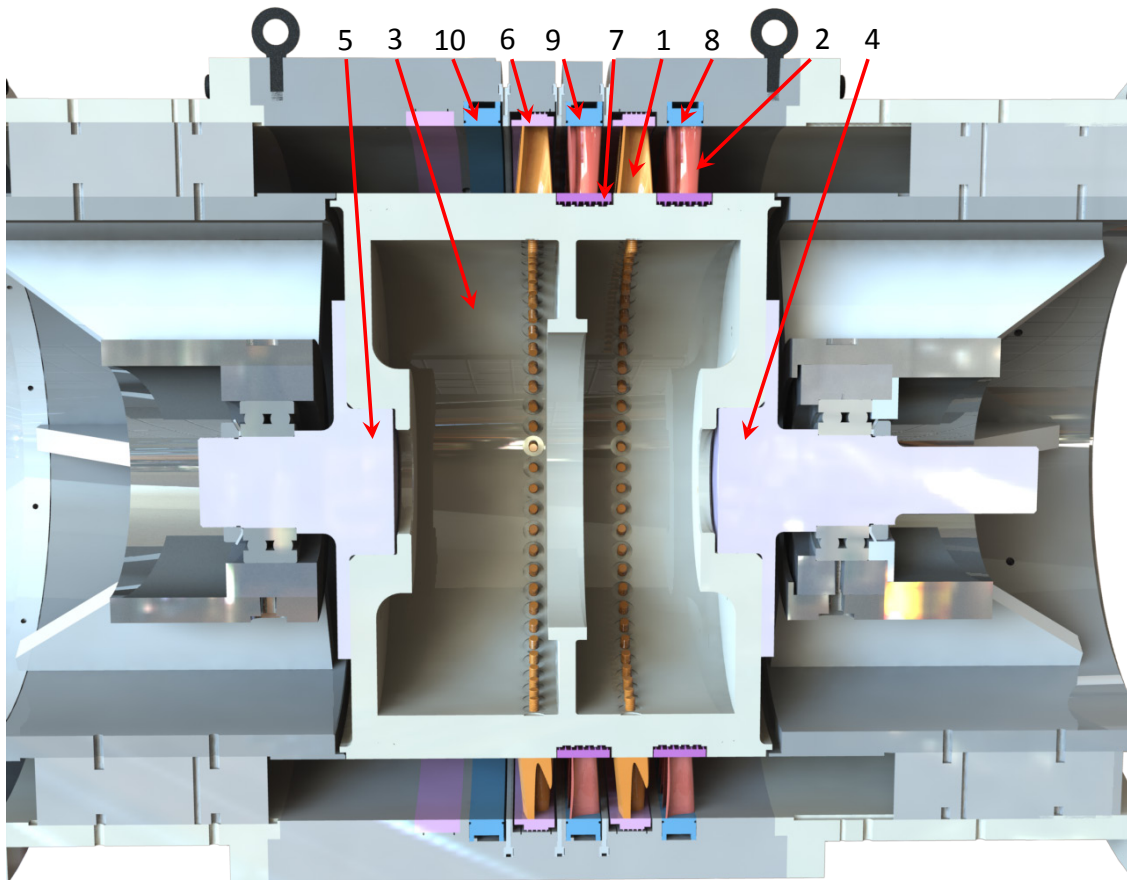


Fig. 16.: Cross sectional view of complete assembly

A set of figures showing the fully assembled machine with all the relevant components is also included in this chapter. Fig. 17, Fig. 18 and Fig. 19 present a fully detailed assembly of the stator rings, rotor hub, bearings and casing.

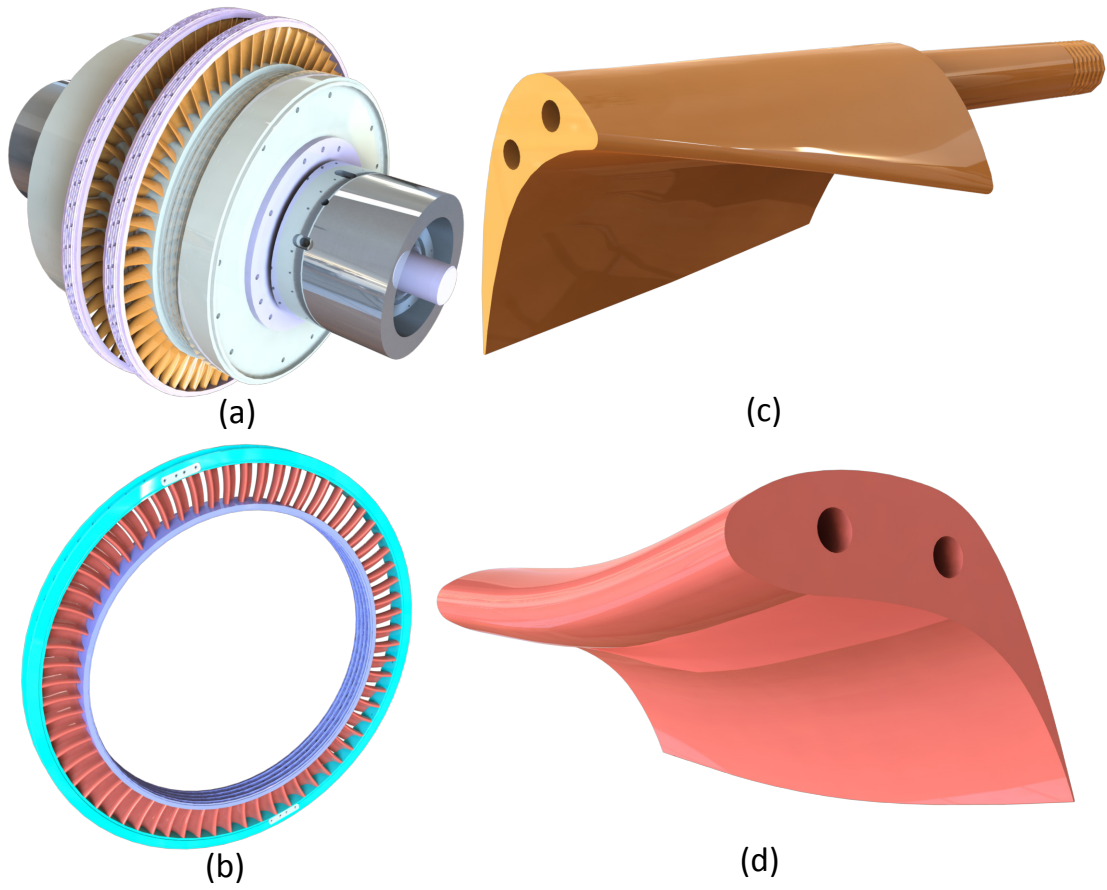


Fig. 17.: (a) Complete hub assembly and bearings with (b) 3-D view of stator ring and 3-d views of (c) Rotor blade and (d) Stator blade

Table I.: Bill of parts for manufacturing

Label	Part Name	Steel Grade	Quantity
1	Rotor Blade	4140	126
2	Stator Blade	4140	132
3	Hub	4140	1
6	Shaft: Fixed Bearing End	4140	1
7	Shaft: Rear End	4140	1
8	Rotor Top Seal (Complete Ring)	4140	2
9	Stator Hub Seal (Complete Ring)	4140	2
10	Stator Ring 10	4140	2
11	Stator Ring 20	4140	2
12	Stator Ring 30	4140	2
13	Stator Ring Connector	4140	12

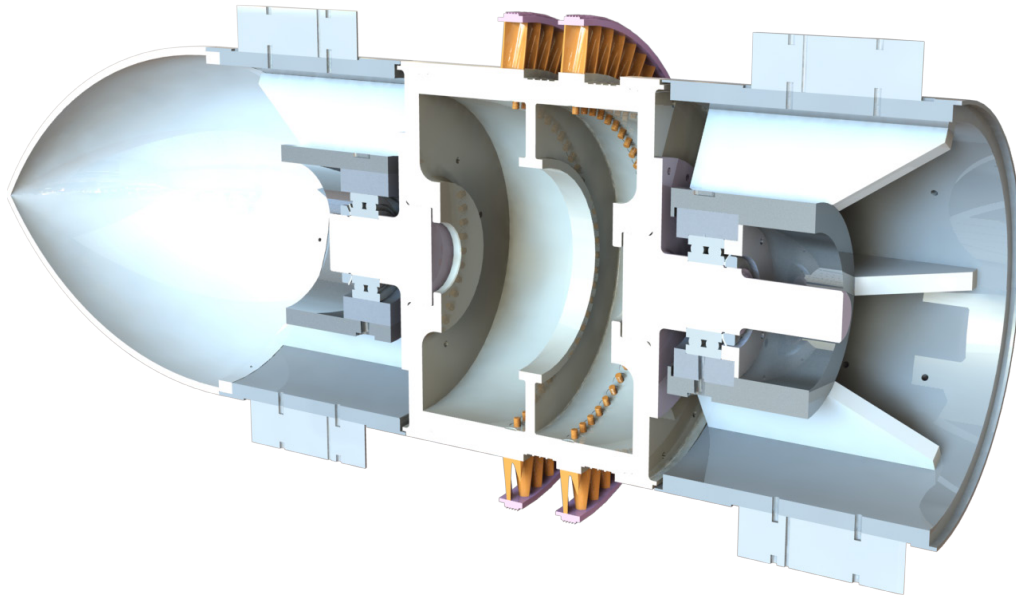


Fig. 18.: Cross sectional view of complete hub assembly, bearings and inner casing

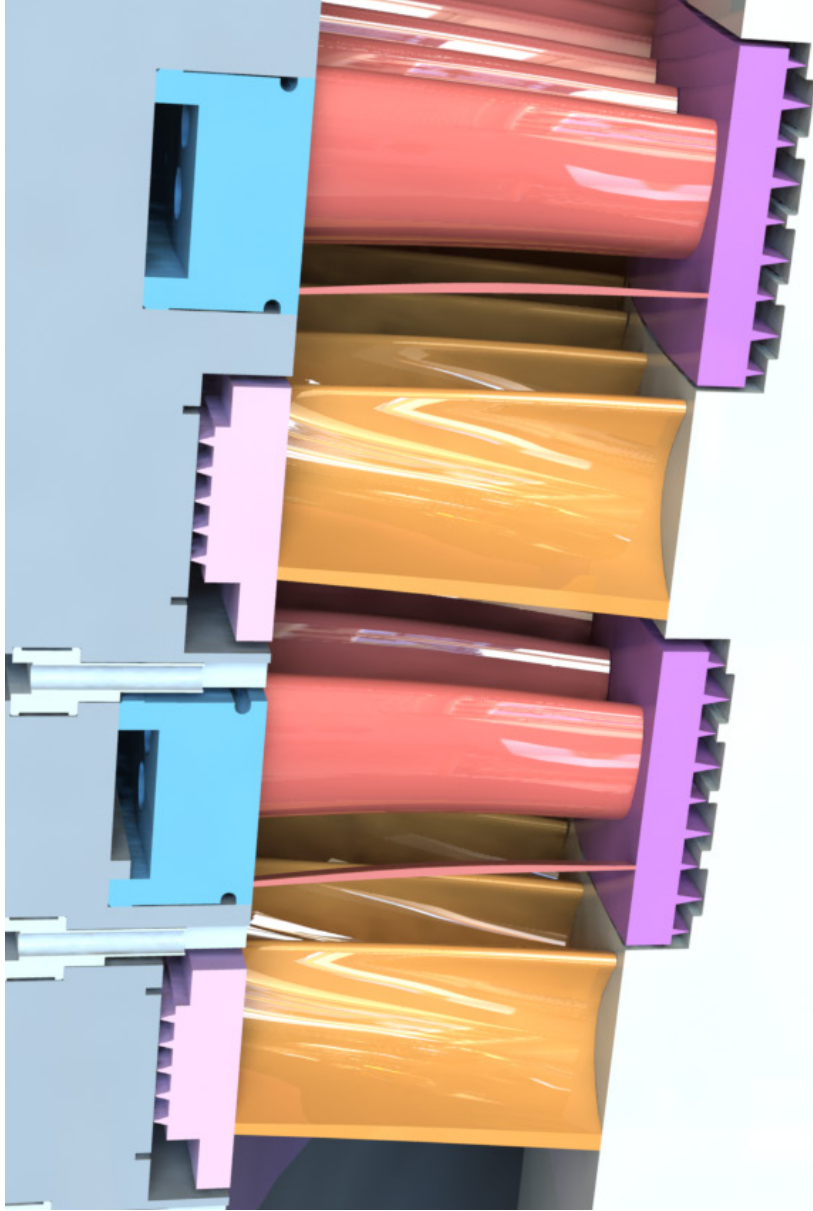


Fig. 19.: Cross sectional view of stator and rotor hub assembly showing the seal profiles used

Shape and dimension of DooSan stator blade is shown in Fig. 20, whereas Fig. 21 shows location of outer mounting holes on stator blade.

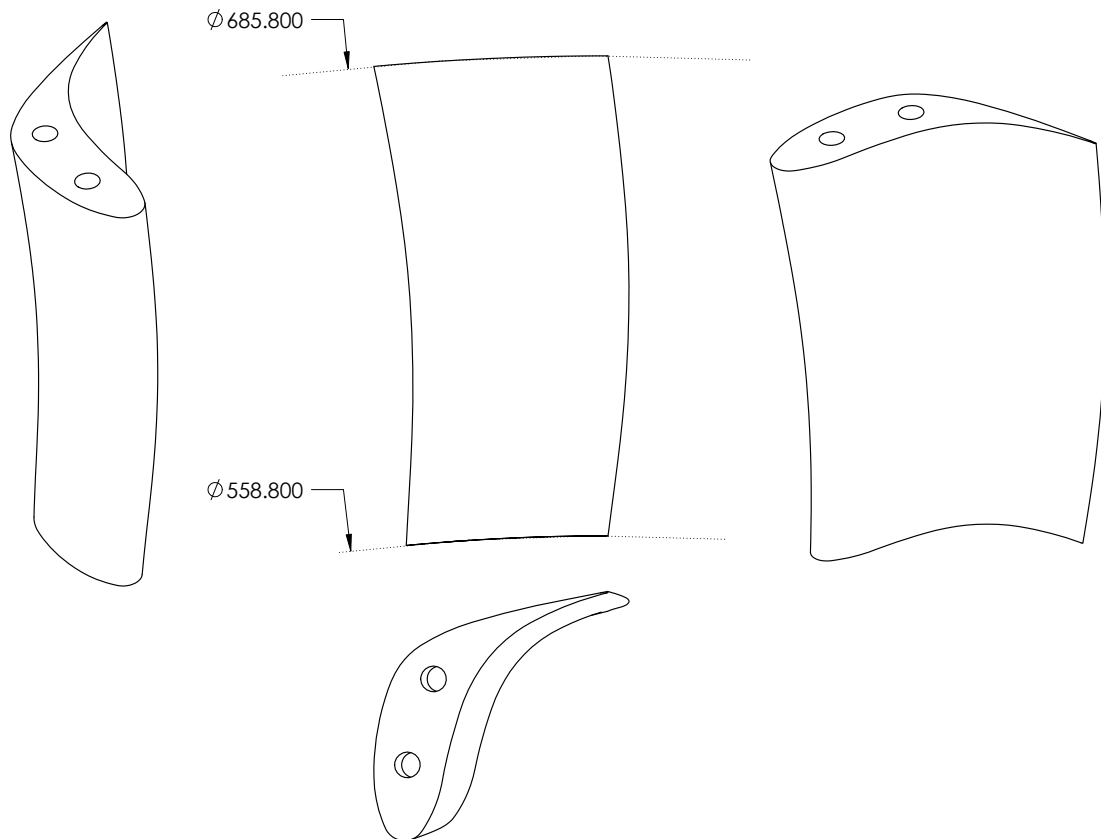


Fig. 20.: Stator blade

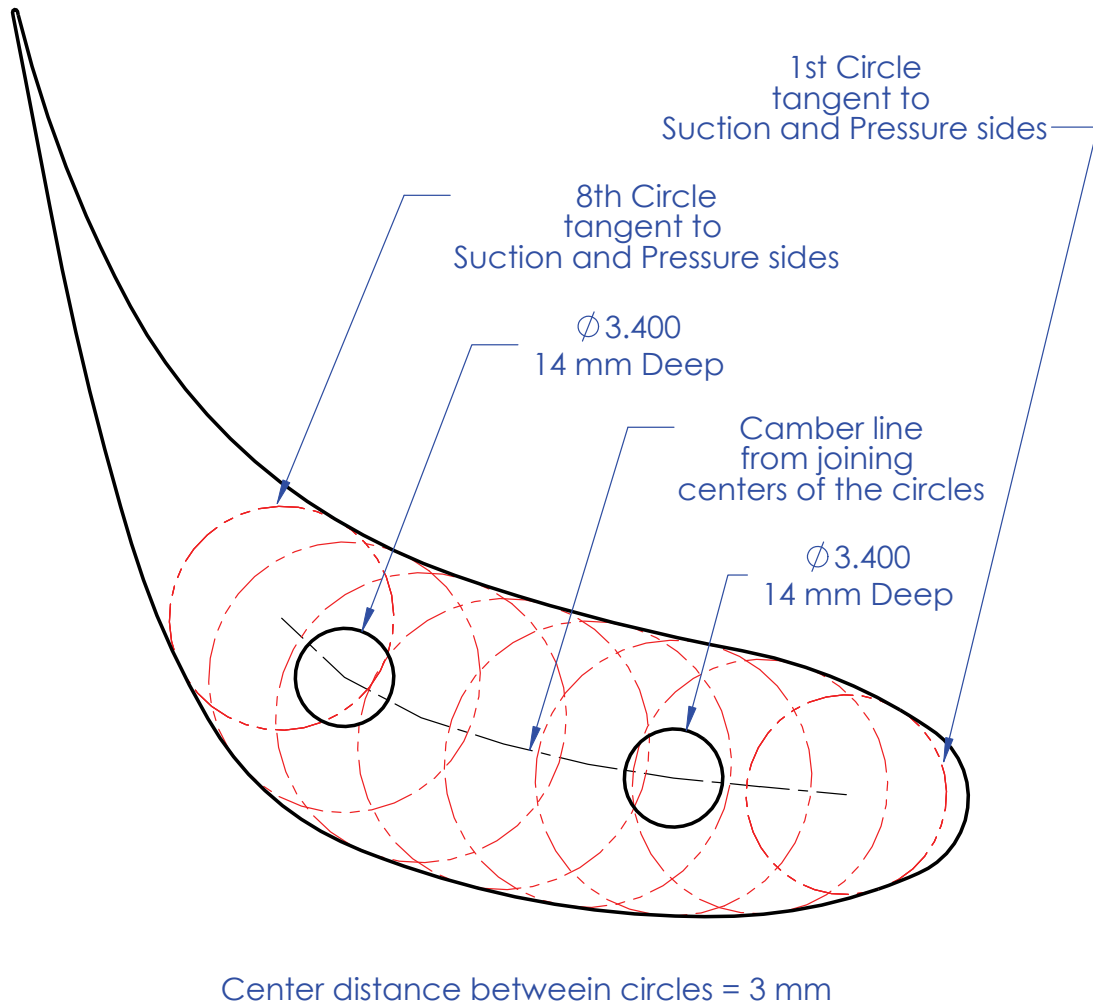


Fig. 21.: Location of outer mounting holes on stator blade

Details of stator assembly with the labyrinth package is shown in Fig. 22.

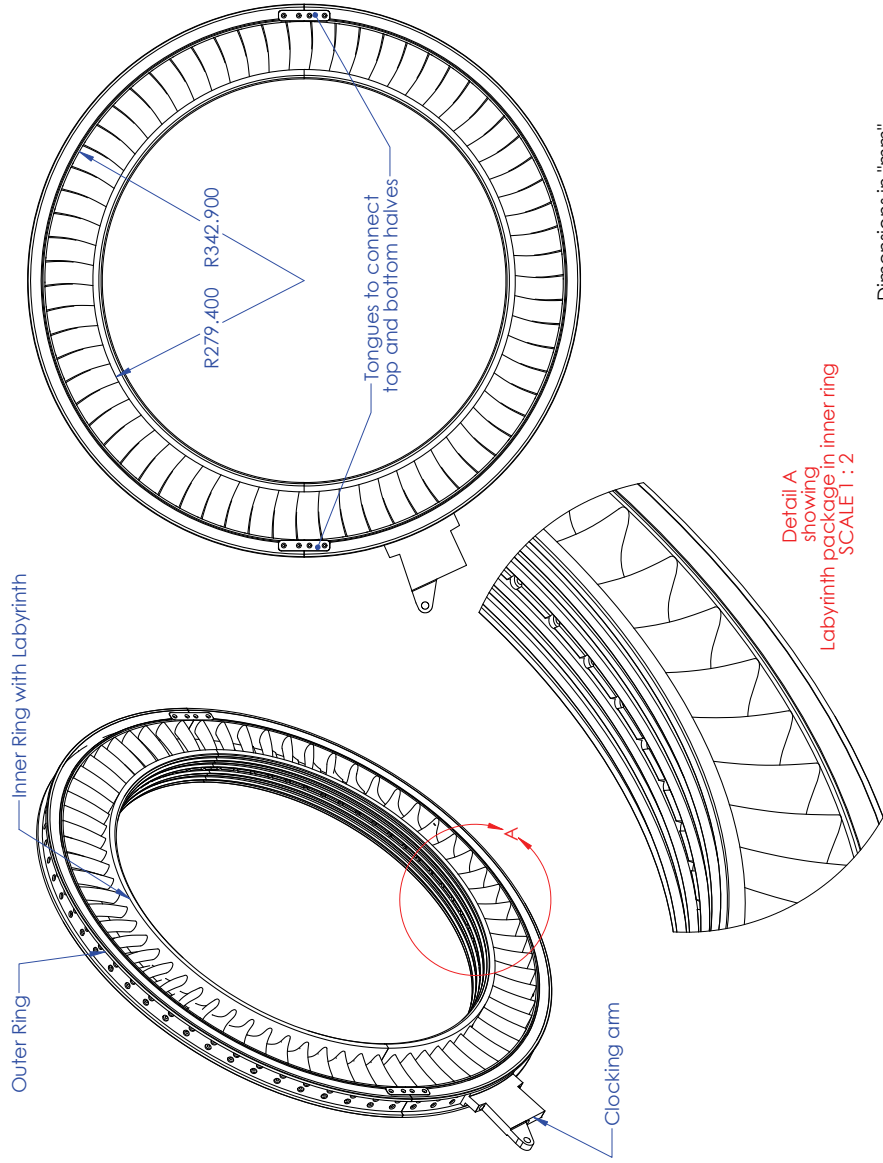


Fig. 22.: Details of stator assembly

Fig. 23 gives the details of DooSan rotor blade and Fig. 24 shows details of rotor assembly along with the labyrinth package for rotor-tip sealing.

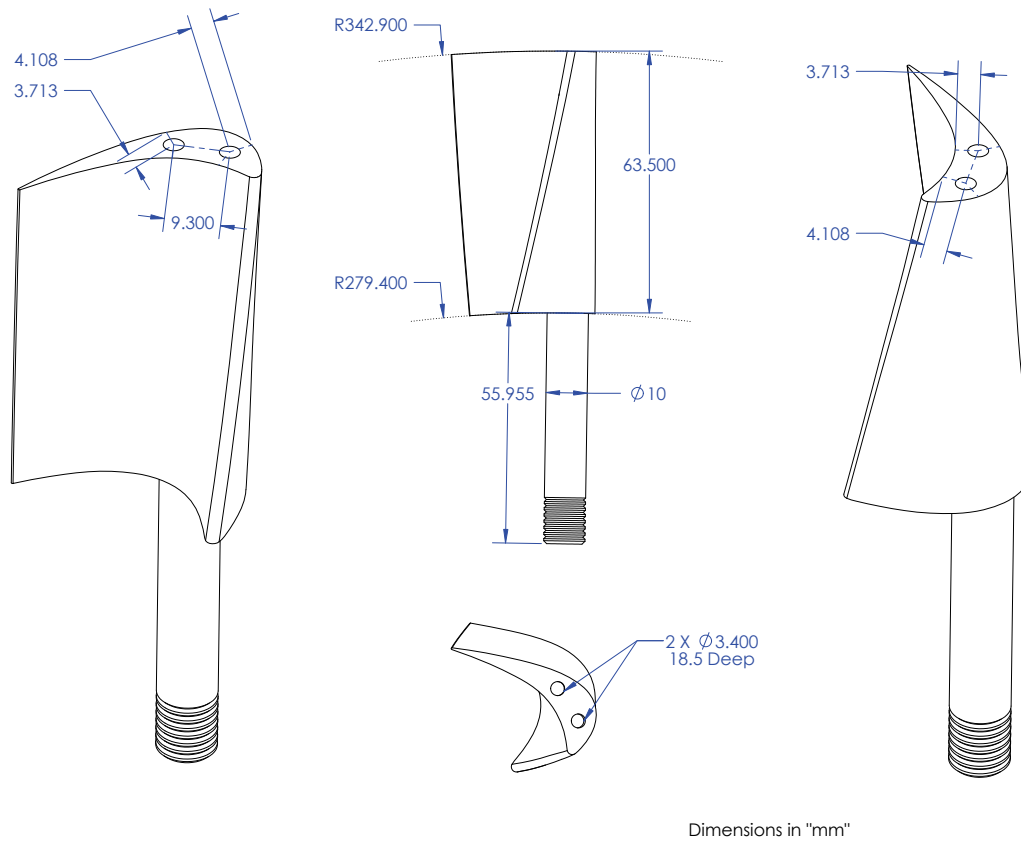


Fig. 23.: Rotor blade

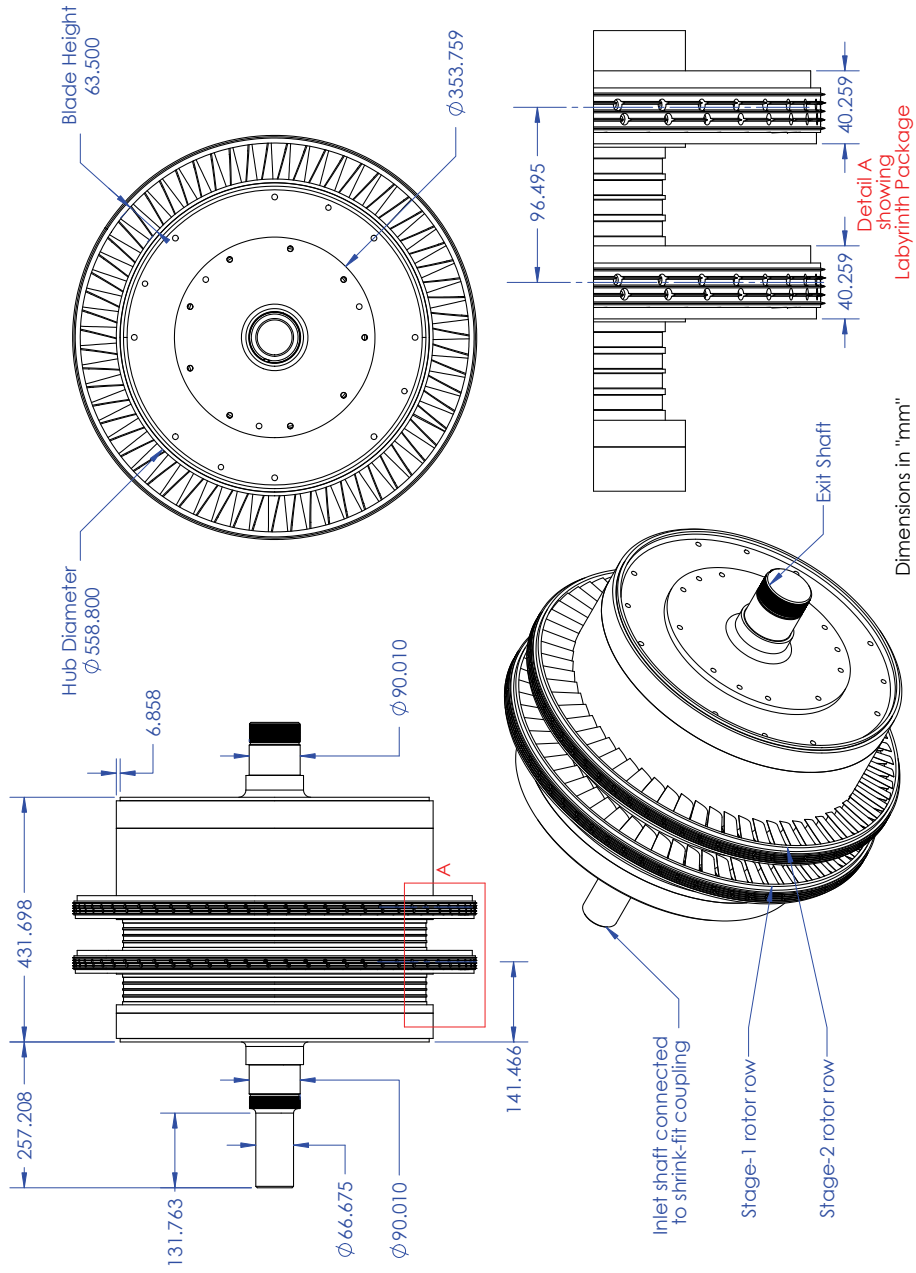


Fig. 24.: Details of rotor assembly

Geometry parameters of DooSan rotor and stator shown in Fig. 25 and Fig. 26 respectively are populated in Table II along with Zweifel coefficients.

Table II.: Blade geometry and Zweifel coefficients

	Axial Chord	Chord	Pitch	Solidity	Zweifel
	C _{ax} (mm)	c (mm)	s (mm)	c/s	Coefficient
Rotor					
Hub	35.29	36.82	27.87	1.32	0.723
Hub-Mid	32.95	36.42	29.39	1.24	0.674
Mid	30.58	36.65	30.91	1.19	0.647
Mid-Tip	28.12	37.39	32.43	1.15	0.622
Tip	25.73	38.57	33.95	1.14	0.602
Stator					
Hub	28.14	37.34	26.60	1.40	0.335
Hub-Mid	26.61	35.63	28.05	1.27	0.409
Mid	29.68	39.05	29.50	1.32	0.368
Mid-Tip	31.22	40.73	30.95	1.32	0.397
Tip	32.8	42.56	32.41	1.31	0.419

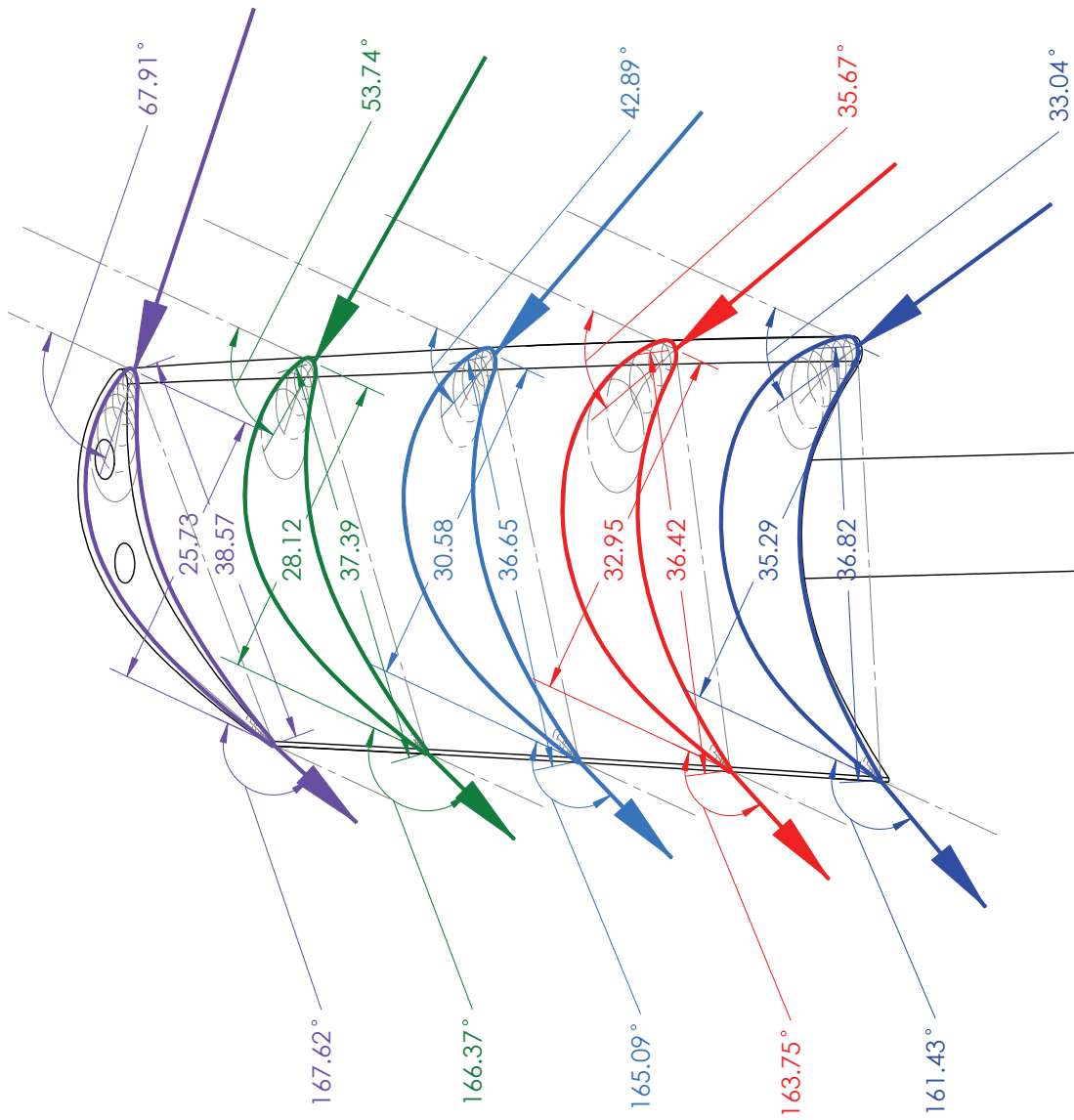


Fig. 25.: Metal angles, axial chord and chord length at various location of rotor blade

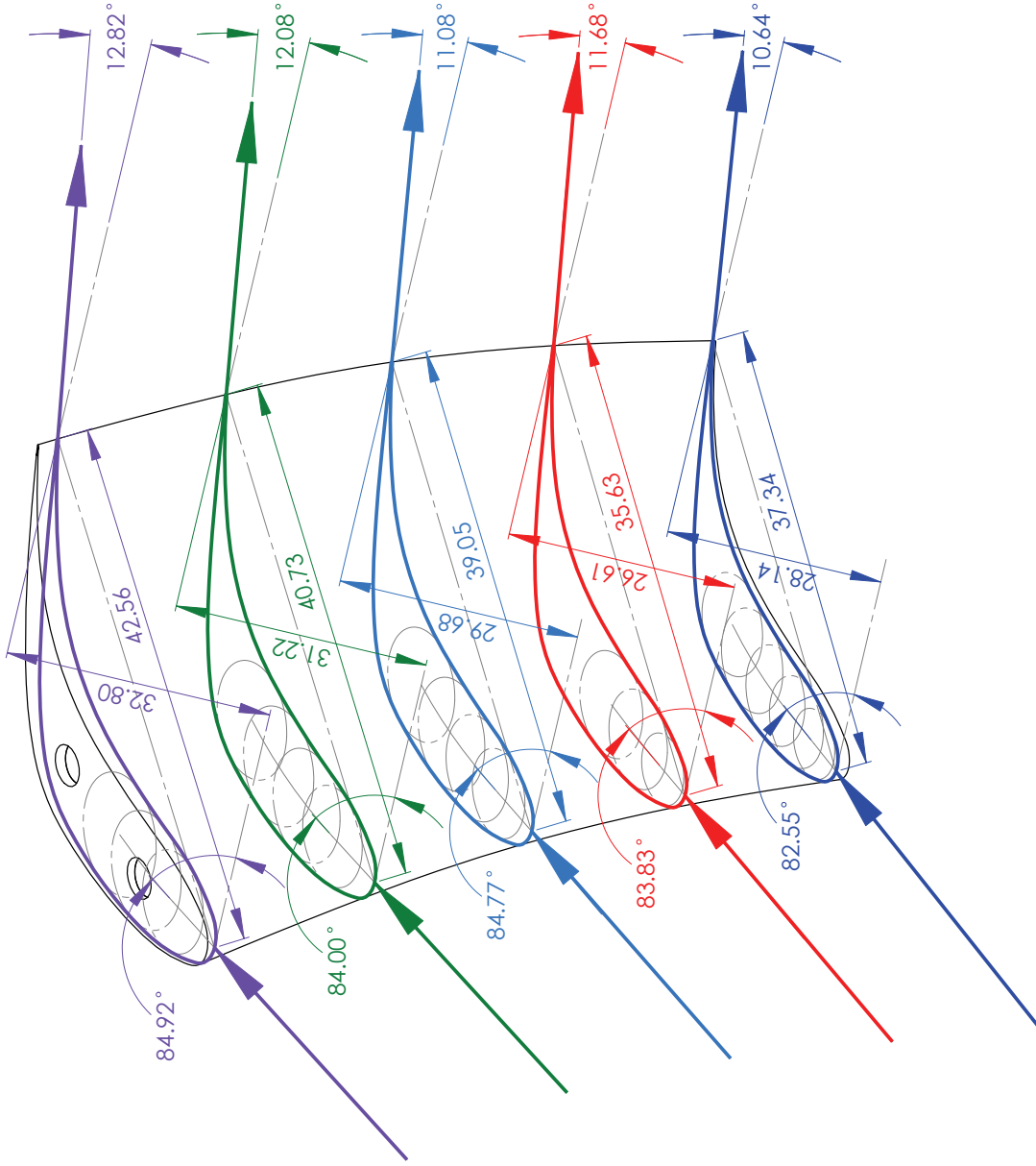


Fig. 26.: Metal angles, axial chord and chord length at various location of stator blade

CHAPTER IV

INSTRUMENTATION

IV.1. Engine Monitoring System

In order to ensure the safety of the personnel and the test facility, the TPFL turbine utilizes several monitoring systems. Vibration velocity-meters are installed at sensitive locations to monitor any unusual vibration levels during the test run. The velocity-meter probes, Bently-Nevada Velomitor PN 330500 (100 mV/in/s) are mounted on the front and back shaft bearings at 6 and 12'o clock positions each. A fifth probe is placed at the base of torquemeter support plate. The output from the five probes is collected using two Bently-Nevada 3300/55 dual velocity monitoring system which give a minimum observable value of 0.05 in/s.

Temperature monitoring thermocouples are placed to monitor critical components within the engine. The thermocouples are J-type thermocouples with 50 ft of extension grade thermocouple wire. The temperature is monitored at the shaft bearings, venturi inlet and at the turbine inlet. The bearings have two thermocouples placed at 6 and 12 o'clock positions, and are used to make sure the shaft bearing temperatures do not exceed 70 °C. For the bearings the use of temperature and vibration level readings act as a simple means to monitor bearing health and determine the need to change bearings. At the venturi inlet, due to the concern for condensation a thermocouple is placed to monitor the temperature of airflow exiting the turbine. The temperature at this point is monitored to make sure it does not go below 21 °C as this would signify condensation. Turbine inlet temperature is monitored and controlled using a feedback loop on the heater controller. The inlet temperature to the

unit is an important parameter for each experimental run and therefore active control of this parameter is necessary. Additionally, the temperature is monitored to make sure it does not exceed safety limits. The output from thermocouples is fed into the Bently-Nevada 3300/30 which allows for a six channel temperature monitoring system. The heater controller utilizes a separate thermocouple for the inlet process temperature that is used in the control loop.

IV.2. Turbine Performance Instrumentation

The pressure and temperature measuring equipment used to obtain engine performance curves included wall static pressure taps, and exit and inlet rakes. Table III gives a list of fixed channels used for understanding flow parameters.

Four combined total pressure and total temperature rakes were placed upstream of the first stator row. They were located radially at 2, 4, 8 and 10 o'clock positions. Each rake consists of 4 total pressure and 3 total temperature probes. The total pressure probes are simply Pitot tubes, and the total temperature are calibrated J-type thermocouples, with their calibration implemented into the performance reduction program. To reduce the wake thickness originated from the trailing edge of the inlet rakes, the rakes were shaped aerodynamically with a round leading edge and a sharp trailing edge.

Four combined total pressure and total temperature rakes were placed downstream of the last rotor row. These are similar to the inlet rakes mentioned above with the exception that they do not have sharp trailing edge and their thermocouples are not calibrated. They are placed in radial positions with similar spacing to the inlet rakes, but are offset in order to prevent interference with the wakes produced due to the inlet rakes.

Table III.: Fixed channels for flow parameters

Parameter	Stations							Total Parameters
	1	2	3	4	5	6	7	
Total Pressure	16	0	0	0	0	0	16	32
Total Temperature	12	0	0	0	0	0	12	24
Static Pressure	4	4	2	2	2	4	4	22
Static Temperature	0	0	0	0	0	0	0	0
Channels/Station	32	4	2	2	2	4	32	78

Stations 1, 2, 6 and 7 are provided with four static pressure taps on the casings. These pressure taps are diametrically opposite to each other in a particular station. Taps on station 2 and 7 are offset by about 10° from the taps at station 1 and 6 respectively. Also, each of the T-rings on station 3, 4 and 5 have 2 static pressure taps at 11 and 1 o'clock positions.

Massflow through the system is measured by a venturi tube from Daniel Flow Products which is connected to the exit diffuser of the turbine. A flow straightener and honey comb are installed at the exit of the diffuser for accurate measurement of mass flow through the venturi. Table IV gives all the geometry parameters for the venturi tube.

Table IV.: Geometry parameters for venturi

	Inner Diameter	Tap Diameter / No.	Cone Angle
Inlet	15.500 in	2 mm / 4	21°
Throat	10.327 in	2 mm / 4	15°
Total Length	69.180 in		

IV.3. Interstage Traversing System

The TPFL facility is equipped with a 4-axis traverse system which allows radial and circumferential traverse of five-hole probes at stations 3, 4 and 5. The traverse system uses five-hole pressure probes to resolve interstage total and static pressures and velocity components. A user defined grid (Fig. 27) can be formed and input as a test script for the traverse system to follow.

Three L-shaped five hole probes were used to resolve interstage pressure contours, velocity components, flow angles and spanwise total pressure loss coefficients. Each probe was calibrated using Bohn's technique in the calibration facility at TPFL. Probes for station 3 and 5 experience exit flow of rotor rows and velocities of approximately 0.1 M, whereas at station 4 (exit of stator), the probe experiences velocities to the range of 0.3 M. Hence, two of the three probes are calibrated at 0.1 M and one of them at 0.3 M. Fig. 28, shows the dimensions of five hole pressure probes used for interstage traverse.

The calibration of five-hole probes required independently placing each probe onto an angular indexing mechanism which was connected to a computer to automatically index the probe through the range of angles (-20° to 20° in pitch and -25° to 25° in yaw), with 1° increments. The stepper motors used for indexing the

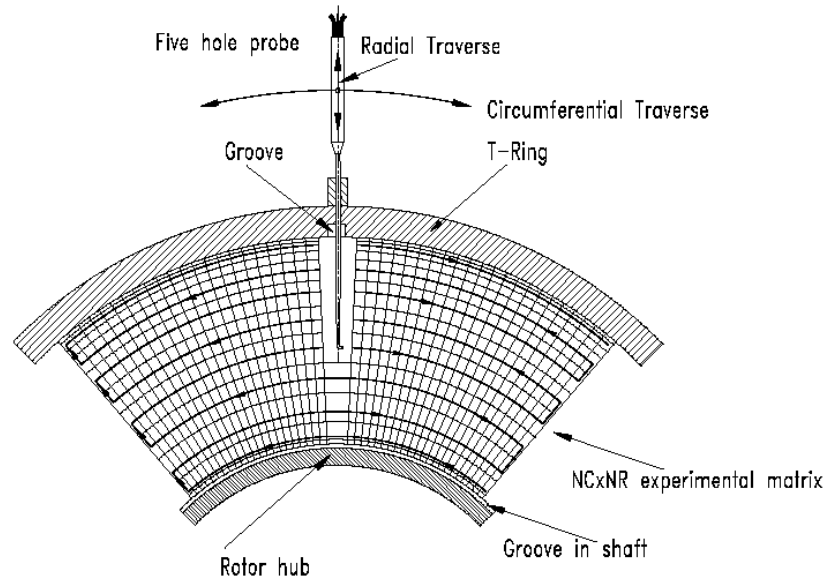


Fig. 27.: Interstage traverse grid [12]

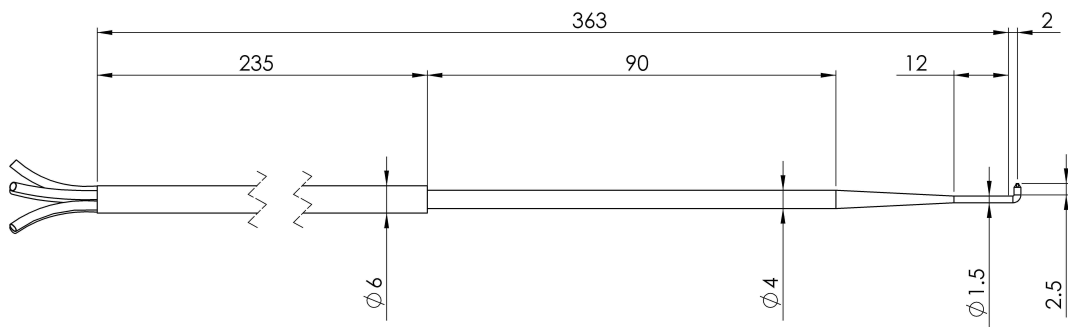


Fig. 28.: Five-hole probe dimensions in mm

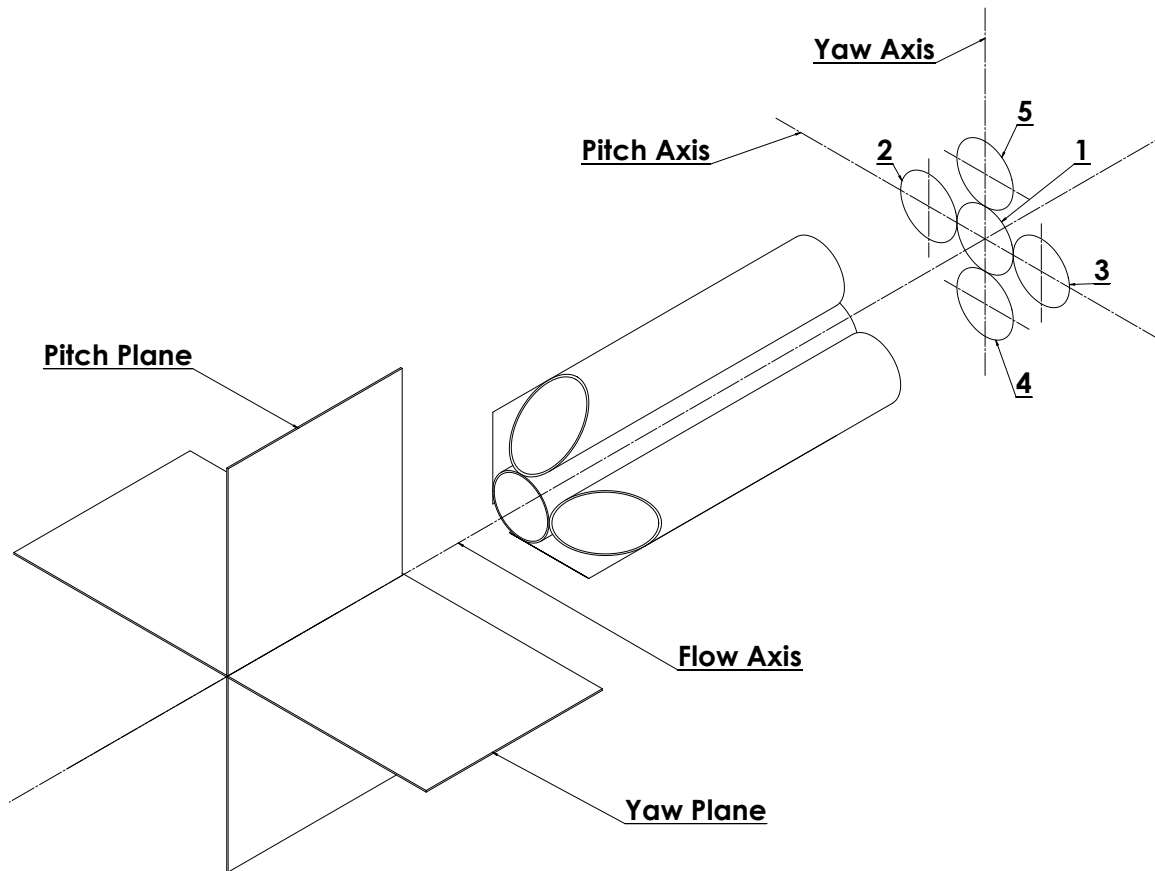
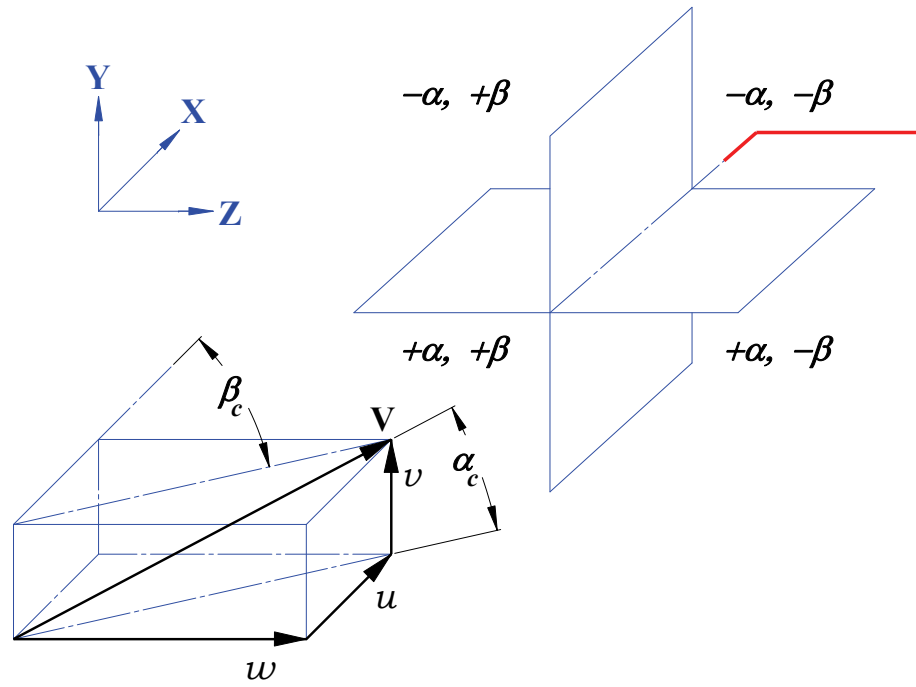


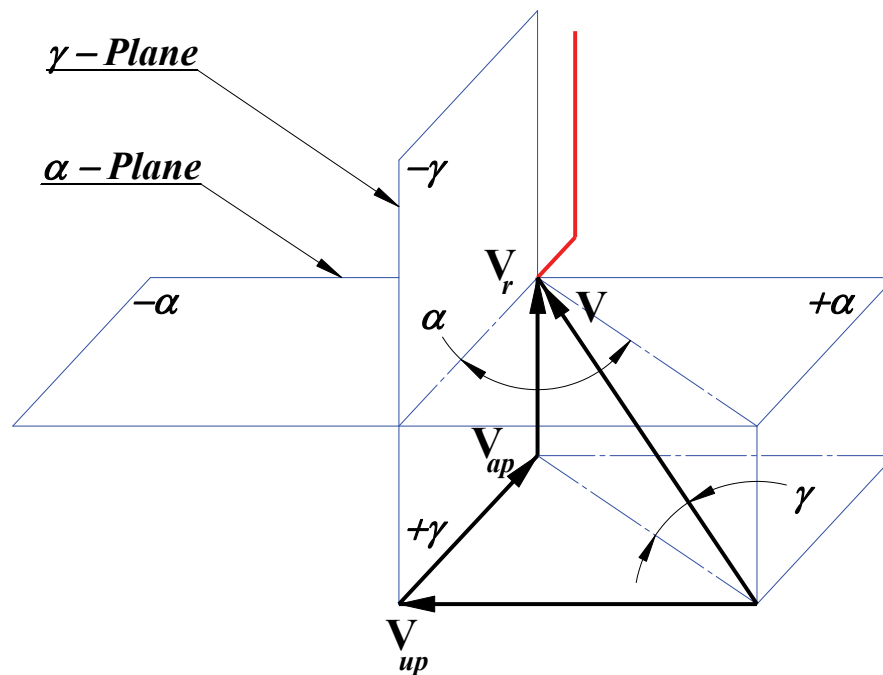
Fig. 29.: Definition of pitch and yaw angles w.r.t. probe axes [12]

probes are controlled by a program developed by E. S. Johansen, J. L. Gilarranz and P. Chakka, which employs the use of an algorithm that creates a user-specific grid of pitch and yaw angles (Fig. 29). The program records the pressure data obtained from channels of pressure scanner for each of the five hole ports as well as the total and static pressure of the calibration flow. The calibration data is analyzed using Bohn's calibration technique to create the calibration surfaces which are used to predict the velocity vector from an unknown velocity field.

Since, mounting of probes in calibration facility and that in turbine is completely different, it is necessary to convert local probe coordinate system to the absolute



(a) Probe coordinate system on calibration facility



(b) Probe coordinate system in turbine

Fig. 30.: Probe coordinate systems [12]

machine coordinate system. The coordinate system in Fig. 30a is referred to as the probe local coordinate system and in Fig. 30b shows the absolute machine coordinate system.

The quadrants in Fig. 30a indicate the sign conventions for pitch (α_c) and yaw (β_c) angles along with that of velocity components u , v and w . This coordinate system is referred to as the probe-local coordinate system in the calibration facility. Following equations govern the conversion between probe local coordinates to machine coordinates:

From Fig. 30a,

$$u = V \cdot \cos \alpha_c \cdot \cos \beta_c \quad (4.1)$$

$$v = V \cdot \sin \alpha_c \quad (4.2)$$

$$w = V \cdot \cos \alpha_c \cdot \sin \beta_c \quad (4.3)$$

Velocity components from Fig. 30b,

$$V_{ap} = V \cdot \cos \alpha \cdot \cos \gamma \quad (4.4)$$

$$V_{up} = V \cdot \sin \alpha \cdot \cos \gamma \quad (4.5)$$

$$V_r = w = V \cdot \sin \gamma \quad (4.6)$$

Thus, the conversion between the angles used in the calibration facility (α_c, β_c) to the angles that are used in the machine system (α, γ) is found from:

$$\alpha = \arctan \left(\frac{\tan \alpha_c}{\cos \beta_c} \right) \quad (4.7)$$

$$\gamma = \arcsin (\cos \alpha_c \cdot \sin \beta_c) \quad (4.8)$$

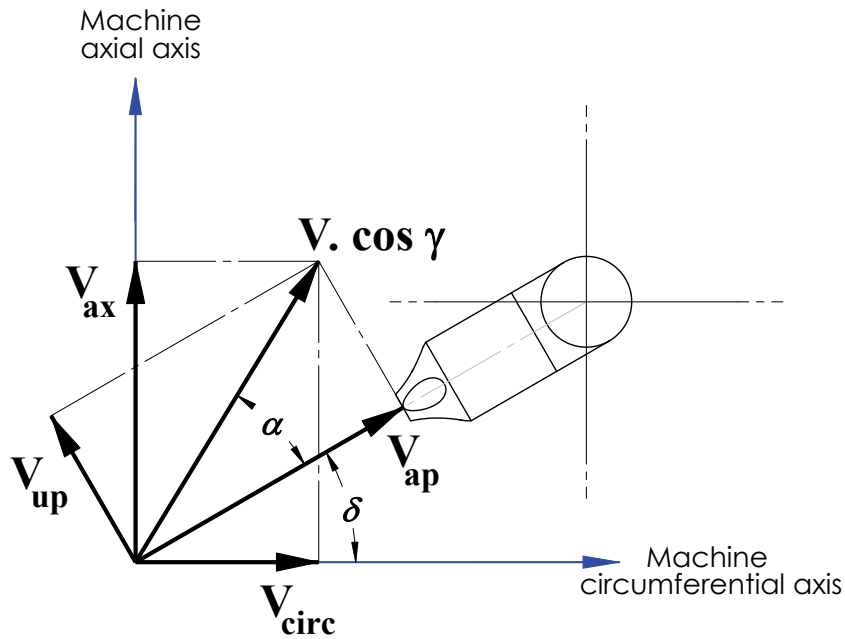


Fig. 31.: Probe velocities w.r.t. to machine axis [12]

The absolute flow angles at stations 3, 4 and 5 in the turbine vary with pressure ratio and rotating speed of the machine. To make sure that the flow angles stay within the calibration ranges for the three probes, the probe tips are aligned with the absolute flow angles at each station. These adjustments were carried out by placing the probes, radially at three different locations: 5 mm from hub, mid-span and 5 mm from tip. The probes were individually adjusted while the machine was running until the pressure ports 2 and 3 of the probes registered equal pressure values, therefore signifying probe being aligned to the flow with respect to the yaw axis. This adjustment angle is referred as δ_i where, subscript “i” is depending on station 3, 4 or 5. These probe adjustment angles can simply be added to the flow angle α . According to Fig. 31 the axial and radial components in machine axis are:

$$V_{ax} = V \cdot \sin(\alpha + \delta) \cdot \cos \gamma \quad (4.9)$$

$$V_{circ} = V \cdot \cos(\alpha + \delta) \cdot \cos \gamma \quad (4.10)$$

IV.4. Uncertainty Analysis

Kline's [27] method is used to calculate and populate the uncertainty of test instruments and its effects on test data. Table V gives all the maximum values for uncertainty of different parameters.

Table V.: Uncertainty data for the test results

Instrument	Parameter	Uncertainty
Five-hole probes	Static Pressure P_s	11.7 Pa
	Total Pressure P_t	35.1 Pa
	Relative Total Pressure P_{tr}	80.9 Pa
	Absolute Velocity V	0.53 m/sec
	Relative Velocity W	0.56 m/sec
	Absolute Flow Angle α	0.30°
	Relative Flow Angle β	0.30°
	Meridional Flow Angle γ	0.36°
	Total Pressure Loss Coefficient (Stator) ζ_s	0.005
Total Pressure Loss Coefficient (Rotor) ζ_r	0.009	
	Efficiency η	0.004
Rakes	Static Pressure P_s	17.0 Pa
	Total Pressure P_t	17.0 Pa
	Total Temperature T_t	0.1°C
Torque-meter	Torque τ	0.14 N m
	Rotational Speed n	1.7 RPM
	Power P	68.9 W
Venturi tube	Massflow \dot{m}	0.012 kg/sec

CHAPTER V

THEORY

This section explains the theory behind efficiency calculations for a turbine. All definitions used in this section are according to Schobeiri [2]. By analyzing the blade losses in spanwise direction, one can calculate the turbine and blade efficiency.

From the first law of thermodynamics, heat transfer (q) and work (w), effect the total enthalpy in an open system. Change in total enthalpy can be written as:

$$\Delta h_0 = q + w \quad (5.1)$$

Total enthalpy of a system is given as follows:

$$h_0 = h + \frac{V^2}{2} \quad (5.2)$$

For a case of no heat transfer, in a non rotating stator stage of a turbine, the enthalpy remains constant as per first law of thermodynamics. Therefore, we can write:

$$\Delta h' = h_2 - h_1 = \frac{V_1^2 - V_2^2}{2} \quad (5.3)$$

However, for a rotor stage in a turbine, Euler's law of turbomachinery combined with the first law of thermodynamics leads to:

$$\Delta h'' = h_3 - h_2 = \frac{W_3^2 - W_2^2}{2} - \frac{U_3^2 - U_2^2}{2} \quad (5.4)$$

For equations (5.3) & (5.4), the assumption that there is no heat transfer is valid as the temperatures in stations 3, 4 and 5 are close to ambient temperature of the

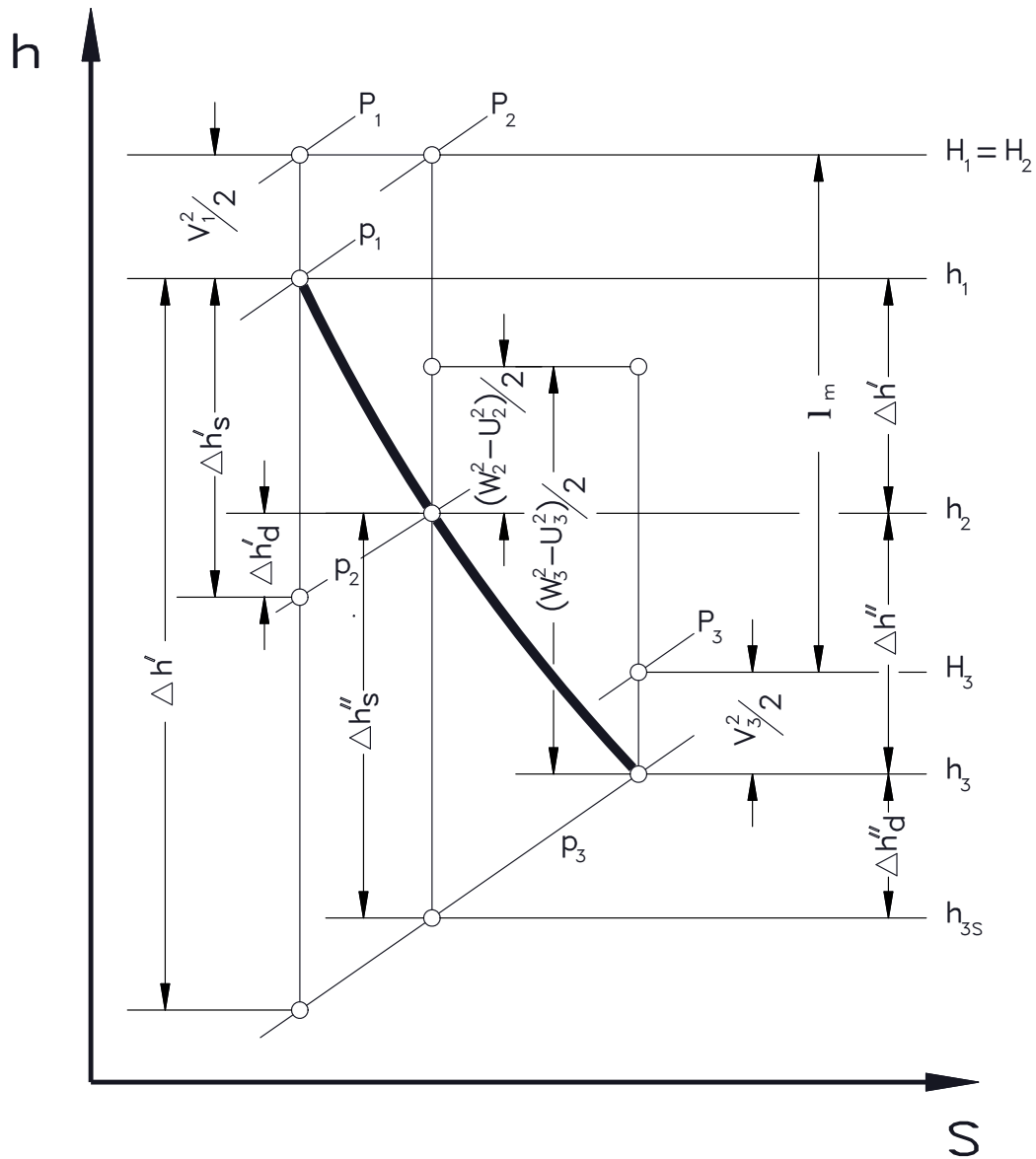


Fig. 32.: $h - s$ diagram for a turbine stage [2]

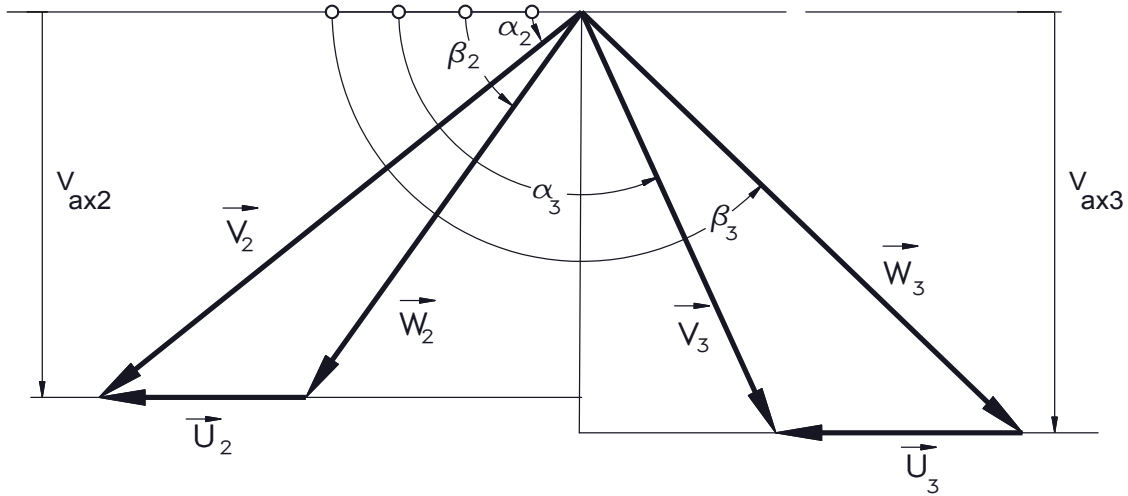


Fig. 33.: Velocity triangle of a typical turbine stage [2]

test cell and hence the heat transfer is negligible.

According to Fig. 32, stage specific mechanical energy, l_m can be written as:

$$H_1 - H_3 = (h_1 - h_2) - (h_3 - h_2) + \frac{V_1^2 - V_3^2}{2} \quad (5.5)$$

and combining equations (5.3) and (5.4) with (5.5), we can write:

$$l_m = \frac{1}{2} [(V_2^2 - V_3^2) + (W_3^2 - W_2^2) + (U_2^2 - U_3^2)] \quad (5.6)$$

Fig. 33 shows the velocity triangle for a typical turbine stage whereas Fig. 34 gives an idea of the velocity triangle of a stage for DooSan blade configuration. In Fig. 33, the subscripts 2 and 3 represent the exit velocity components of stator and rotor respectively. Subscripts i and e , represent inlet and exit for the stator row in Fig. 34.

Schobeiri [2] introduces few dimensionless parameters that completely determine the stage velocity diagram. One of them is degree of reaction, r and is defined as the

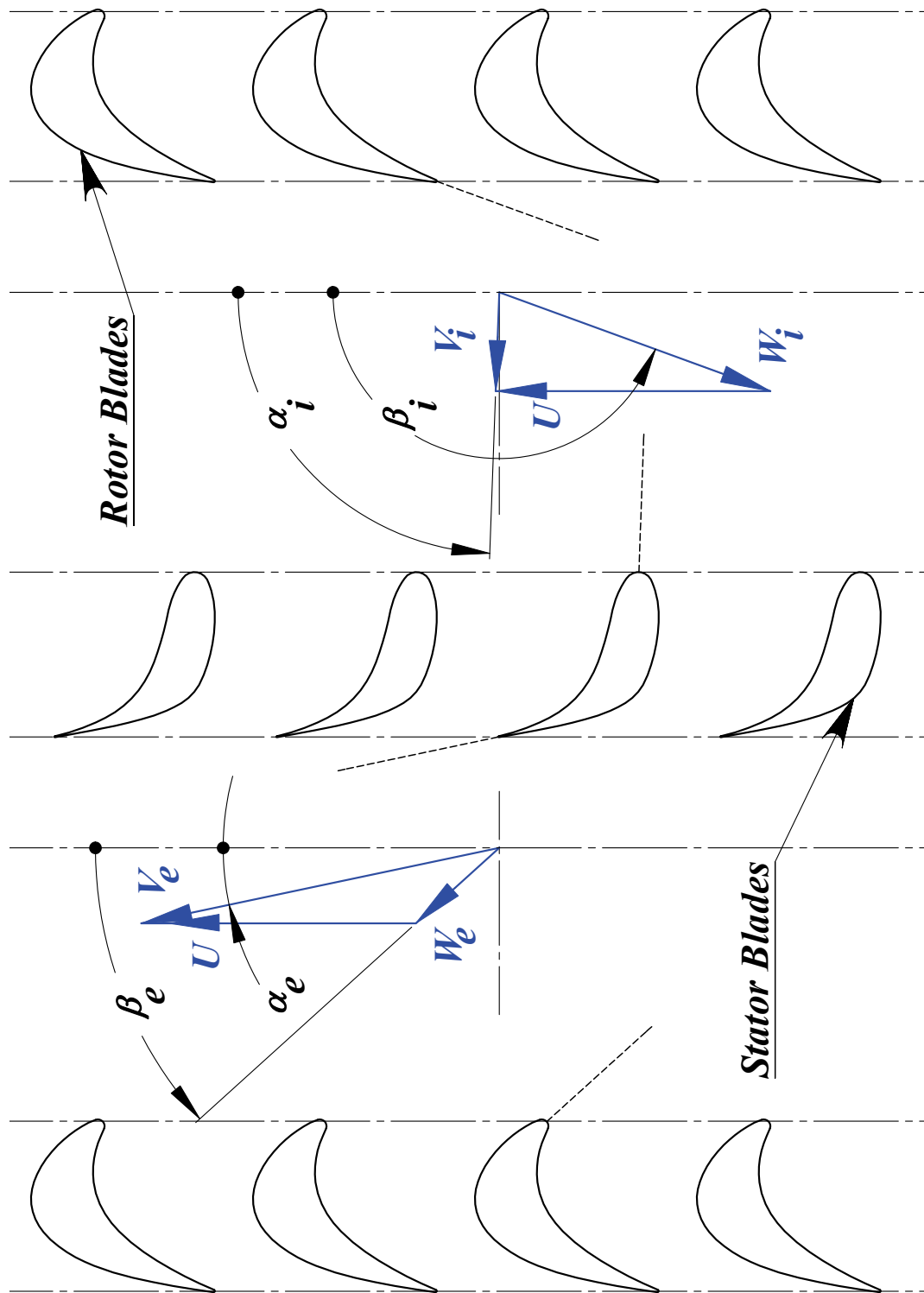


Fig. 34.: Velocity triangle for stator stage of DooSan blade configuration

ratio of static enthalpy difference in rotor row to that in the entire stage.

$$r = \frac{\Delta h''}{\Delta h'' + \Delta h'} \quad (5.7)$$

From equations (5.3) & (5.4) we get,

$$r = \frac{\Delta h''}{\Delta h'' + \Delta h'} = \frac{W_3^2 - W_2^2 + U_2^2 - U_3^2}{W_3^2 - W_2^2 + U_2^2 - U_3^2 + V_2^2 - U_1^2} \quad (5.8)$$

Another dimensionless parameter, stage load coefficient, λ is defined by Schobeiri as ratio of specific stage mechanical energy to exit circumferential kinetic energy from rotor. The stage load coefficient describes the work provided by a stage and can be directly related to the flow deflection in the stage. For the rotor, flow deflection can be given by the difference in inlet and flow exit angles i.e., $\alpha_3 - \alpha_2$.

$$\lambda = \frac{l_m}{U_3^2} \quad (5.9)$$

CHAPTER VI

PERFORMANCE TESTS

Performance tests carried out on TPFL turbine facility give an insight into the following characteristics of the blade configuration:

1. Power
2. Windage losses
3. Bearing losses
4. Total to total efficiency
5. Total to static efficiency

Performance tests are carried out in following ways:

Varying rotational speed with fixed mass flow: Here, mass flow through the turbine section can be fixed to a desired value by controlling the compressor frequency and rotational speed is varied using dynamometer.

Varying mass flow with fixed rotational speed: In this case, rotational speed of turbine is fixed using the dynamometer and mass flow through the turbine is varied by varying compressor output frequency.

Data analysis program for the performance tests was first written using FORTRAN by J. Gillaranz and E. Johansen under the supervision of Dr. Schobeiri and since has modified by T. Neuenschwander and lately by H. Chibli. This program analyzes data by reading specified columns from the raw data file generated from

Turbo.vi and hence care should be taken during instrumentation that similar connection map is followed for all channels, failure of which will lead to erroneous results. Care should also be taken to check for any failed channels or channels with erroneous values and such channels should be neglected from being used in the analysis by modifying *effeciency.f90* file before compilation. This program reads raw data file by neglecting first six columns including the column for “Time”. A MATLAB program was developed by the author of this report which helps to check for bad/erroneous channels and is attached as Appendix-D.

VI.1. Testing Procedure

1. Make sure that there are no leakage points in the turbine section. Masking tape can be used around traverse system to seal any leakage.
2. Refer Appendix-F and start-up the turbine to desired compressor frequency and engine speed.
3. Generate a test script file as shown in Fig. 35. Here the main traverse axis is considered to be at 12 o'clock and hence the script file has the position at 500, so as to not move the traverse. 500 sample points are collected after waiting for 2000 milliseconds.
4. To allow for flow stabilization, wait for about 10 minutes after varying engine

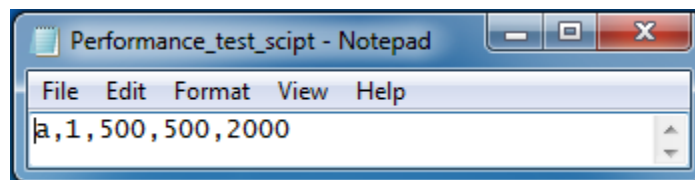


Fig. 35.: Test script code for performance test

speed or compressor frequency before collecting data. Usually, following routine is followed to conduct performance tests:

Varying rotational speed with fixed mass flow: Engine speed is varied from 1800-3000 rpm with increments of 100 rpm.

Varying mass flow with fixed rotational speed: Compressor frequency is varied from 40-65 Hz with increments of 2.5 Hz.

VI.2. Calculations

According to the Diploma thesis report [12], following steps are used by the analysis program *efficiency.f90* for calculation of efficiencies:

Mass flow rate through Venturi: Sutherland law is used to calculate the flow viscosity as follows:

$$\mu = \mu_0 \cdot \left(\frac{T_i}{T_0} \right)^{1.5} \cdot \frac{T_0 + S}{T + S} \quad (6.1)$$

where,

$$\text{Reference viscosity: } \mu_0 = 1.716E - 05 \text{ N} \cdot \text{s}/\text{m}^2$$

$$\text{Reference temperature: } T_0 = 273.0 \text{ K}$$

$$\text{Sutherland constant (Effective temperature): } S = 111.0 \text{ K}$$

Calibration sheet for the venturi flow meter provides a compressibility factor, $Z = 0.99959$ to calculate the density:

$$\rho = \frac{p}{T \cdot R \cdot Z} \quad (6.2)$$

Following equation is used to calculate the adiabatic expansion factor:

$$\gamma = \tau^{2/\kappa} \cdot \left(\frac{\kappa}{\kappa - 1} \right) \cdot \left(\frac{1 - \tau^{\frac{\kappa-1}{\kappa}}}{1 - \tau} \right) \cdot \left(\frac{1 - \beta^4}{1 - \beta^4 \cdot \tau^{2/\kappa}} \right) \quad (6.3)$$

where,

τ = pressure ratio between throat and inlet pressure

$\beta = D_t/D_i$ = ratio between throat and inlet diameter

κ = isentropic exponent

Pressure difference between venturi inlet and throat in inches of water, Δp_w along with an initial guess of discharge coefficient, C_d can be used to calculate the mass flow rate by:

$$\dot{m} = 0.09970190 \cdot C_d \cdot \gamma \cdot D_t^2 \cdot \sqrt{\frac{\rho \cdot \Delta p_w}{1 - \beta^4}} \quad (6.4)$$

The throat Reynold's number can be calculated as:

$$Re_t = \frac{4 \cdot \dot{m}}{\pi \cdot D_t \cdot \mu} \quad (6.5)$$

The calculated Reynold's number is then checked to be within the calibrated range ($532,770 < Re_t < 1,572,700$). A new discharge coefficient is then calculated from the calibration curve of venturi meter given by following equation:

$$C_d = a + b \cdot (Re_t)^{0.5} \quad (6.6)$$

With coefficients $a = 1.00258$ and $b = -4.18287$ determined by calibration, discharge coefficient obtained from equation (6.6) is then compared the initially assumed value and if it is within 0.05% of assumed value, the calculations are complete. If the values differ by more than 0.05%, the assumed discharge coefficient is replaced with the last calculated discharge coefficient to calculate new mass flow, Reynold's number and discharge coefficient. This procedure is repeated until the assumed and calculated discharge coefficient values are within 0.05%.

Total to static efficiency based on torque meter: Values of torque, M_T and engine speed, N acquired using torque meter are used in the following equation to calculate power output:

$$L_T = M_T \cdot \frac{2\pi N}{60} \quad (6.7)$$

Since, this power output is equal to the specific enthalpy difference, we get:

$$\Delta h_T = \frac{L_T}{\dot{m}} \quad (6.8)$$

However, when all the calculated windage and bearing losses are considered, we have:

$$\Delta h = \frac{L_T + L_{windage} + L_{bearing}}{\dot{m}} \quad (6.9)$$

The isentropic total to static enthalpy difference is calculated by:

$$\Delta h_s = c_p \cdot T_{01} \cdot \left(1 - \left(\frac{p_7}{p_{01}} \right)^{\frac{\kappa-1}{\kappa}} \right) \quad (6.10)$$

where,

c_p = specific heat capacity of air

T_{01} = total temperature at turbine inlet (station-1)

p_7 = static pressure at turbine exit (station-7)

p_{01} = total pressure at turbine inlet (station-1)

And hence, isentropic total to static efficiency of the turbine is given by the following equation:

$$\eta_{ts} = \frac{\Delta h}{\Delta h_s} \quad (6.11)$$

The dimensionless parameter, u/c_0 is given by following:

$$u = \omega \cdot r_{mean} \quad (6.12)$$

$$c_0 = \sqrt{\Delta H_i} \quad (6.13)$$

where,

r_{mean} = average machine radius

ΔH_i = change in total enthalpy from machine inlet to exit

VI.3. Results

A series of cases were run for both, varying engine speeds and massflow rates, the results are presented in the following plots. The total to static efficiency obtained from calculations is plotted as a function of machine mass flow rate in Fig. 36 and u/c_0 in Fig. 37.

First, the turbine was operated at a fixed pressure ratio of 1.45 with varying rotational speeds from 1750 to 3000 RPM and then the rotational speed was fixed at 3000 RPM and the pressure ratio was varied from 1.45 to 1.16 to get a complete curve in Fig. 37. As explained earlier, mechanical power from torque-meter adjusted with bearing and windage losses of the turbine is used for efficiency calculations. At u/c_0 of 0.75, maximum efficiency (85.2%) is observed. As we move away from the design point, it can be seen that for a lower u/c_0 , the drop in efficiency is considerable (17.6%) because of the distortion of velocity triangles, however for a value of u/c_0 higher than design point, drop of only 3.7% is seen in total to static efficiency.

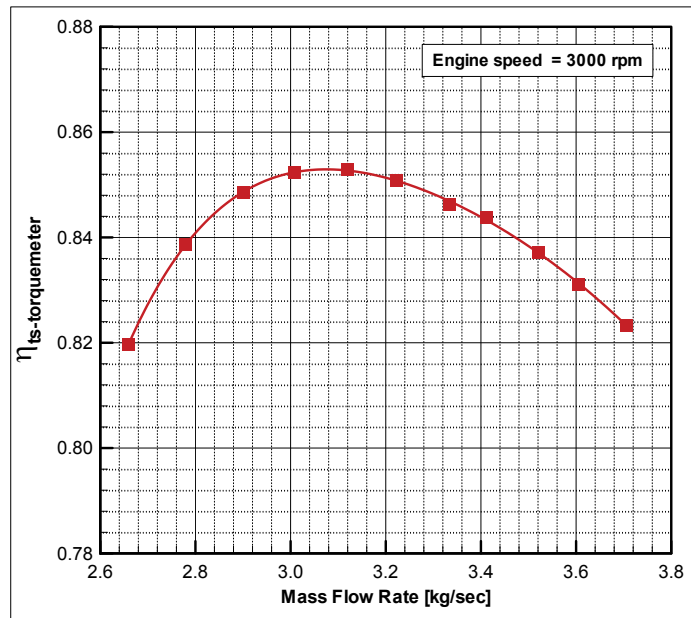


Fig. 36.: Isentropic total-static efficiency of DooSan two-stage turbine as a function of mass flow

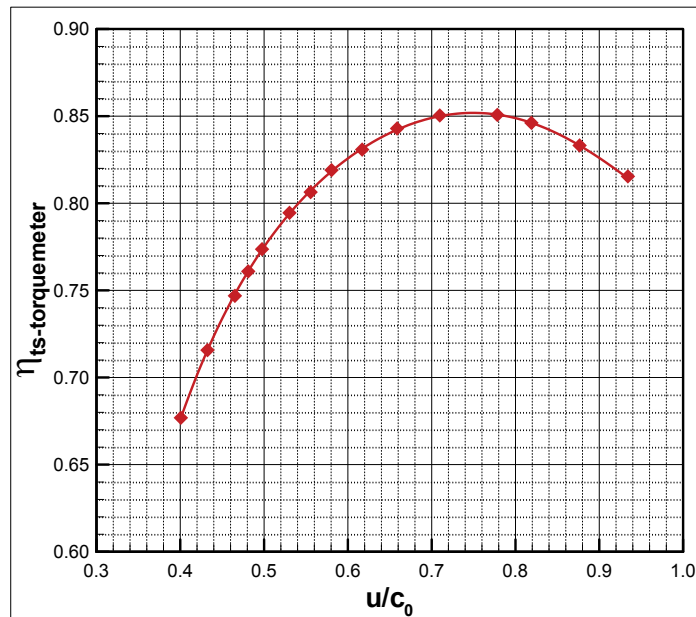


Fig. 37.: Isentropic total-static efficiency of DooSan two-stage turbine as a function of u/c_0

CHAPTER VII

INTERSTAGE TESTS

VII.1. Testing Procedure

1. Refer Appendix-C to generate a test script file for desired test grid.
2. Refer Appendix-F and start-up the turbine to desired compressor frequency and engine speed.
3. Switch “ON” the switch for traverse controllers in test-cell and run the data acquisition program, *Turbo.vi* from data acquisition computer to get a main window as shown in Fig. 38.
4. Click *Edit→I/O config* to get a window as Fig. 39.
5. Any or all of the traversing controllers or pressure modules can be switched “ON” or “OFF” by clicking their respective switches, which are long, red colored vertical bars next to them. A glowing bar indicates “ON” mode. Make sure, all the traversing controllers and pressure modules are “ON”.
6. Check the physical location of traverse motors in test-cell and enter their respective locations as their “Initial Pos(mm)”. For circumferential traverse motor (A-1), 12 o’clock position is referred as 500 *mm*, whereas, for all radial traverse motors (A-2, B-1 and B-2), hub-position is referred as 100 *mm*. Do not modify any other values for traverse controllers on this screen.
7. Now, click *ConfigTraverse* at the bottom to initialize all traverse motors.
8. All eight pressure modules can be initialized together by clicking *ConfigPress*.

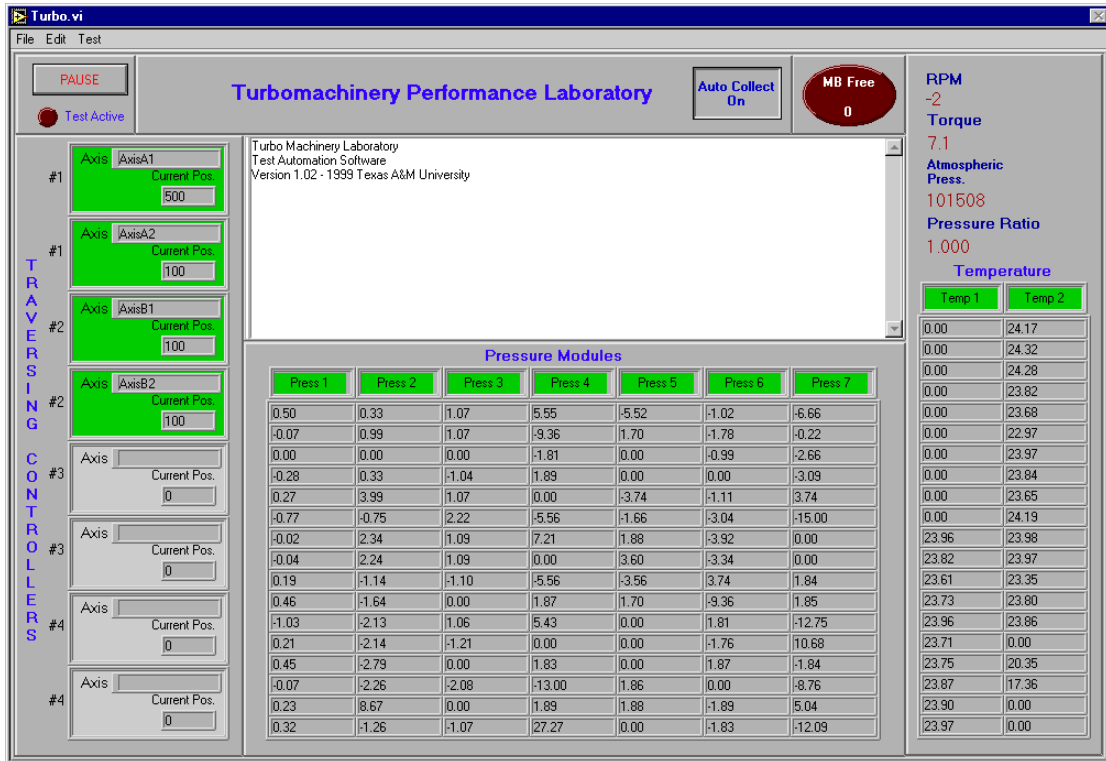
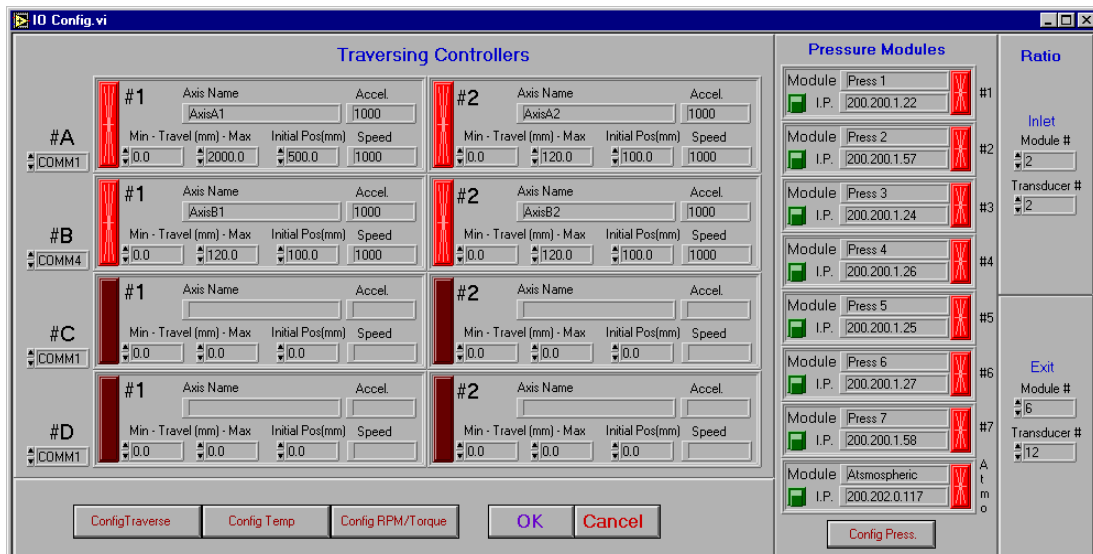
Fig. 38.: Main screen of data acquisition program, *Turbo.vi*

Fig. 39.: I/O configuration window for data acquisition program



Fig. 40.: Temperature configuration window for data acquisition program

9. To configure both temperature modules, click *Config Temp* to the a window as shown in Fig. 40.
10. Click the drop-down menu under Module No: and choose “2” before clicking *Initialize*.
11. At this point, we need to configure the test run. Click *Edit*→*Test Config* to get a window shown in Fig. 41.
12. Enter any information as header as desired, however, the header should NOT exceed one line.
13. Select the archive path by browsing to any desired directory.
14. Type a desired test filename for raw data file which will be generated at the end of test-run.

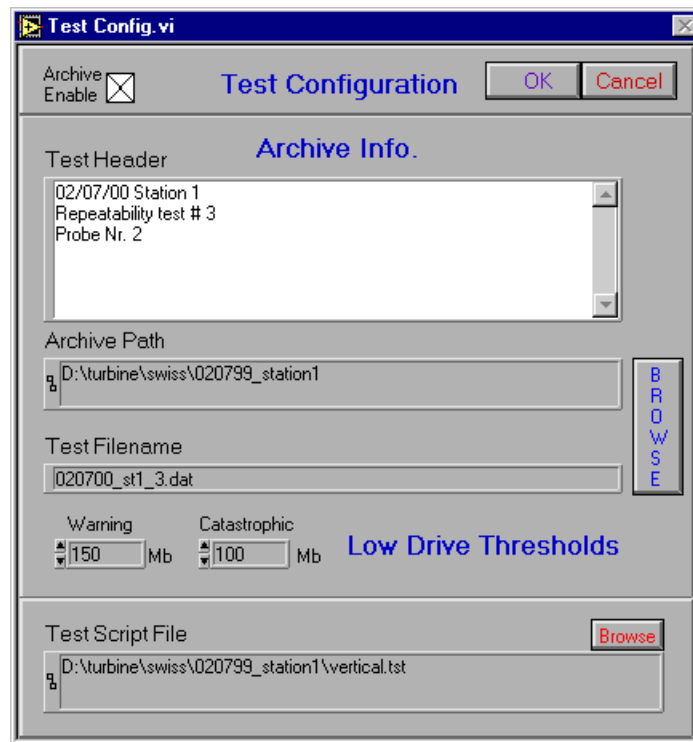


Fig. 41.: Test configuration window for data acquisition program

15. Browse to the test script file which was generated earlier for this test-run.
16. This completes all the necessary steps for starting the test-run. However, to check whether all the channels are infact working, click *Auto Collect On* button on main window of data acquisition. Changing values of pressure and temperatures indicate that all pressure and temperature modules have been initialized correctly.
17. Click *Test→Start* to start the test run. Make sure the door for test-cell is not opened for the entire duration of test-run.

VII.2. Calculations

The data analysis program for interstage measurements developed by H. Chibli, uses following definitions for interstage loss and efficiency calculations:

Loss coefficients:

Stator loss coefficient (between stations 3 and 4):

$$\zeta_S = \frac{P_{t3} - P_{t4}}{P_{t3} - P_{s4}} \quad (7.1)$$

Rotor loss coefficient (between stations 4 and 5):

$$\zeta_R = \frac{P_{tr4} - P_{tr5}}{P_{tr4} - P_{s5}} \quad (7.2)$$

Efficiency definitions:

Stator efficiency:

$$\eta_S = \frac{\frac{1}{2}V_4^2}{\Delta h_s + \frac{1}{2}V_3^2} \quad (7.3)$$

where,

$$\begin{aligned}\Delta h_s &= h_3 - h_{4s} \\ h_{4s} &= h_3 \cdot \left(\frac{P_4}{P_3}\right)^{\frac{\kappa-1}{\kappa}}\end{aligned}$$

Rotor efficiency:

$$\eta_R = \frac{\frac{1}{2}(W_5^2 - U_5^2)}{\Delta h_s + \frac{1}{2}(W_4^2 - U_4^2)} \quad (7.4)$$

where,

$$\begin{aligned}\Delta h_s &= h_4 - h_{5s} \\ h_{5s} &= h_4 \cdot \left(\frac{P_5}{P_4}\right)^{\frac{\kappa-1}{\kappa}}\end{aligned}$$

Stage efficiency:

$$\eta_{stage} = \frac{\frac{1}{2}(W_5^2 - U_5^2 + V_4^2)}{\Delta h_s + \frac{1}{2}(V_3^2 + W_4^2 - U_4^2)} \quad (7.5)$$

Machine isentropic total to static efficiency:

$$\eta_{ts} = \frac{1 - \frac{T_{tout}}{T_{tin}}}{1 - \left(\frac{P_{tout}}{P_{tin}}\right)^{\frac{\kappa-1}{\kappa}}} \quad (7.6)$$

VII.3. Results

Attached below are the result plots for interstage measurements carried out with engine speed of 3000 rpm at 65 Hz compressor frequency and heater temperature of 55°C . From the calculations, it was found that in this condition the mass flow rate through the turbine section was 3.7233 kg/s.

VII.3.1. Line plots

All the line plots are pitch averaged and plotted with immersion ratio, r^* as the abscissa. Immersion ratio is a normalized spanwise location in the turbine and is given by:

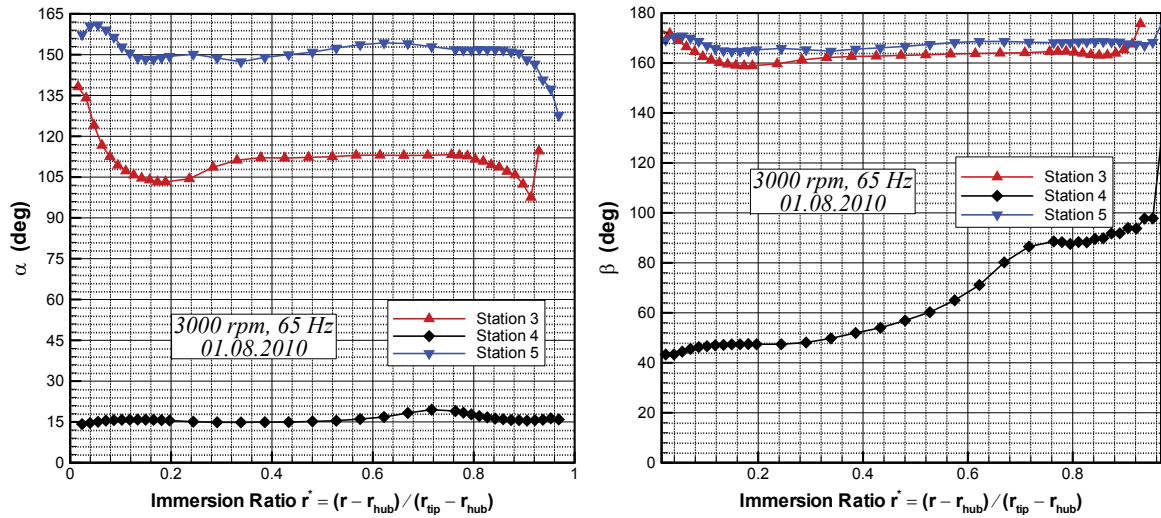
$$r^* = \frac{r - r_{hub}}{r_{tip} - r_{hub}}$$

Table VI.: Metal angles for stator and rotor blades of DooSan turbine

r^*	Rotor		Stator	
	Inlet Angle (°)	Exit Angle (°)	Inlet Angle (°)	Exit Angle (°)
0	33.04	161.43	82.55	10.64
0.125	33.87	162.78	81.75	10.37
0.25	35.67	163.75	83.83	11.68
0.375	39.54	164.48	84.88	10.82
0.5	42.89	165.09	84.77	11.08
0.625	47.68	165.70	83.68	11.04
0.75	53.74	166.37	84.00	12.08
0.875	60.37	166.97	84.67	11.97
1	67.91	167.62	84.92	12.82

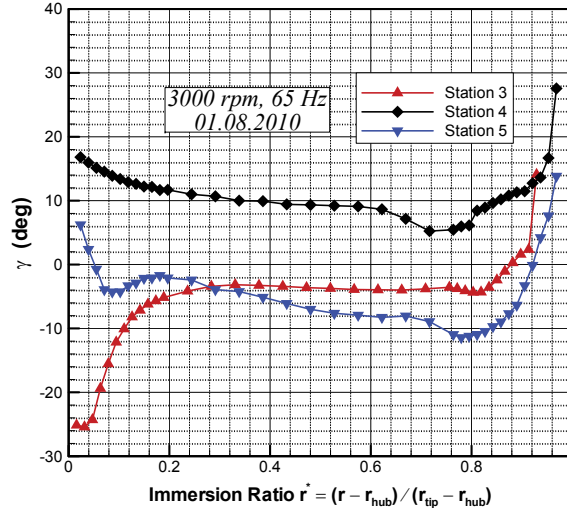
Fig. 42 gives the absolute and relative flow angles measured at each of the stations and Table VI populates metal angles at various spanwise locations, measured from SolidWorks© assembly of DooSan turbine. Relative flow angles from Fig. 42b are

comparable to the metal angles of rotor, however, at hub and tip regions endwall vortices lead to the deviation of flow angles from metal angles. Relative flow angle at stator exit (station-4) should be equal to inlet metal angle of the rotor blade.



(a) Absolute velocity flow angle

(b) Relative velocity flow angle



(c) Meridional flow angle

Fig. 42.: Absolute, relative and meridional flow angles

Comparing the rotor inlet metal angles from Table VI and station-4 relative flow angle from Fig. 42b, a difference of 15° to 30° is noted from hub to tip respectively.

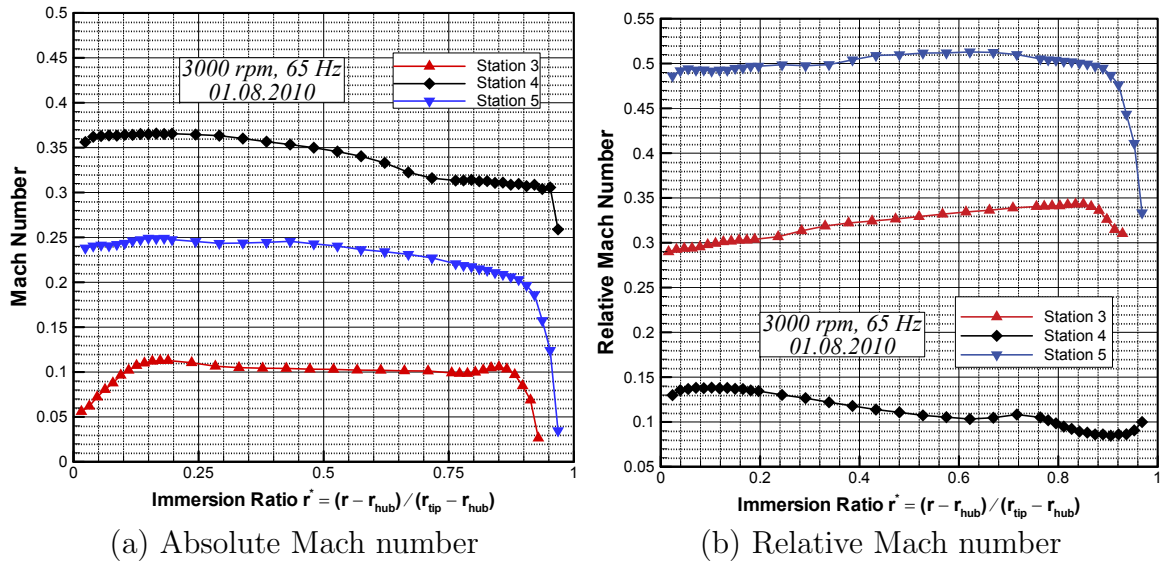


Fig. 43.: Absolute and relative Mach numbers

this difference can be attributed to the fact that the interstage measurements are not at the design point condition and hence the rotor blades experience a positive incidence.

Fig. 43 gives the absolute and relative Mach numbers. It can be seen clearly that the measured absolute Mach number for stator is higher than that of rotors. Static pressure observed for three stations is shown in Fig. 44. Absolute and relative total pressures from each station in Fig. 45 are used to calculate total pressure loss coefficients for stator and rotor. Mass flow rate through a row (stator or rotor) can be calculated from axial flow velocities shown in Fig. 46a. Even, flow streamlines can be estimated from axial flow velocities and from the total pressure difference for a streamline at inlet and exit plane of the row, one can calculate total pressure loss coefficient for respective streamline in a row. Various radial streamlines are used to calculate individual total pressure loss coefficient and then averaged to get total pressure loss coefficient of a specific row (stator or rotor).

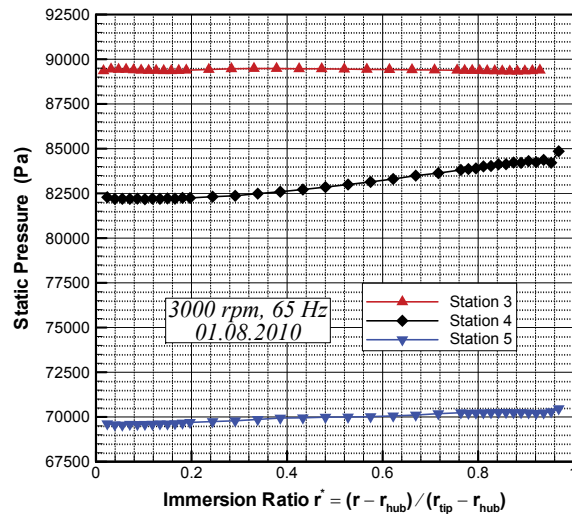


Fig. 44.: Static pressure *vs.* immersion ratio

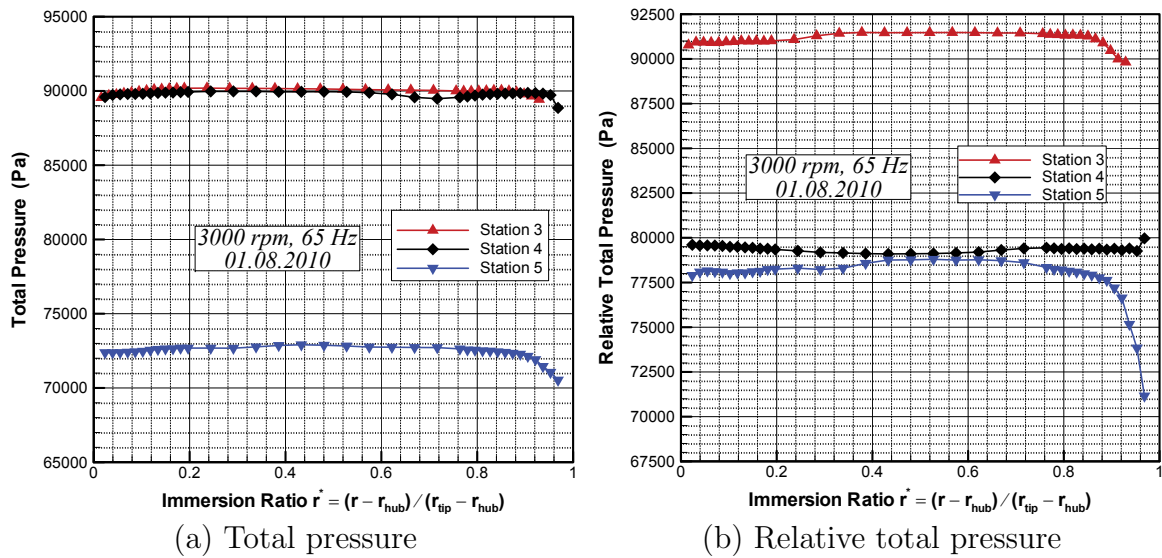


Fig. 45.: Absolute and relative total pressures

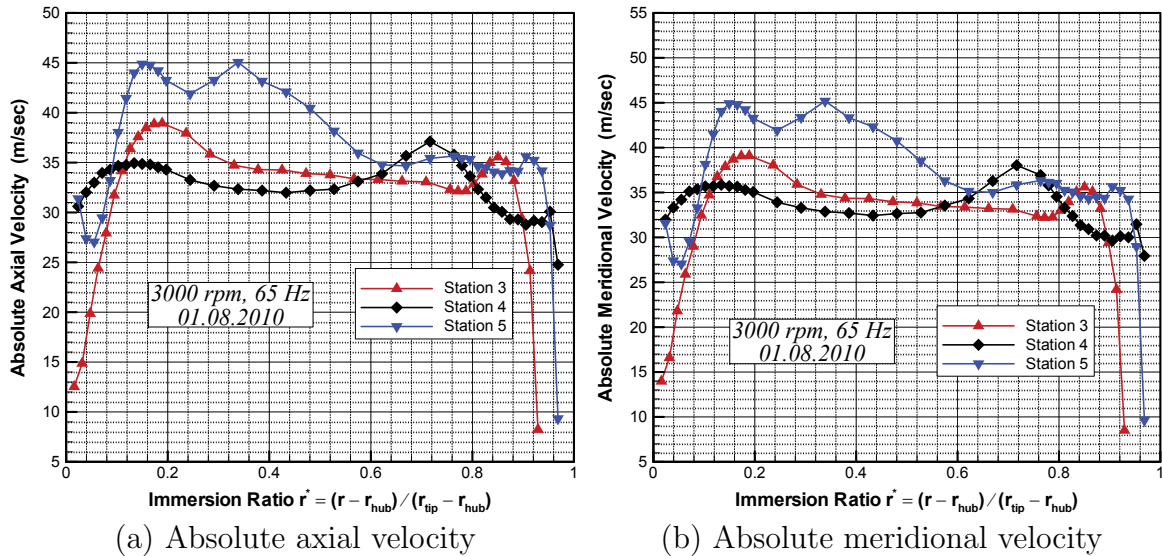


Fig. 46.: Absolute axial and meridional velocities

Table VII.: Summary of row and stage performance parameters

Parameter	Stator	Rotor	Stage
Total pressure loss coefficient (ζ)	0.04932	0.16947	—
Efficiency (η)	0.9606	0.8488	0.8913
Isentropic efficiency (η_{isen})	—	—	0.8415

Fig. 47a gives the total pressure loss coefficient for stator and rotor rows. Row and stage efficiencies are plotted in Fig. 47b and Fig. 48 gives the isentropic stage efficiency for the DooSan turbine. Table VII gives a quick summary of the row performance parameters.

Absolute and relative flow velocities is given in Fig. 49 and Fig. 50 shows the static temperature measured along with the static enthalpy calculated for three stations. Values for absolute and relative total enthalpy is shown in Fig. 51

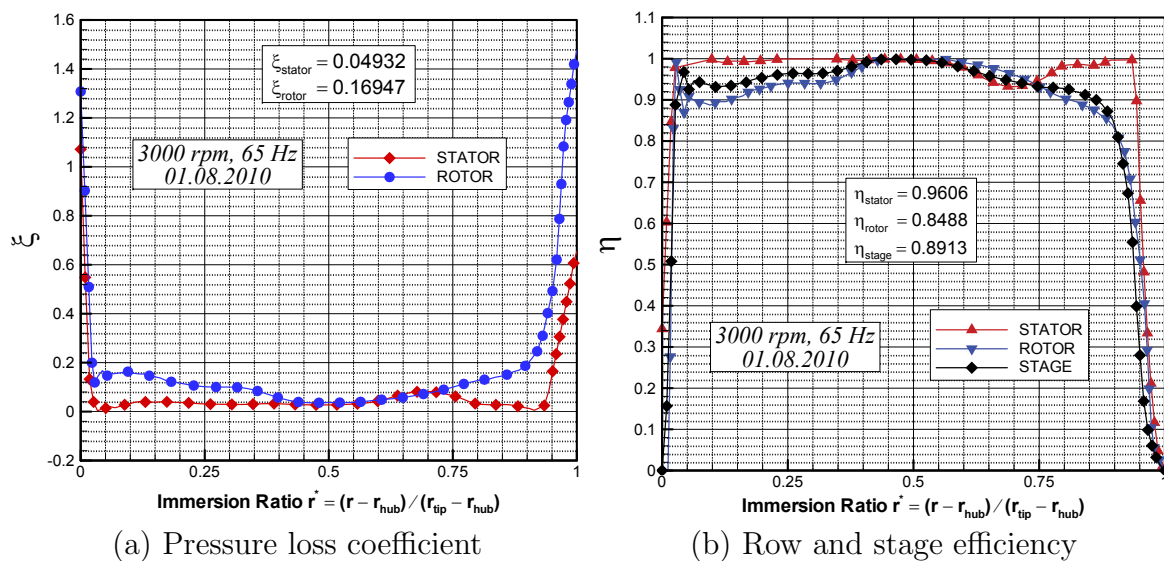


Fig. 47.: Stage loss coefficients and efficiencies

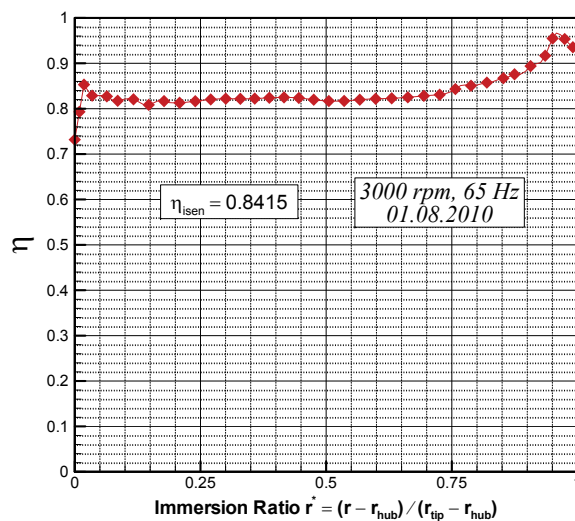


Fig. 48.: Isentropic stage efficiency vs. immersion ratio

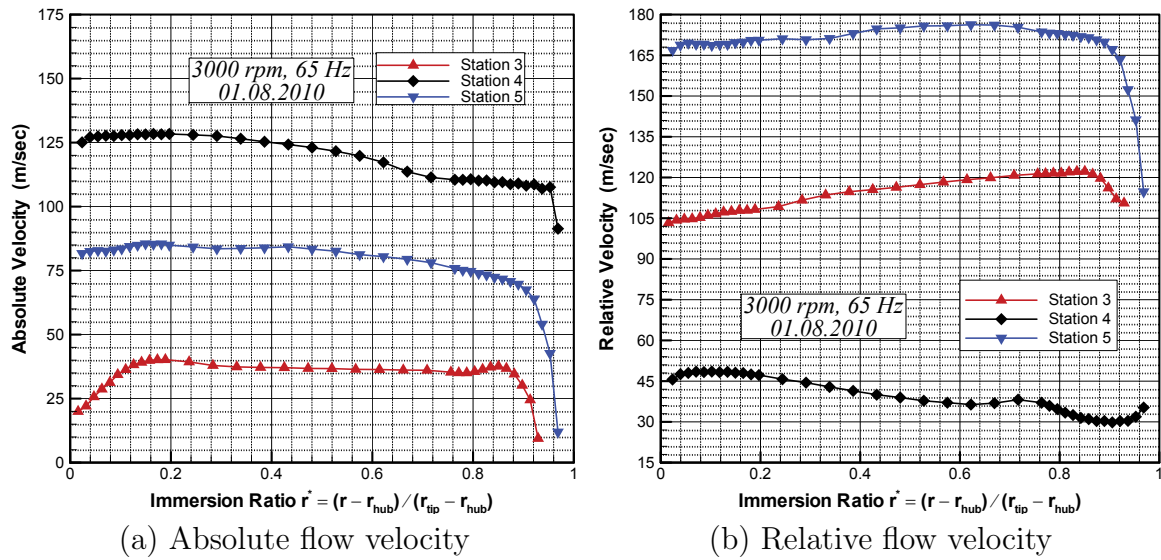


Fig. 49.: Absolute and relative flow velocities

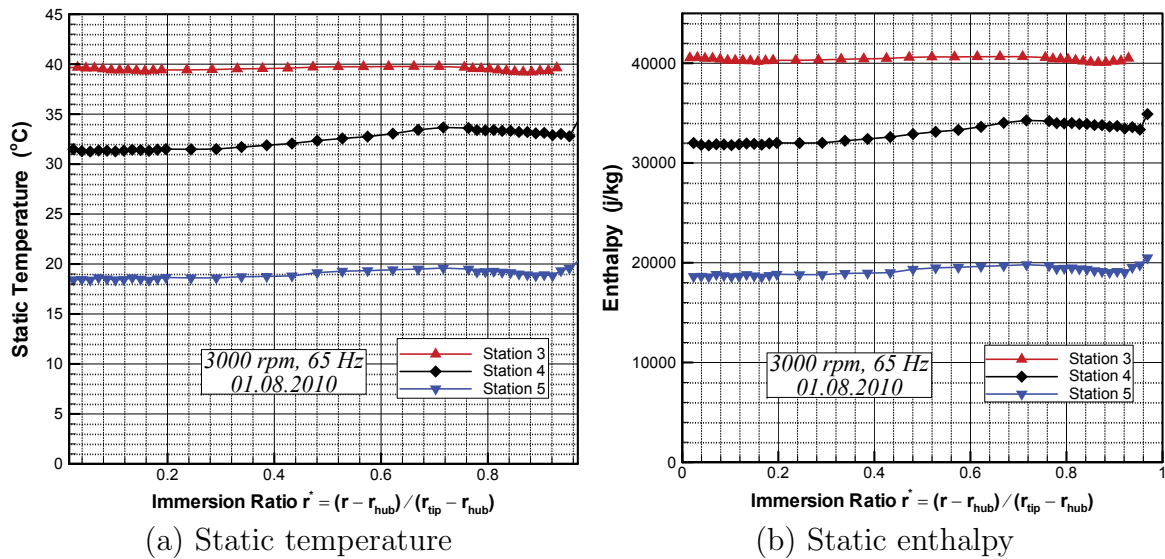


Fig. 50.: Static temperature and enthalpy

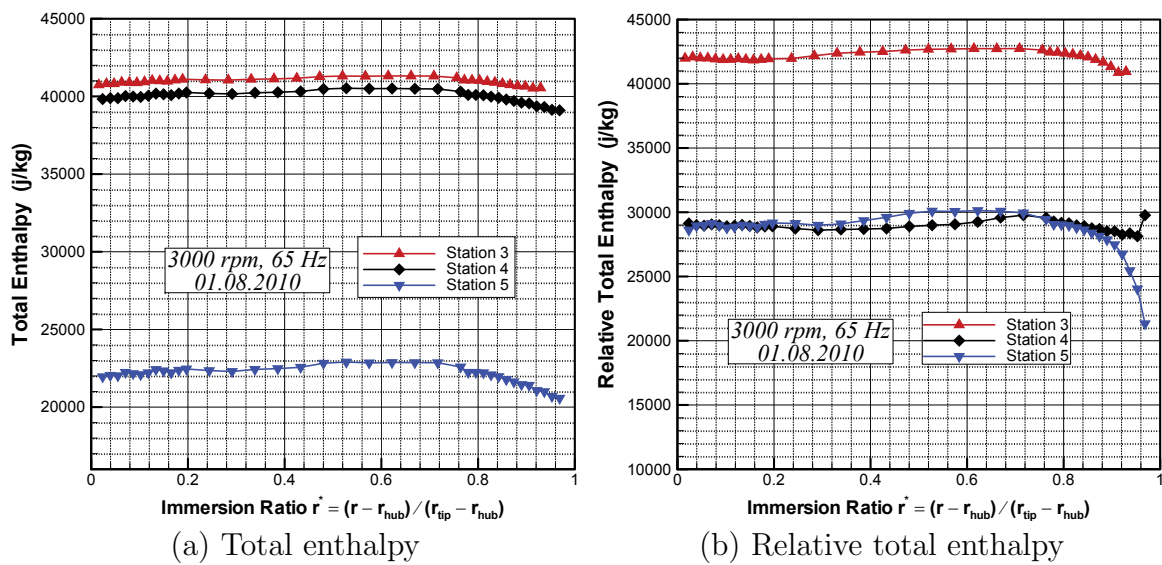


Fig. 51.: Absolute and relative total enthalpy

VII.3.2. Contour plots

It can be observed from Fig. 52a that for rotor exit (station-3), the absolute flow angle varies by about 60° in spanwise direction however, for stator exit (station-4) as seen in Fig. 52b the variation is only about 7° . This can be attributed to the turbulent flow at rotating endwalls. Fig. 53 shows the Mach numbers across the interstage test window for station 3 and 4. Five-hole probes used at the rotor exit plane were calibrated at 0.1 M and the speed range experienced by these probes is comparable to the calibrated speed range, however, probe at stator exit experienced Mach numbers close to 0.37 M which is higher than the range for which this probe was calibrated.

In Fig. 54a, one can clearly see a circumferential asymmetry to the range of 650 Pa in contour plot for static pressure. Though, this asymmetry could not be accounted for, it is believed to be because of some leakage flow from slots provided in the turbine casing for clocking of stators. This asymmetry is also seen in total pressure contour plots, however, it is more prominent in the static pressure contour plots.

Fig. 54c shows the relative total pressure at the exit of rotor. Regions with higher pressure values indicate free stream passage whereas lower pressure values on the plot represents wakes from the blade. Hence, a keen look indicates, distinct wakes from 3 rotor blades and approximately, 2.5 of free stream passage. At the tip of all three blade wakes, a distinct drop of pressure attest the presence of tip vortex at the shrouded endwall. Three well-defined regions with lower pressure values near the hub region enunciate the presence of secondary flow vortex.

Total pressure observed at the exit plane of stator is produced in Fig. 54d. Here, two distinct blade profiles can be seen as indicated by the low pressure regions. The blade wake is curved in the direction of rotor rotation as this is the absolute total

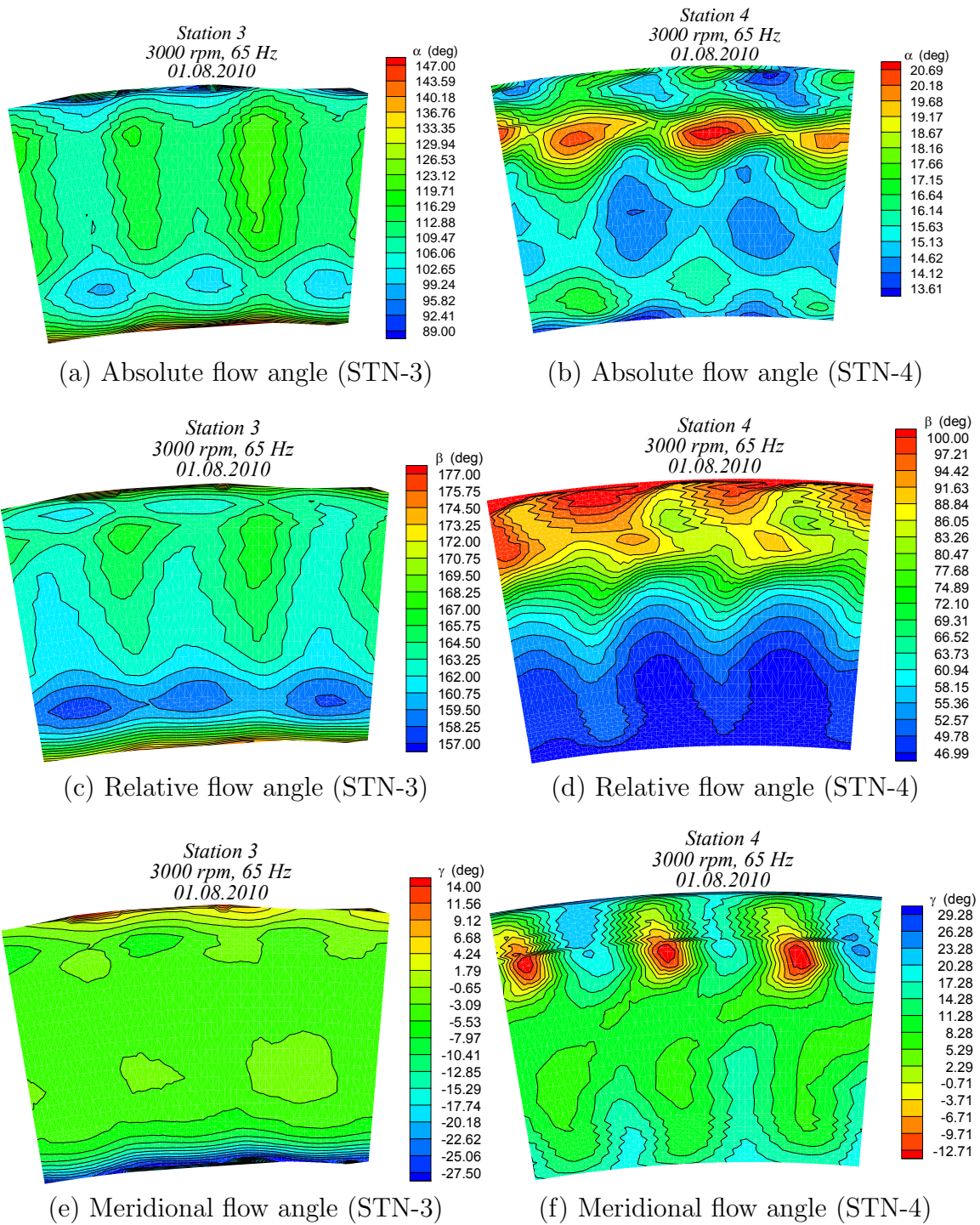
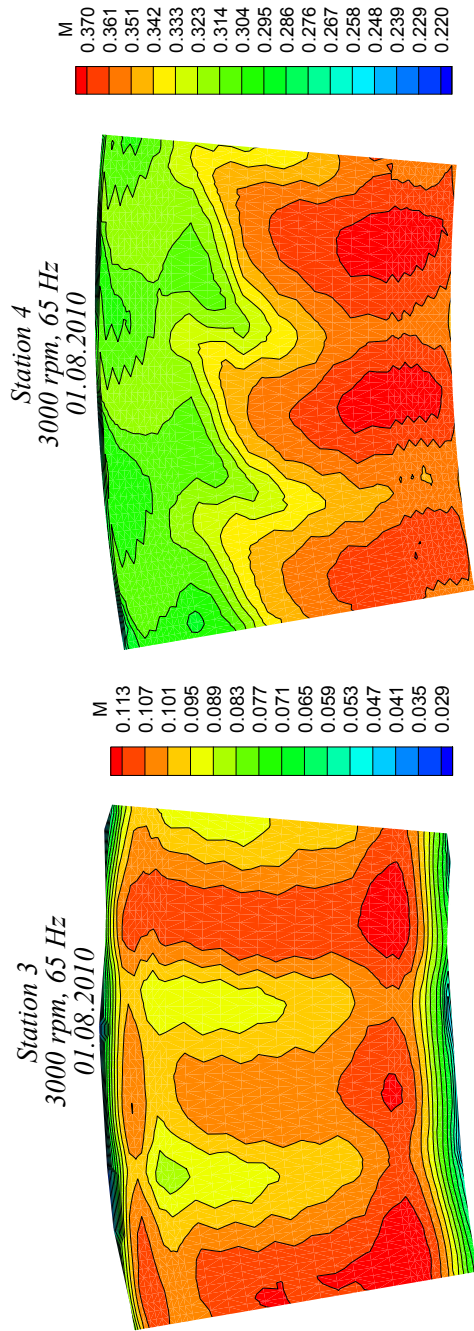
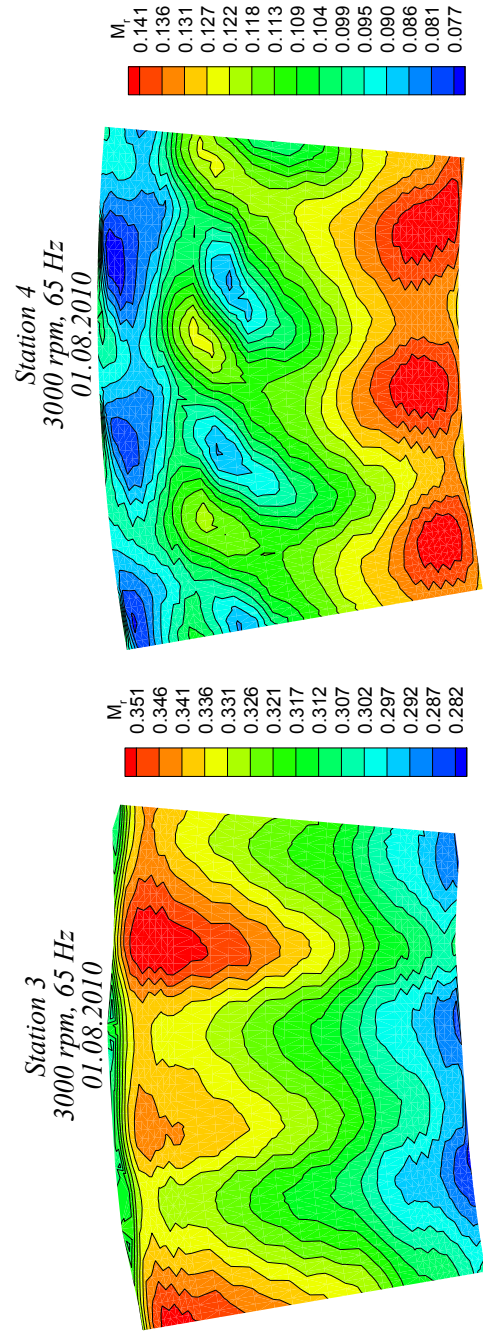


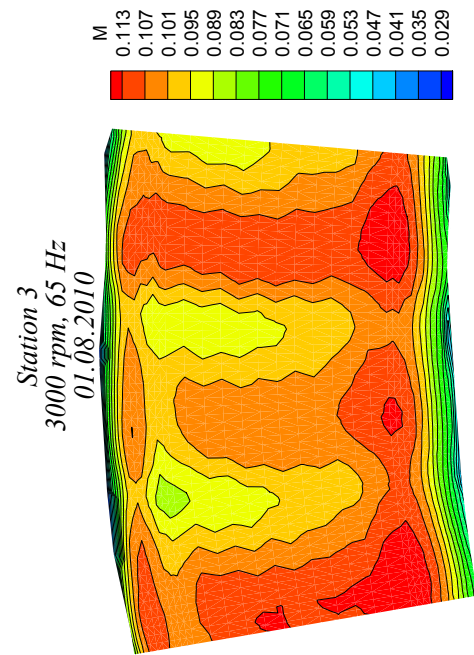
Fig. 52.: Contour plots for absolute, relative and meridional flow angle



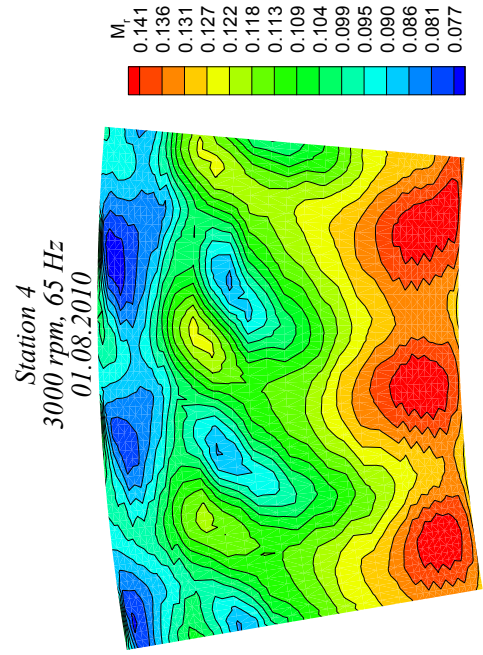
(a) Absolute Mach number (STN-3)



(b) Absolute Mach number (STN-4)

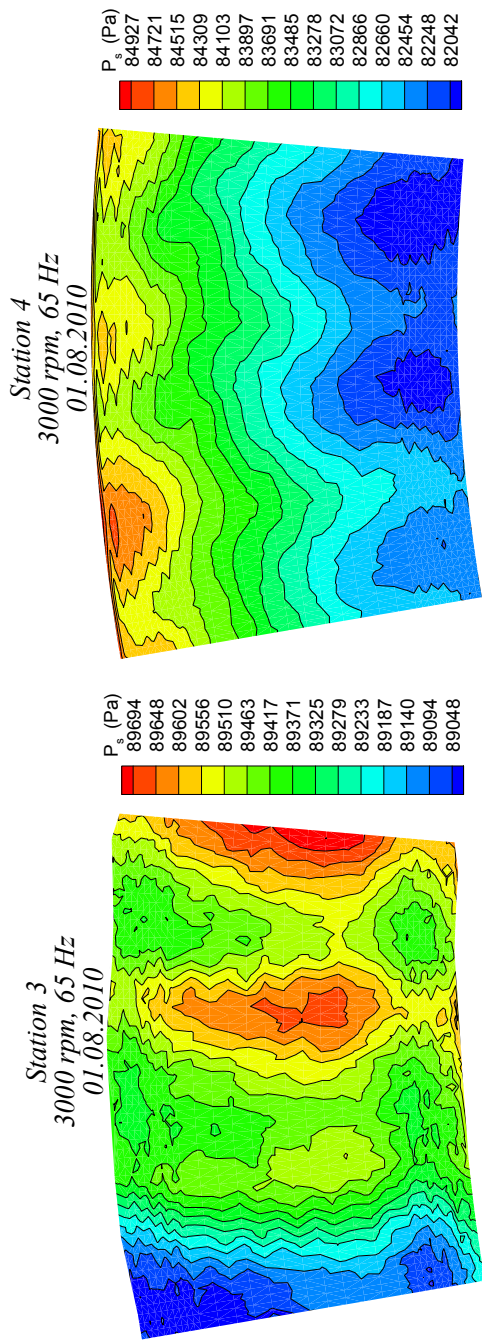


(c) Relative Mach number (STN-3)



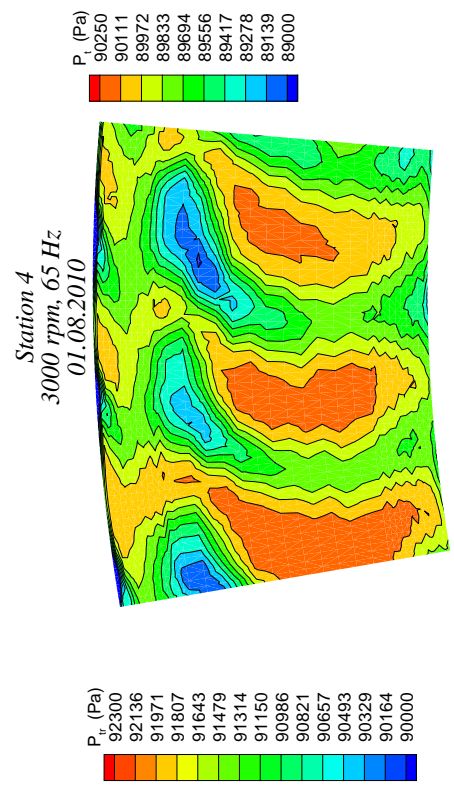
(d) Relative Mach number (STN-4)

Fig. 53.: Contour plots for absolute and relative Mach number

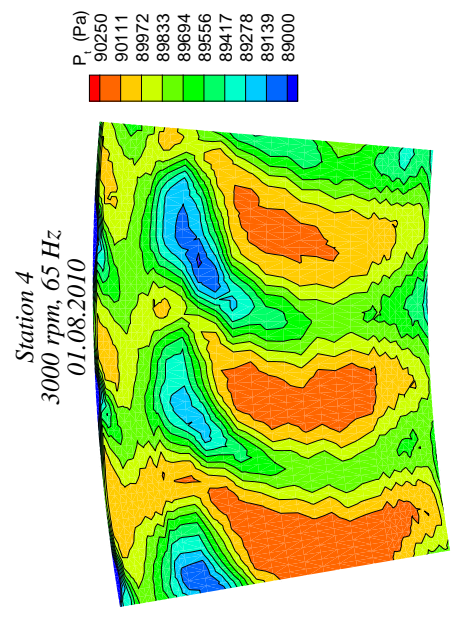


(a) Static pressure (STN-3)

(b) Static pressure (STN-4)



(c) Relative total pressure (STN-3)

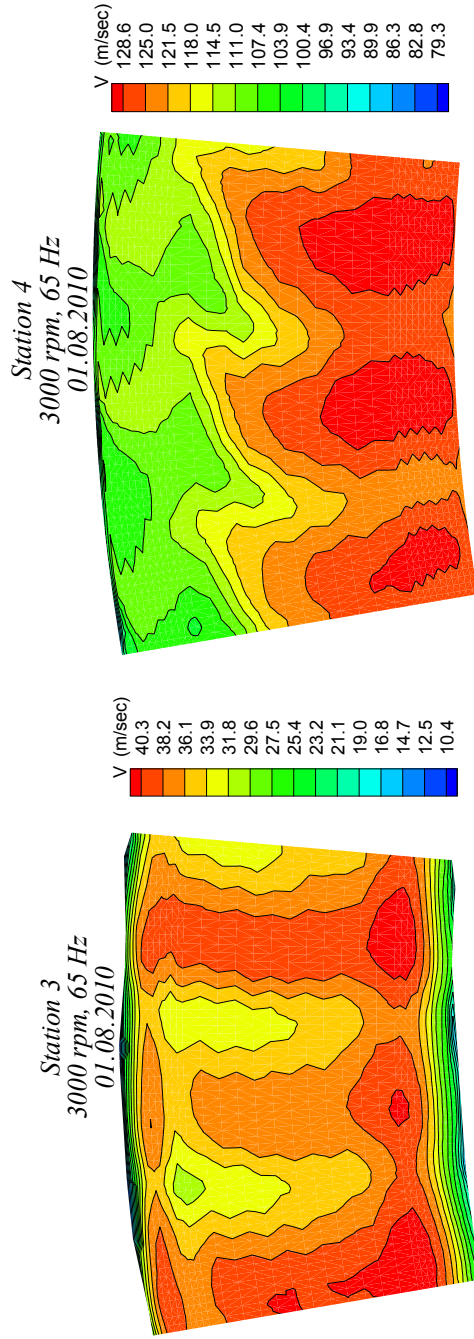


(d) Total pressure at (STN-4)

Fig. 54.: Contour plots for static and relative total pressure

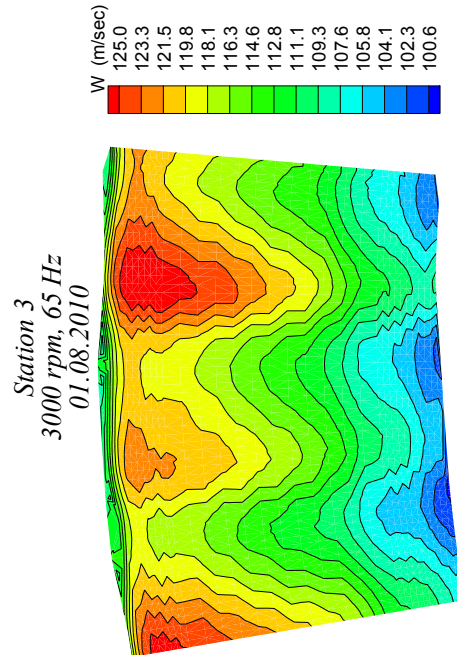
pressure unlike Fig. 54c which shows relative total pressure.

Fig. 55 gives a picture of absolute and relative flow velocities whereas Fig. 56 shows the axial and meridional components of flow velocity for stator (STN-4) and rotor (STN-3) exits.

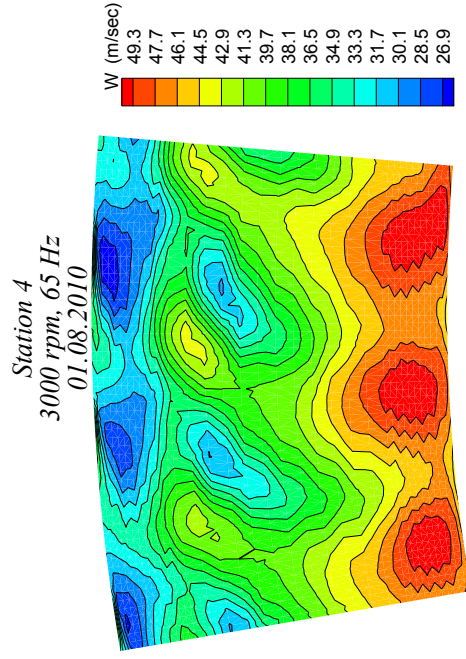


(a) Absolute flow velocity (STN-3)

(b) Absolute flow velocity (STN-4)

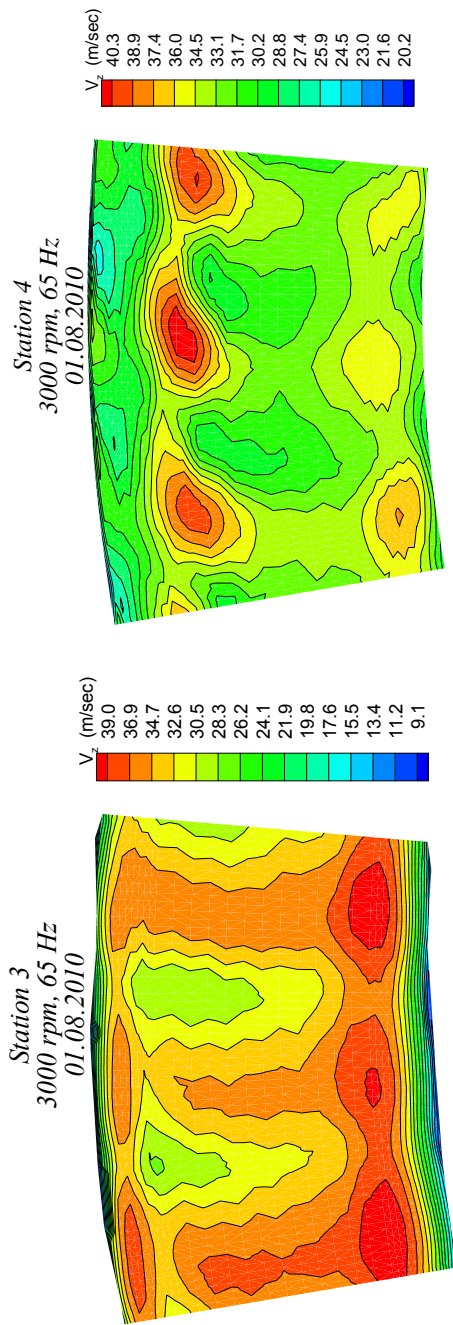


(c) Relative flow velocity (STN-3)

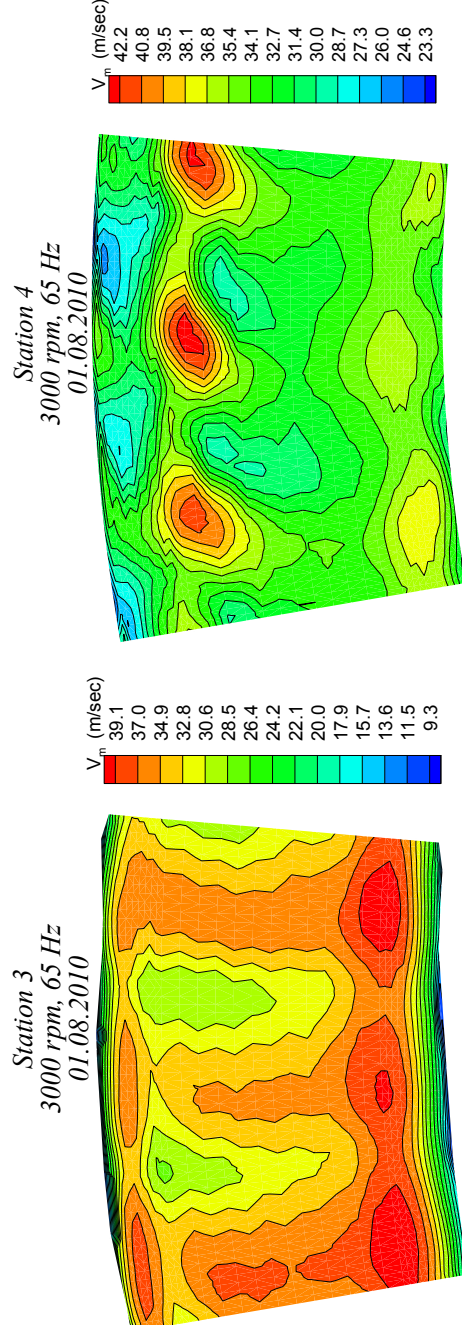


(d) Relative flow velocity (STN-4)

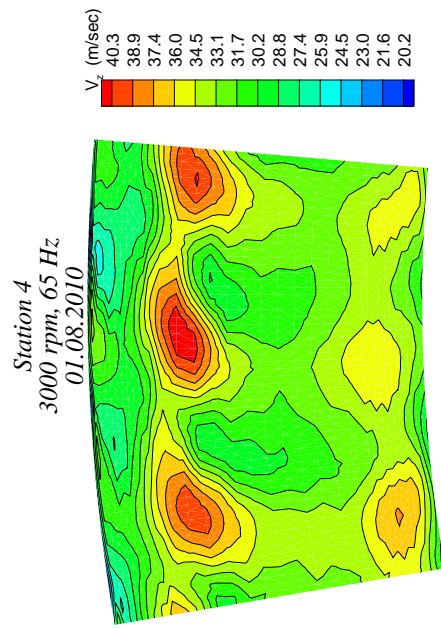
Fig. 55.: Contour plots for absolute and relative flow velocity



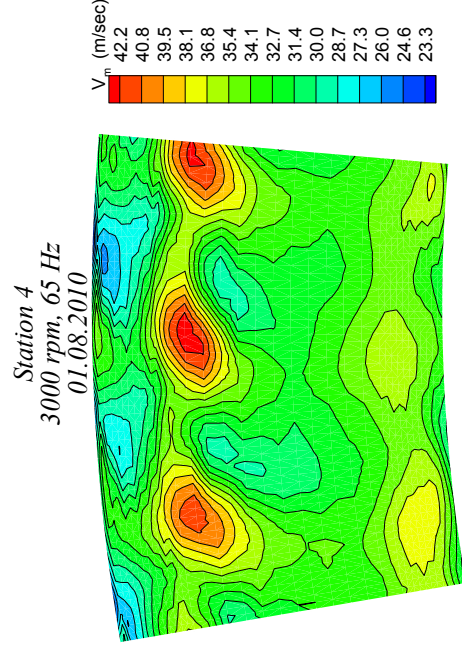
(a) Axial flow velocity (STN-3)



(c) Meridional flow velocity (STN-3)



(b) Axial flow velocity (STN-4)



(d) Meridional flow velocity (STN-4)

Fig. 56.: Contour plots for axial and meridional flow velocity

CHAPTER VIII

CONCLUSION

The test case with engine speed of 3000 rpm and compressor frequency of 65 Hz discussed in this report represents a highly loaded operational mode, with the greatest pressure ratio of 1.4465 and mass flow rate of 3.7233 kg/s. Figures 42 and 42c show line plots for various velocity flow angles. As expected the absolute velocity flow angle at the stator exit point (station 4) is relatively constant at 15° . The relative flow angles for stations 3 and 5 are constant for most of the hub to tip region. Figures 43a and 43b show the absolute and relative Mach numbers respectively. As expected the stator exit exhibits a higher absolute velocity when compared to the rotor exit points.

Loss coefficients as seen in Fig. 47a are very minimal near the mid-span region for both stator and rotor rows, however, the values are higher near end walls, more prominently close to the tip for rotor. Low pressure loss coefficients clearly reflect in efficiency values (Fig. 47b), 96.06% for stator and 84.88% for that of rotor. The overall stage efficiency is noted to be 89.13%. There is a scope of design improvement to reduce loss coefficients close to tip region which will help in an increase of overall stage efficiency.

It was observed that it is difficult to see any distinct patterns in contour plots for station 5 because of turbulent mixing of flow at station 5 and hence are not shown in this report.

It was observed during data analysis that it was difficult to get convergence for data close to end walls. This was attributed to very turbulent flow close to end walls leading the data to fall outside calibration range of probes.

REFERENCES

- [1] Bradshaw, P., 1996. “Turbulence modeling with application to turbomachinery,” *Progress in Aerospace Sciences*, **32** (6) , pp. 575–624.
- [2] Schobeiri, M., 2005. “Losses in turbine and compressor cascades,” in *Turbomachinery Flow Physics and Dynamic Performance*. Springer Berlin Heidelberg, New York, pp. 177–214.
- [3] Langston, L., 1980. “Crossflows in a turbine cascade passage,” *Journal of Engineering for Power*, **102** (4) , pp. 866–874.
- [4] Sharma, O. P., and Butler, T. L., 1987. “Predictions of endwall losses and secondary flows in axial flow turbine cascades,” *Journal of Turbomachinery*, **109** (2) , pp. 229–236.
- [5] Goldstein, R. J., and Spores, R. A., 1988. “Turbulent transport on the endwall in the region between adjacent turbine blades,” *Journal of Heat Transfer*, **110** (4a) , pp. 862–869.
- [6] Wang, H. P., Olson, S. J., Goldstein, R. J., and Eckert, E. R. G., 1997. “Flow visualization in a linear turbine cascade of high performance turbine blades,” *Journal of Turbomachinery*, **119** (1) , pp. 1–8.
- [7] Acharya, S., and Mahmood, G., 2006. “Turbine blade aerodynamics,” in *The Gas Turbine Handbook*. National Energy Technology Laboratory (NETL), Albany, pp. 363–390.
- [8] Eckerle, W. A., and Langston, L. S., 1987. “Horseshoe vortex formation around a cylinder,” *Journal of Turbomachinery*, **109** (2) , pp. 278–285.

- [9] Boletis, E., and Sieverding, C. H., 1991. “Experimental study of the three-dimensional flow field in a turbine stator preceded by a full stage,” *Journal of Turbomachinery*, **113** (1) , pp. 1–9.
- [10] Arndt, N., 1993. “Blade row interaction in a multistage low-pressure turbine,” *Journal of Turbomachinery*, **115** (1) , pp. 137–146.
- [11] Schobeiri, M. T., and Pappu, K., 1997. “Experimental study on the effect of unsteadiness on boundary layer development on a linear turbine cascade,” *Experiments in Fluids*, **23** (4) , pp. 306–316.
- [12] Neuenschwander, T., and Jermann, C., 2000. Flow measurements and investigation of data acquisition and averaging for a three stage model turbine. Diploma thesis, Texas A&M University.
- [13] Schlienger, J., Kalfas, A. I., and Abhari, R. S., 2005. “Vortex-wake-blade interaction in a shrouded axial turbine,” *Journal of Turbomachinery*, **127** (4) , pp. 699–707.
- [14] Porreca, L., Behr, T., Schlienger, J., Kalfas, A. I., Abhari, R. S., Ehrhard, J., and Janke, E., 2005. “Fluid dynamics and performance of partially and fully shrouded axial turbines,” *Journal of Turbomachinery*, **127** (4) , pp. 668–678.
- [15] Porreca, L., Kalfas, A. I., Abhari, R. S., Yun, Y. I., and Song, S. J., 2009. “Interstage flow interactions and loss generation in a two-stage shrouded axial turbine,” *Journal of Turbomachinery*, **131** (1) , p. 011002.
- [16] Tan, C., Zhang, H., Chen, H., Dong, X., Zhao, H., and Yamamoto, A., 2009. “Flow separation control by using bowed blade in highly loaded turbine cas-

- cares,” *Science in China Series E: Technological Sciences*, **52** (6) , pp. 1471–1477.
- [17] Harrison, S., 1992. “The influence of blade lean on turbine losses,” *Journal of Turbomachinery*, **114** (1) , pp. 184–190.
- [18] Devenport, W. J., Agarwal, N. K., Dewitz, M. B., Poddar, K., and Simpson, R. L., 1990. “Effects of a fillet on the flow past a wing-body junction,” *AIAA Journal*, **28** (12) , pp. 2017–2024.
- [19] Sauer, H., Müller, R., and Vogeler, K., 2001. “Reduction of secondary flow losses in turbine cascades by leading edge modifications at the endwall,” *Journal of Turbomachinery*, **123** (2) , pp. 207–213.
- [20] Shih, T. I.-P., and Lin, Y.-L., 2003. “Controlling secondary-flow structure by leading-edge airfoil fillet and inlet swirl to reduce aerodynamic loss and surface heat transfer,” *Journal of Turbomachinery*, **125** (1) , pp. 48–56.
- [21] Zess, G. A., and Thole, K. A., 2002. “Computational design and experimental evaluation of using a leading edge fillet on a gas turbine vane,” *Journal of Turbomachinery*, **124** (2) , pp. 167–175.
- [22] Boletis, E., 1985. “Effects of tip endwall contouring on the three-dimensional flow field in an annular turbine nozzle guide vane: Part 1—experimental investigation,” *Journal of Engineering for Gas Turbines and Power*, **107** (4) , pp. 983–990.
- [23] Harvey, N. W., Rose, M. G., Taylor, M. D., Shahpar, S., Hartland, J., and Gregory-Smith, D. G., 2000. “Nonaxisymmetric turbine end wall design: Part I

- three-dimensional linear design system,” *Journal of Turbomachinery*, **122** (2) , pp. 278–285.
- [24] Hartland, J. C., Gregory-Smith, D. G., Harvey, N. W., and Rose, M. G., 2000. “Nonaxisymmetric turbine end wall design: Part II - experimental validation,” *Journal of Turbomachinery*, **122** (2) , pp. 286–293.
- [25] Dossena, V., Perdichizzi, A., and Savini, M., 1999. “The influence of endwall contouring on the performance of a turbine nozzle guide vane,” *Journal of Turbomachinery*, **121** (2) , pp. 200–208.
- [26] Schobeiri, M. T., Gilarranz, J. L., and Johansen, E. S., 2004. “Aerodynamic and performance behavior of a three-stage high efficiency turbine at design and off-design operating points,” *International Journal of Rotating Machinery*, **10** (1) , pp. 33–44.
- [27] Kline, S. J., and McClintock, F. A., 1953. “Describing uncertainties in single-sample experiments,” *Mechanical Engineering*, **75** (1) , pp. 3–8.

APPENDIX A

TURBINE ASSEMBLY INSTRUCTIONS

Read the following **CAREFULLY** before starting the assembly :-

1. Follow the instructions and execute everything step by step exactly in the given order.
2. Print this instruction sheet and tick mark each step as it is completed to keep a track of the assembly.
3. Keep all the required tools at reach for convenience.
4. Starting from inlet casing, in the direction of air-flow, the turbine casing is divided into following five sections, each having top and bottom halves: **1.** Inlet Casing **2.** Middle Casing **3.** Exit Casing **4.** Casing # 4 and **5.** Casing # 5.

A.1. Assembly of bottom half of stator sings

- Remove bottom halves of all the T-rings and place it outside with a correct label on each.
- Remove any rust and clean all the slots in the bottom casing using clean paper towel and alcohol.
- Slide the labeled clocking arms into respective slots in the bottom casing.
- Use aluminum tape to properly secure thermocouples from blades at 3 o'clock and 6 o'clock upto 3rd hole for clocking arm on the shrouds.

- Bolt the tongues into shrouds of all three bottom stator halves.
- Lift bottom portion of stage-1 stator ring using a webbing sling (yellow lifting belt) with the crane and carefully slide it into the bottom turbine casing. The stator ring has to be supported and guided by hand to ensure proper alignment.
- Make sure that the shroud is flush with bottom turbine casing surface at 3 o'clock and 9 o'clock positions.
- From 9 o'clock position, slide both stage-2 and stage-3 stator half rings one by one into their respective locations in the casing. Make sure that the shrouds are flush with bottom turbine casing surface at 3 o'clock and 9 o'clock positions.
- FOR ALL 3 STAGES: Thermocouples from blades at 3 o'clock and 6 o'clock need to be pulled out from clocking slots on casing using tweezers/nose-pliers. Make sure these thermocouples are routed below the clocking arm.
- Bolt all 3 clocking arms to their respective positions.

– *End of this step.*

A.2. Assembly of 5600 series rotor

- Clean rotor hub and blades using fine grit sand-paper and then alcohol to remove any rust before starting the assembly.
- Place bottom part of exit bearing housing (the one with pins) on bottom casing. Match the leading edge of bearing housing with the etched-mark on bottom casing.

- Place bottom part of Inlet-bearing housing (the one with pins) with all the respective shims on the bottom casing. Make sure that the bearing housing can have no movement in flow direction due to thrust.
- Clean inside surface of bearing housings with alcohol and clean paper towel.
- Now lift the rotor with crane and steel cables making sure the rotor is perfectly horizontal when lifted (use a digital/spirit level).
- Clean the bearing outer races with alcohol and clean paper towel.
- Place the rotor slowly into bottom casing while taking care of the following:-
 1. Rotor blades do not hit anywhere and get damaged.
 2. Brass sealing ring is aligned properly to match the recess in bottom part of 1st stage stator.
 3. Inlet bearing slides smoothly in bottom bearing housing with respective shims in place. Make sure that the bearing can have no movement in flow direction due to thrust.
 4. Rotor rotates smoothly after loosening the steel cables used for lifting. **DO NOT TAKE OFF THE STEEL CABLES AS OF NOW.**
- Carefully slide bottom part of slip ring cover on exit shaft and bolt it with bottom bearing housing.
- While ensuring that the pins go in smoothly, place top portions of both inlet and exit bearing housings on respective bottom portions. Bolt the halves of bearing housings together.

- Now lift the rotor up by JUST a millimeter so that both inlet and exit bearing housings can be rotated to bring bottom halves on the top.
- Insert thermocouples in both inlet and exit bottom bearing housings and use contact pins to ensure proper contact of thermocouples with the bearings. This can be checked using a multi-meter.
- Turn both bearing housings back to the correct orientation.
- Connect the inlet and exit bottom bearing thermocouples to the respective connectors on the bottom inlet and exit casings.
- Lower the rotor and take off the steel lifting cables. Make sure that the rotor still runs smoothly.
- Insert thermocouple into top half of inlet bearing housing through top portion of slip ring cover and use the contact pin to secure it in place. Make use of a multi-meter to check for a proper contact.
- Insert brass shim and then the front cover of inlet bearing housing and tighten the bolts.
- Insert and tighten the bolts that hold inlet and exit bearing housings to the bottom casing.

– *End of this step.*

A.3. Assembly of slip ring and coolant pipe

- Carefully slide the slip ring on the exit end of shaft.

- Connect thermocouples on shaft to the ones on slip ring according to the connection map.
- Turn slip ring in order to get the white electrical connector on top.
- Hold top portion of slip ring cover over the bottom portion and connect the white electrical connector.
- Now place top portion of slip ring cover flush with bottom portion.
- Turn the slip ring slowly and carefully without disturbing bottom thermocouple. Pin on the slip ring should be aligned with the hole at 6'o clock on bottom portion of slip ring cover.
- Screw the brass stopper in bottom portion of slip ring cover to hold the slip ring in place through the pin.
- Tighten all three equally spaced set-screws on the slip ring.
- Insert thermocouple into top half of exit bearing housing through the top portion of slip ring cover and use the contact pin to secure it in place. Make use of a multi-meter to check for a proper contact.
- Carefully assemble the slip ring cap and tighten all four screws. Make sure to check for any noises while turning the rotor. If there is any noise, loosen the screws on the cap a little bit.
- Align 4 holes on long coolant pipe with matching holes on slip ring cap and bolt them together.

- Route the flexible hoses from the long coolant pipe to outside through the holes provided on the window at the exit of the turbine. Make sure there is no crimp on these flexible hoses.

– *End of this step.*

A.4. Assembly of flex-coupling and shaft

1. FOLLOWING STEPS ARE VERY CRITICAL
 2. IN CASE OF ANY DOUBT, REFER TO THE FLEX-COUPLING INSTALLATION INSTRUCTIONS IN THE BOX-FILE.
- Clean the inlet end of rotor shaft and bore (internal surface) of the shrink-fit hub with alcohol. Make sure these surfaces are free of any oil/grease.
 - Clean outer surface of the shrink-fit hub with alcohol and then apply a thin film of WD-40 oil using a paper towel. (Wet the paper towel with WD-40 and then use it.)
 - Slide both shrink discs (being held together with 7 bolts) on shrink-fit hub and then slide shrink-fit hub on inlet end of rotor shaft.
 - Tighten all the 7 bolts by hand making sure shrink discs are parallel to each other.
 - Use a torque-wrench with a torque of 22 in-lb to tighten the bolts in CW/CCW direction one after another, quarter turn each time.
 - Use the semicircular wooden supports for keeping the shaft in place.

- Use C-clamps to compress the flex-coupling on the shaft to get it inside the shoulder on both sides.
- Insert the numbered bolts in correct positions on both sides of the shaft.
- On both engine and dynamometer side, hand tighten the bolts and then use a torque wrench to give a torque of 44 in-lb to all the bolts with quarter turn each time in CW/CCW direction.
- CHECK - Check whether alignment of shaft is needed and call the professionals if required.
 - *End of this step.*

A.5. Assembly of top half of stator rings

- Use aluminum tape on top half of all stator rings to properly secure thermocouples placed in blades at 9 o'clock and 12 o'clock on the shrouds.
- Bolt the tongues into shrouds of all top three stator halves. Do not tighten the tongues completely as of now and allow some play.
- Assemble top half of stator rings with bottom halves and tighten all the tongues at this point.
- Route the thermocouples out of respective slots from top of clocking arms.
 - *End of this step.*

A.6. Assembly of top casings

Inlet and exit top casings

- Clean the mating surfaces on bottom exit casing with alcohol and clean paper towel.
- Insert four dowel pins in bottom casing near the exit bearing housing. Apply little grease to the exposed dowel pins after inserting them in casing.
- A steel pipe between two eye-bolts is needed to lift the top exit casing. Use a digital/spirit level to make sure the casing is perfectly horizontal when lifted.
- Insert two short guide pins on each side of top exit casing through the non-threaded holes. The nuts on these guide pins should be threaded to only 2-3 threads at this time.
- Lower exit top casing slowly and carefully making sure that dowel pins in bottom casing slide in easily into the corresponding holes on top casing. Also, make sure that the top exit bearing thermocouple does not get crimped anywhere.
- At this point, four short guide pins should come out easily from the top casing. In case any of them gets stuck, use some washers between top casing and the nut(s). Tightening the respective nut(s), pulls the pin(s) out.
- There should be no gap between the top and bottom casing if the top exit casing was lowered correctly.
- Connect the top exit bearing thermocouple connector to the respective connector on the top exit casing. Make sure the thermocouple is secured properly using cable ties and is not close to the rotor.

- Repeat all the above steps for top inlet casing.
 - *End of this step.*

Middle top casing

- Clean bottom half of all T-rings and apply a thin layer of silicon lubricant before sliding them into their respective slots in bottom casing. The ends of T-rings should be flush with the surface of bottom casing.
- Slide labeled halves of dummy rotor shrouds into their respective slots in bottom casing.
- Place corresponding top halves of dummy rotor shrouds over the bottom shrouds.
- Clean mating surfaces on bottom casing with alcohol and clean paper towel.
- Thread two long guide pins on each side of the bottom casing. Use the threaded holes at extreme ends on bottom middle casing.
- Use steel pipe with a larger diameter between the two eye-bolts to lift the top middle casing. Use a digital/spirit level to make sure the casing is perfectly horizontal when lifted.
- Insert two short guide pins on each side of top middle casing through the non-threaded holes. These guide pins have nuts on them which should be threaded to only 2-3 threads at this time.
- While the top casing is lifted up by the crane, remove the top half of T-rings and clean them using a clean paper towel and alcohol.
- Apply a thin layer of silicon lubricant and slide the T-rings back into their respective positions.

- Align top middle casing over the bottom casing in both flow and lateral directions.
- Slowly and carefully lower the top casing until it is half-way down between inlet and exit casings. Beyond this point, keep the top casing rocking (moving up and down) while lowering it down further.
- On both sides, regularly measure distance between the mating surfaces of top and bottom casings as they start getting closer. Use C-clamps to keep the distances equal.
- When the distance between mating surfaces is about 2 cm. keep an eye on the tongues of T-rings and ensure none of the bottom halves of T-rings is pushed up from any side.
- If done correctly, there should be no gap between the mating surfaces of top and bottom middle casings. However, to close any small gap, C-clamps can be used after lowering the top casing completely.
- At this point, four short guide pins should come out easily from the top casing. In case any of them gets stuck, use some washers between top casing and the nut(s). Tightening the respective nut(s), pulls the pin(s) out.
- Un-screw all four long guide pins and take them out.
- Insert all eight horizontal hex bolts in middle casing and tighten them completely.
- CHECK: Make sure that the rotor turns easily and freely.

- CHECK: All three T-rings should be sliding easily and smoothly in respective slots. After the check, adjust the holes in all three T-rings inline with etched mark at 12 0'clock on casing.
- Insert six horizontal hex bolts each on inlet and exit casings and tighten them completely.
- Insert and tighten all circumferential hex bolts to connect middle casing with inlet and exit casing.
 - *End of this step.*

Exit cone, casing # 4 & casing # 5

- Connect the transparent hoses used for cooling of slip ring to the two brass fittings on slip ring cap. These hoses are routed from below through bottom halves of casing # 4 and exit cone. Seal all the gaps around the hoses and holes on casing # 4 and exit cone.
- The thermocouples from slip ring should be taken outside through the small hole in the center, between the ones for transparent hoses in exit cone and casing # 4.
- Seal all open holes and any gaps on the exit cone using aluminum tape. If needed use the conical rubber plugs.
- Apply 3 layers of electrical tape on the mating surfaces of bottom half of exit cone to provide proper sealing after assembly.
- Use 2 eye-bolts and a D-shackle on each to lift the top half of the exit cone.

- Carefully and slowly slide the top half of exit cone into its position and make sure all holes are properly aligned.
- Using 2 hex bolts through the bottom half of exit cone, bolt two halves together at small end of the cone. Insert and tighten all circumferential bolts connecting top half of exit cone to the exit casing.
- Two persons can lift top half of casing # 4 and place it in the right position. Use 2 bolts on each side to connect the horizontal flanges together and all circumferential bolts to connect casing # 4 with top exit casing.
- Again, two persons can lift the top half of casing # 5 and place it in the right position. Use 2 bolts on each side to connect the horizontal flanges together and all circumferential bolts to connect casing # 4 with casing # 5.
- Outside the test cell, near the compressor, use a hydraulic jack between structural frame and flange on the long pipe to push the pipe towards the compressor. This creates a distance between casing # 5 and the long green pipe. BE EXTREMELY CAREFUL, IF NOT DONE PROPERLY, THE JACK CAN SNAP OFF AND CAUSE BODILY INJURY.
- Insert the 2 halves of steel sealing rings in casing # 5. The half rings should sit properly in the shoulder provided.
- Carefully and slowly release the hydraulic jack to reduce distance between long pipe and steel sealing ring. The gap between these 2 is sealed using the rubber gasket.
 - *End of this step.*

A.7. Assembly of heater

- Pass the long threaded bolt through a 2.5 in. spacer to maintain right distance of exit passage between outer and inner cylinders and thread it completely on the inner cylinder.
- Now on this long bolt, lock two nuts against each other such that bottom nut is flush with outer cylinder.
- By means of two jack screws on the sides ensure uniform air passage of 2.5 in. all around. Use a vernier calliper.
- Un-screw the long bolt from inner cylinder without disturbing nuts on it and remove the spacer between two cylinders.
- Screw the long bolt back completely into bottom circular steel plate.
- Pass a steel cable loop with turn-buckle through the jaw on long threaded bolt and around the bar on heater top.
- Connect crane hook to the bar on heater top and move the crane up just enough to move the round bar but not heater.
- Tighten the turn-buckle to ensure that there is no slack in the steel cable loop.
- Lift up the top half of heater on crane and ensure that the honey-comb is intact and in proper place.
- Align top half of heater with bottom half and slowly lower it to about few millimeters from the bottom half.

- Move top half of heater towards the turbine such that both inner and outer cylinders of heater exit slide into the shoulders on inlet turbine casing. It might be required to loose turn-buckle a little bit to facilitate this.
- Use C-clamps to completely push the outer cylinder into shoulder of inlet casing.
- Slide two big bolts into horizontal flange of the heater, do not tighten them yet.
- Insert and tighten all circumferential bolts between heater and inlet casing. Now, tighten the horizontal flange bolts completely.
- Bolt all four, curved steel plates, labeled A, B, C and D at their respective places to connect top and bottom halves of heater.
- Bolt two small bolts on each of the four horizontal flanges of heater.
- Use aluminum tape to seal any gap between top and bottom half of inner and outer cylinders.
- Connect top and bottom halves of perforated screen for air passage using two small screws on each side. Slide this screen on inner cylinder in flow direction until it is flush to the wall of outer cylinder.
- Insert the inner flow deflector sheet between the heater elements and connect the ends together using three screws such that the sheet is flush with all heater elements from inside.
- Slide this inner flow deflector sheet in the flow direction so that its edge is flush with wall of the outer cylinder.
- Encircle all heater elements with outer flow deflector sheet and connect the ends together using three small screws.

- Slide this outer flow deflector sheet towards the dynamometer until its edge is flush with wall of outer cylinder.
- Assemble the perforated screen over top half of heater and secure it using small screws at various circumferential positions.
- Cover this perforated screen with an air-filter and use nylon thread to secure it in place.
- Route the electrical cables to respective locations and make the connections carefully. The nine black electrical cables are labeled as L1-1 to L1-3, L2-1 to L2-3 and L3-1 to L3-3.
- Three green ground cables are connected to the same location.
- Two yellow cables are connected to the thermocouples. Make sure to cover these thermocouple connections with electrical tape and properly secure them using cable ties.

– *End of this step.*

A.8. Instrumentation

A.8.1. Four-axis traverse system

- Insert all three labeled fingers inside their respective slots. Make sure fingers are inserted in the right direction (side labeled 3 o'clock should be facing 3 o'clock).
- Each of these fingers are connected to T-rings using four small hex bolts. Ensure that each T-ring still moves freely, if not, loosen these hex bolts and check again.

- Assemble the traverse base on top of these T-rings in correct direction (base has etched markings). Base is connected to each of the fingers using two long hex bolts.
- Make sure that the base and T-rings slide smoothly and easily after assembly. It may be needed to loosen some or all of these six bolts for T-rings and base to slide smoothly.
- Move traverse frame to the original position and bolt its four legs to the ground.
- Attach all five labeled unistruts to their respective positions on walls.
- CHECK: The traverse frame should be firm.
- The main traverse which is hanging on the frame using steel cable should be lowered slowly onto the traverse base by loosening the turnbuckle.
- Each of the three traversing pillars are connected to traverse base using three hex bolts. At this point, connect traverse pillars for station-3 and station-5 to the base.
- Traverse pillar for station-4 needs to be turned to make space for electrical connection. Pivot traverse pillar for station-4 by removing two of the three hex bolts connecting it to the top plate of the main traverse and loosening the third.
- Make electrical connection of thick stepper motor cable for station-4 and assemble the traverse pillar back to its original position. Bolt traverse pillar for station-4 with traverse base at this point.
- Apply 1 layer of silicon tape on smaller diameter of all three brass pieces for 5-hole probes and slide them carefully in through traverse base at respective stations.

- There is one big stepper motor which controls the radial motion of each 5-hole probe and one big stepper motor to control circumferential movement of all three 5-hole probes together. Each of these big stepper motors have following three electrical connections:
 1. One thick cable for stepper motor.
 2. One cable for controller.
 3. One cable for encoder.

One of these connection is completed in previous step, now connect the remaining labeled connections carefully without making any mistakes.

- Do not connect electrical cables to small stepper motors used to turn 5-hole probes.
 - *End of this step.*

A.8.2. Five-hole probes

- Use LabView program, *Turbo.vi* to move all three radial traverse systems to their bottom mechanical stops.
- Station-4 probe assembly is different than that of station-3 and station-5. Following steps are for station-4 probe assembly.
- Slide the following one by one on 5-hole probe from the probe-tip end: Worm gear (Fig. 57a), Round spacer (Fig. 57b), Steel sleeve (Fig. 57c) & Hex nut (Fig. 57d). Fig. 57e shows all these four parts on the probe.
- Place the probe between two halves of probe holder such that the steel sleeve is inside the two halves. For station-4 probe, the stepper motor needs to placed

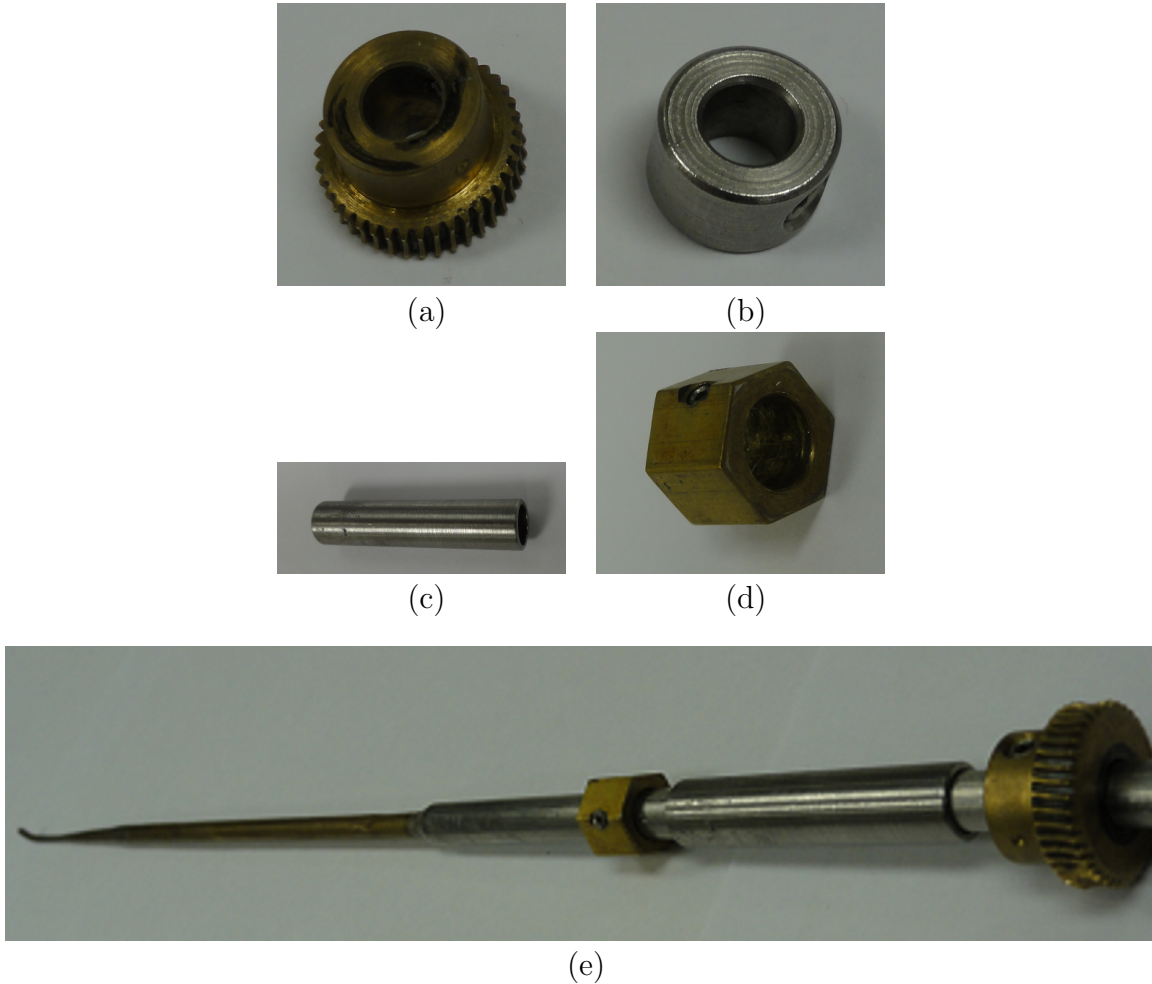


Fig. 57.: Various parts used on 5-hole probes during assembly

along with top half of probe holder and a aluminum spacer at this step, but do not tighten the probe holer yet.

- The round spacer, worm gear and hex-nut should be tightened on probe using set screws so that they are flush to each other and probe holder as shown Fig. 58. Care should be taken that, probe still turns freely. Also, the set-screws should be pointing in the direction os probe-tip.
- Now mesh the worm gear with stepper motor and tighten all four screws of

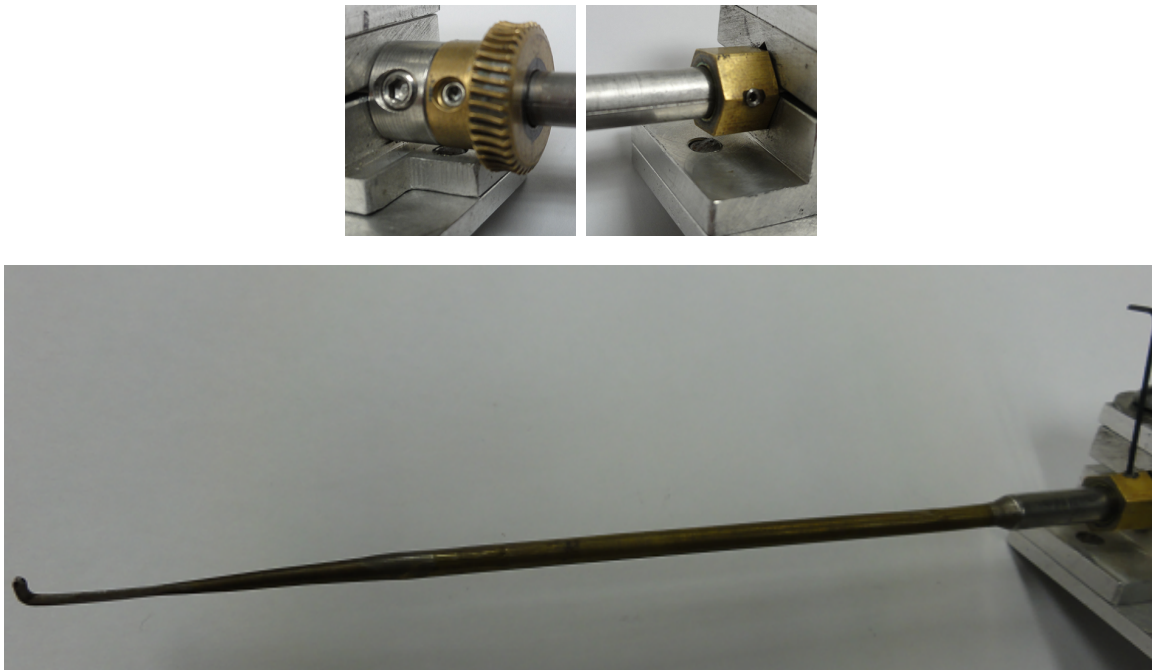


Fig. 58.: Spacer and hex-nut flush with probe holder and set-screws aligned with probe-tip

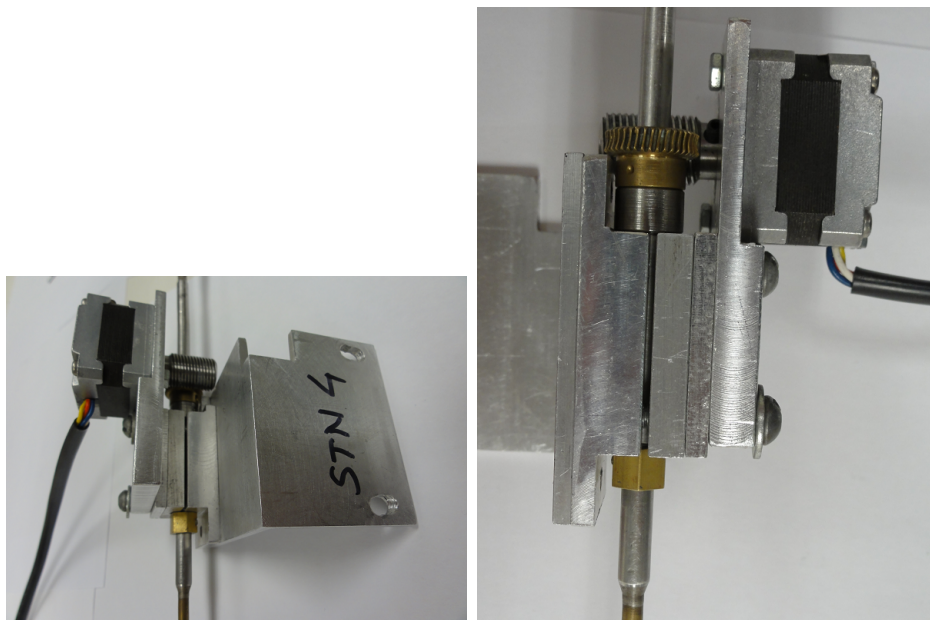


Fig. 59.: Station-4 probe assembly

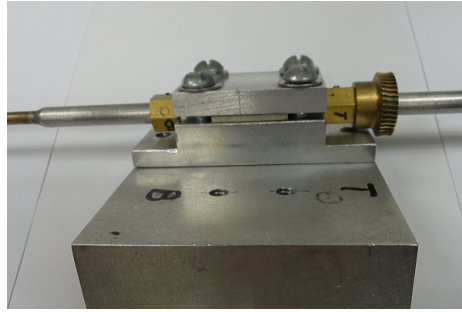


Fig. 60.: Set-up for station-3 and station-5 probes in probe holder

probe holder. After tightening, make sure:

1. Probe turns freely in both directions by turning the worm of stepper motor.
2. Both halves of probe holder are parallel to each other.

Station-4 probe assembly looks as shown in Fig. 59.

- For station-3 and station-5 probe assembly steps are similar and explained below.
- As shown in Fig. 57, slide small parts like worm gear, spacer, steel sleeve and hex-nut on respective probes.
- Place each of these probes with small parts between the halves of probe holder and tighten two halves together using four screws each (Refer Fig. 60).
- Similar to Fig. 58, spacers, worm gears and hex-nuts need to be tightened with their set-screws aligned in the direction of probe-tip.
- For both these probes, the stepper motor can be aligned and meshed using two small screws each. Make sure, the probes turn freely by turning worms of stepper motors after assembly. Assembled station-3 and station-5 probes are shown in Fig. 61.

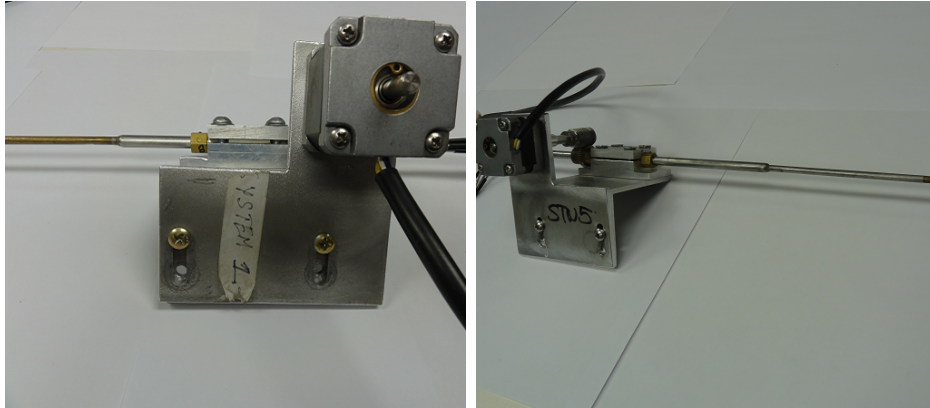


Fig. 61.: Station-3 and station-5 probe assembly

- 5-hole probe for station-4 needs to be assembled in the traverse system before any other probe.
- Wrap a single layer of silicon tape on the smaller diameter of brass piece for station-4 and push it inside traverse base on the machine.
- Carefully insert station-4 probe assembly between traverse pillars for station-3 & station-4 as shown in Fig. 62a and then turn it in counter-clockwise direction to get it in a position as shown in Fig. 62b. Slide it inside through the brass piece. Make sure the probe-tip is pointing towards 9 o'clock position (Fig. 63) before sliding it in.
- Place the brass shim between probe holder and traverse system of station-4 and use two small screws to assemble these together.
- At this point all four screws of probe holder have to be loosened just a little bit to disengage the worm gear from stepper motor. Now, while holding the probe from top, loosen both worm gear and spacer.
- Very slowly and carefully, slide the probe inside until it rests on hub surface. Re-

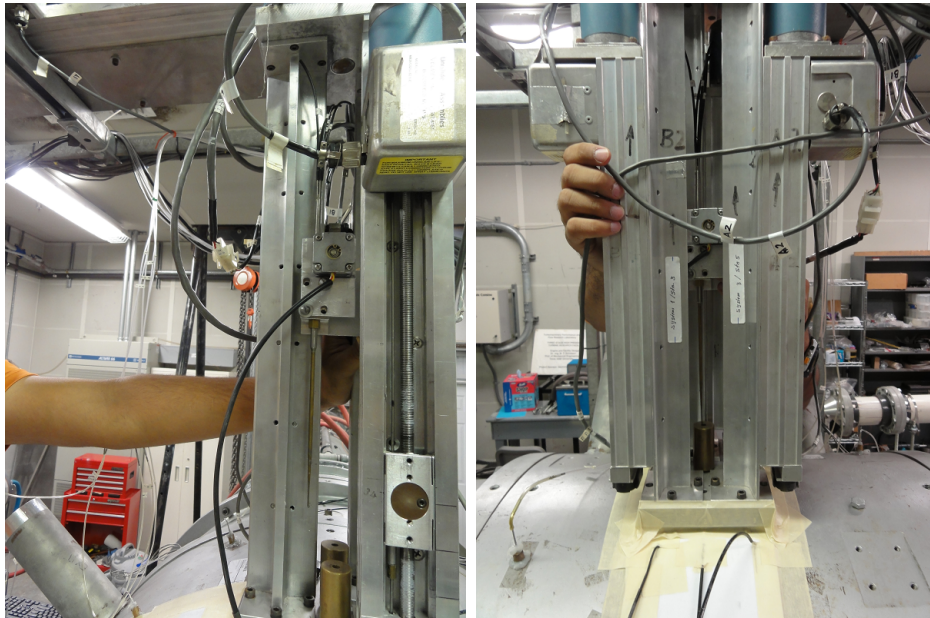


Fig. 62.: Steps for sliding station-4 probe assembly into traverse system

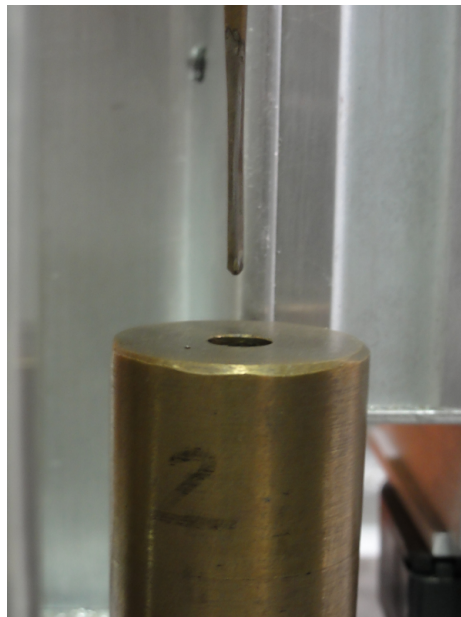


Fig. 63.: Figure showing station-4 probe tip pointing towards 9 o'clock

tighten both, spacer and worm gear flush to probe holder and their set screws aligned with that of the hex-nut.

- Now, loosen hex-nut and slide it up so that it is flush with probe holder and tighten it back with its set screw aligned with that of worm gear and spacer.
- Mesh the worm gear back and tighten all four screws of probe holder. Make sure that the probe rotates freely by turning worm of stepper motor by hand. This completes the assembly of station-4 probe on traverse system.
- **VERY CRITICAL:** At this moment, use *Turbo.vi* program to lift the probe at station-4 up from hub surface by only 1 *mm* and initialize this location as 100 *mm*. Make sure the probe is traversed upwards or else you will damage the probe.
- Now, wrap a single layer of silicon tape on the smaller diameter of brass piece for station-5 and push it inside traverse base on the machine (Fig. 64a does not show any silicon tape on brass piece, however it should be there).
- Slide this brass piece on the probe as shown in Fig. 64a and then carefully slide top of the probe behind the electrical connector of station-4 as shown in Fig. 64b.
- Once the probe is vertical, make sure the probe tip is pointing towards 9 o'clock and then first slide the brass piece in to traverse base and then slowly slide the probe inside to align probe holder with traverse system (Refer Fig. 64c) . Use two small screws to secure probe holder with traverse system.
- Steps to make the probe tip rest on hub surface is similar to that of station-4. However, station-5 probe assembly might have to be taken outside the machine

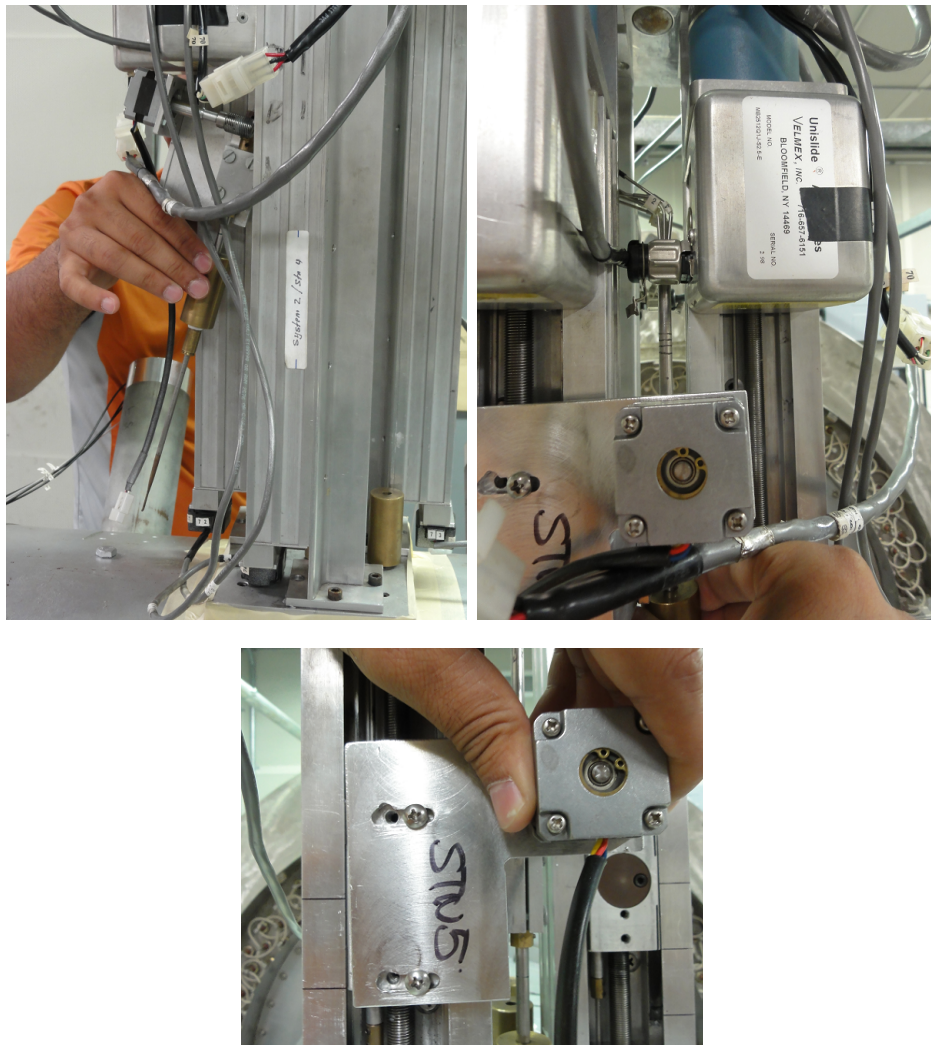


Fig. 64.: Steps for sliding station-5 probe assembly into traverse system

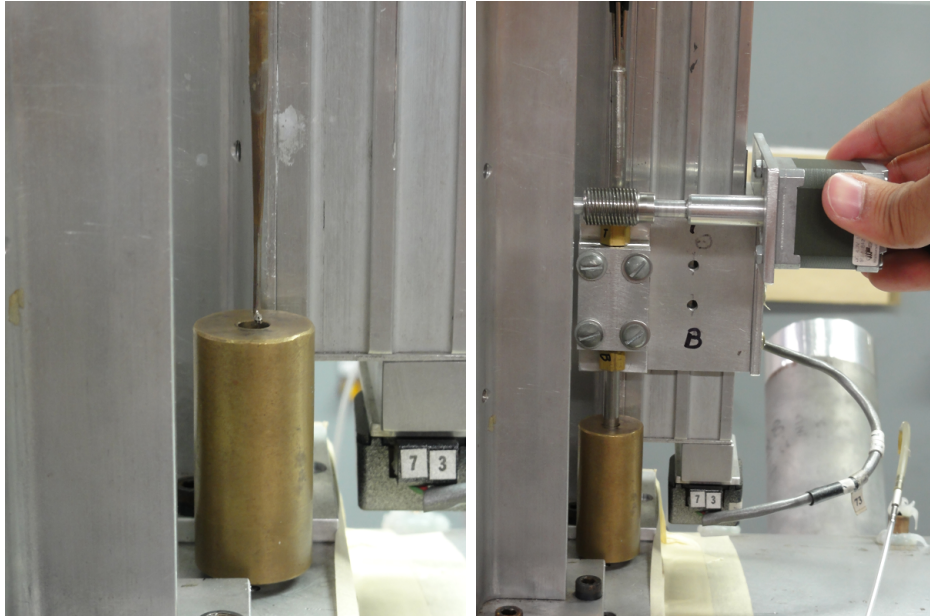


Fig. 65.: Steps for sliding station-3 probe assembly into traverse system

to mesh the worm gear once the probe is set at right height on probe holder.

- Similar to that of station-4, lift probe traverse by 1 *mm* and initialize this location of probe traverse as 100 *mm*.
- Assembly of probe at station-3 is exactly similar to the assembly of station-5, infact for station-3, the brass piece can be put inside traverse base before sliding the probe inside machine (Refer Fig. 65).
- Similar to that of station-4 and station-5, lift probe traverse by 1 *mm* and initialize this location of probe traverse as 100 *mm*.

– *End of this step.*

A.8.3. Inlet and exit rakes

There are four rakes to get the total pressure and temperature, both at inlet and exit of the turbine. All the rakes should be assembled as follows:-

- Remove the aluminum plugs out.
- Insert the labeled rake to its respective location while ensuring the following:
 1. The probe tips are facing the flow.
 2. The probe is not touching rotor hub.
- Tighten all four hex bolts on the brass cap.
 - *End of this step.*

APPENDIX B

INSTRUCTIONS TO CALIBRATE 5-HOLE PROBES

Five hole probes need to be calibrated using the calibration facility in TPFL as follows:-

1. In order to get a steady flow for calibration, start all three *Ingersoll Rand* oil-free compressors for atleast an hour before the start of calibration.
2. 5-hole probe calibration usually runs for about 6-10 hours depending on the grid needed. Check with all other groups in Turbolab that none of them would be using High Pressure (HP) air for the duration of your calibration run.
3. Place the calibration facility clear of walls and connect both electrical cables from the controller to respective stepper motors.
4. Connect one end of the long RS-232 cable to controller and other end to data acquisition computer.
5. Do not connect the controller to power supply yet.
6. Unscrew the aluminum plug from turn-table where 5-hole probe is mounted and use a small screw-driver to push the slotted silicon sleeve out.
7. Carefully slide the 5-hole probe from back side of turn table without touching probe-tip to anything.
8. Now, push the slotted silicon sleeve over the 5-hole probe from front. Screw the aluminum plug to check whether the probe tip is in the center of exit nozzle of flow tunnel. Silicon sleeve on the probe might need to be adjusted to get the probe-tip in the center of exit nozzle.



Fig. 66.: Icon for SetZero program



Fig. 67.: Icon for NetScanner program

9. Connect the 5-hole probe to pressure transducer suitably rated for the required calibration pressure. Note channel number of these connections. Also, note the IP address of the module.
10. Connect total and static pressure tubes from the flow tunnel to same transducer used in above step and note channel numbers.
11. Use *SetZero* program from the desktop to zero all pressure transducers. The program icon looks as Fig. 66.
12. Open the test cell window.
13. Connect the blue flexible hose to HP air outlet pipe in test cell. Check routing of this hose to ensure that the air from HP pipe goes through two filters on calibration table before going in to the flow tunnel.
14. Partially open butterfly valve on HP pipe to start the air flow and use *NetScanner Start V1.04* (Icon for this program looks as Fig. 67) software to keep a check on the flow pressure and limit of pressure transducers being used.

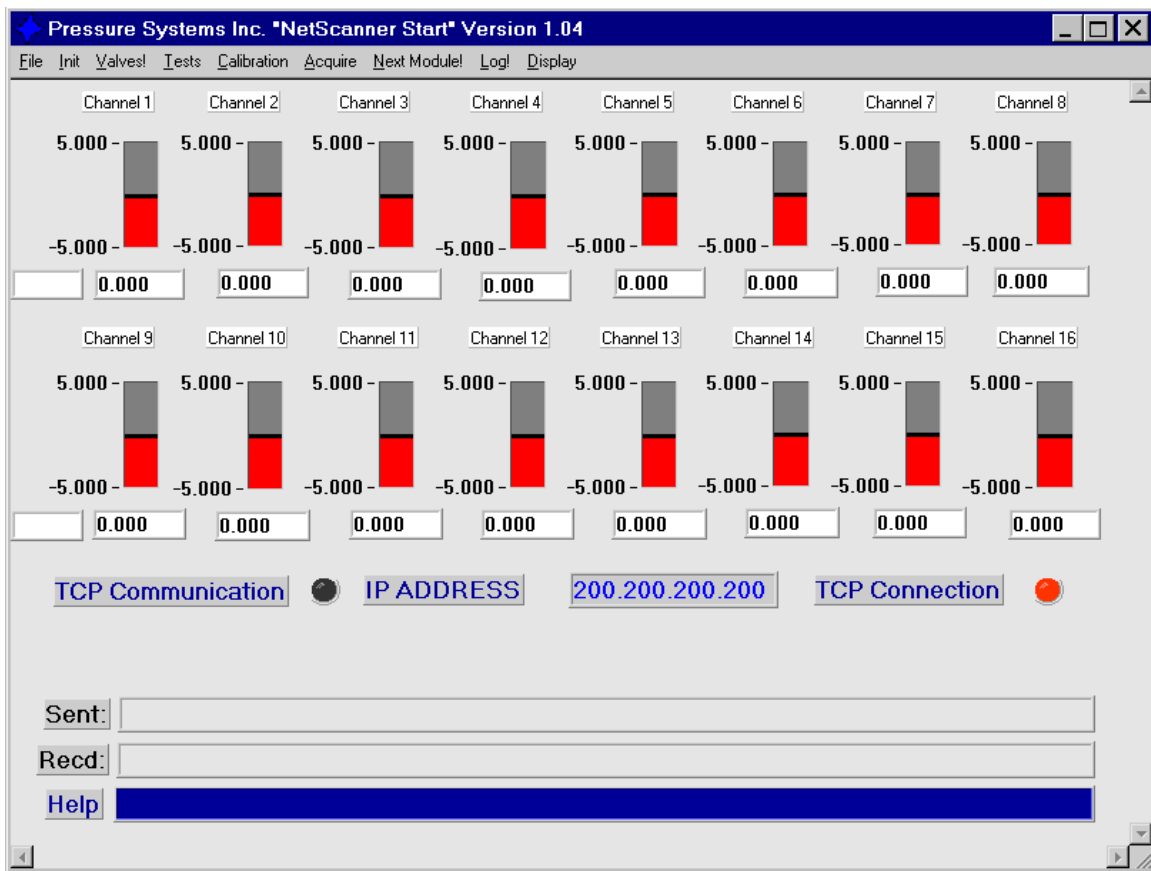


Fig. 68.: Main window of NetScanner program

15. Fig. 68 shows the main window of *NetScanner* program.
16. To use *NetScanner* program, click *Init*→*NetScannerModules*. Now, choose *Read IP Addresses From a File* and click *OK*. Select the text file with all IP addresses to initialize all pressure modules.
17. Now jump to the pressure module in use by clicking *File*→*Select Module* and entering the correct IP address.
18. To check the pressure values, click *Acquire*→*Acq.Data*. Desired units for pressure can be chosen by clicking *File*→*Unit of Measure*.
19. Using total and static pressure of the flow along with its temperature from the thermocouple in flow tunnel, actual Mach number of the flow can be calculated.
20. Butterfly valve and throttle valve on High Pressure (HP) pipe can be adjusted to achieve required Mach number for a particular 5-hole probe (Fig. 69).



Fig. 69.: Butterfly and throttle valves for calibration facility



Fig. 70.: Icon of TurboProbe program

21. Now, adjust both the turn tables by hand so that the probe holes for pitch and yaw read same pressures. Refer Fig. 29 for pitch and yaw angle definitions with respect to probes axes.
22. Note these pitch and yaw angle readings on respective turn tables. These are the zero-setting angles for the probe.
23. Both pitch and yaw turn tables need to be set at negative range chosen for the probe calibration. Hence, adjust both turn tables by hand to a value of negative range (usually ± 25 or ± 30) from zero-setting angles on both turn tables.
24. Now, connect the controller to power supply and ensure that it is “ON”.
25. At this point close the test cell door from outside. Do not open the door for entire calibration run.
26. Open *TurboProbe* program (Icon for this program looks as Fig. 70) from desktop of data acquisition computer. Click *Connect* to get a window as shown in Fig. 71.
27. Controller and pressure transducers are connected as follows:-
 - (a) COM1 Connection is used for connecting the computer with controller.
 - (b) Pressure transducer is connected through TCP/IP connection by typing correct IP address. Port value should be 9000.

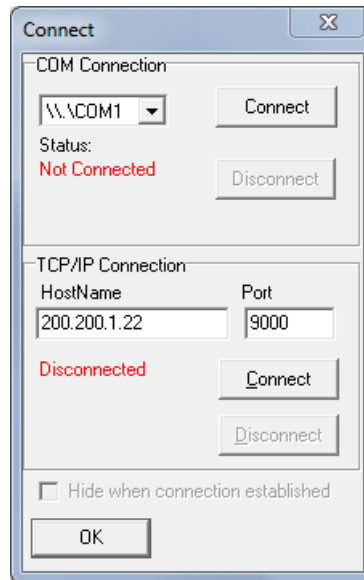


Fig. 71.: Connection window for probe calibration

Once both the connections are successful, click *OK* to close the connection window.

28. Click *Setup*→*Grid* to get a *Grid Configuration* window as shown in Fig. 72. Here, number of points for pitch and yaw is equal to $2 \times n + 1$, where n = calibration range (usually $n = 20, 25, 30, 35, \dots$). Also, enter the range for pitch and yaw.
29. Make sure *Run in AUTO MODE* is ticked before clicking *OK*.
30. Click *Setup*→*Pressure Configuration* to get a window as shown in Fig. 73. Choose 7-hole probe configuration instead of 5-hole probe as this enables you to choose two more channels one of which can be set for static pressures and the other can be any random channel. Make sure correct channel numbers are used during this configuration.

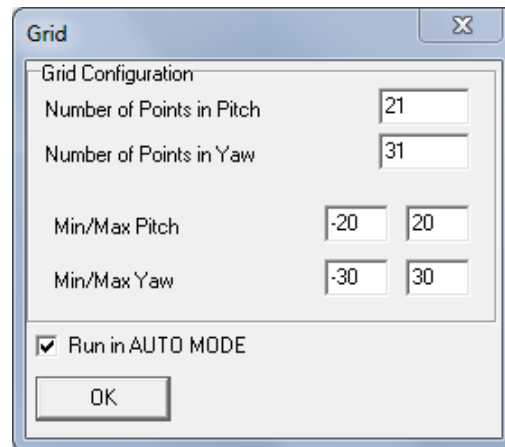


Fig. 72.: Grid configuration window for probe calibration

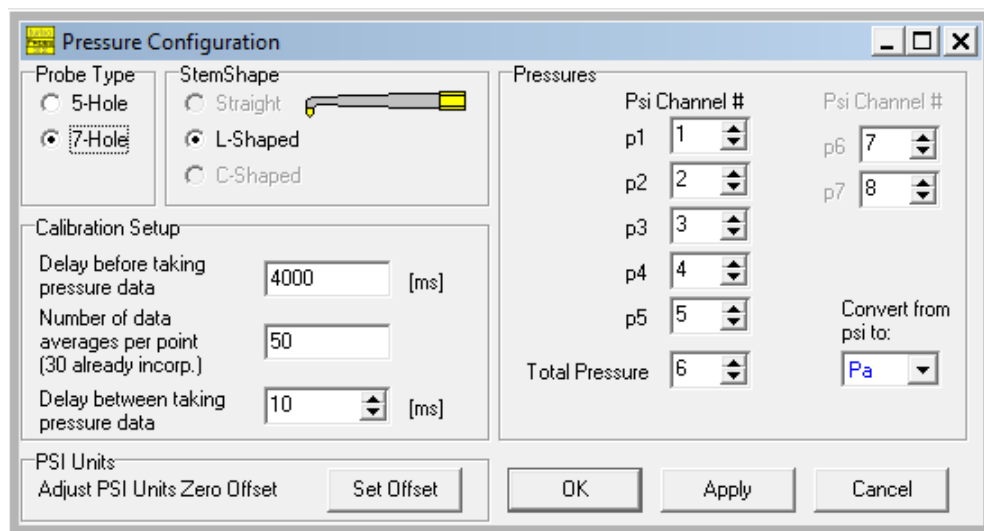


Fig. 73.: Pressure configuration window for probe calibration

31. Click *Apply* and then *OK* without changing anything else on this window.
32. Do not change anything in the *Traverse Configure* window.
33. Click *Calibration*→*Start* to start the calibration.

APPENDIX C

INSTRUCTION MANUAL FOR GENERATING TEST SCRIPT

1. Test script file can be generated using the *GenFile* program. The icon looks as shown in Fig. 74



Fig. 74.: Icon for *GenFile* program

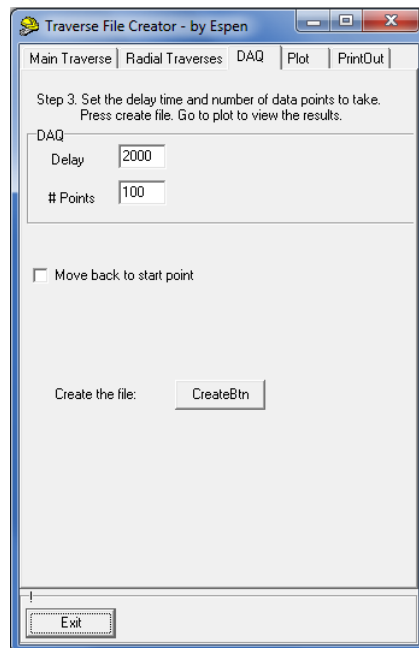


Fig. 75.: Default window of *GenFile* program

2. Main window for this program looks as shown in Fig. 75 and has five different tabs on the top. Default view for the main window is *DAQ* where the user needs to set *Delay* time in milliseconds and *# Points*.

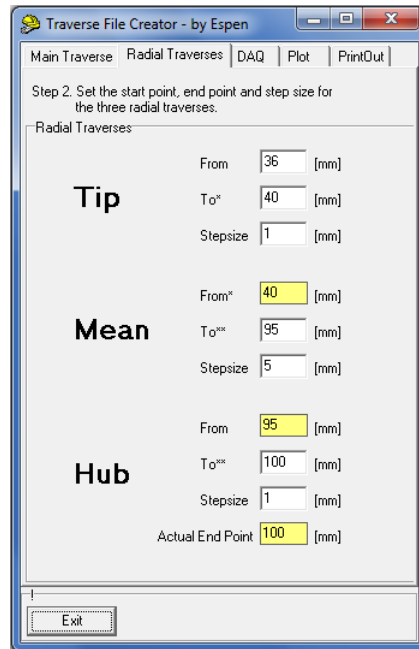


Fig. 76.: Radial traverse tab from *GenFile* program

3. Here, *Delay* time means the wait time between movement of probes and data acquisition by pressure scanners, whereas, *# Points* sets the number of samples in test data. The default values are “2000” and “100”.
4. Go to *Main Traverse* to set the range of movement and step size for circumferential traverse. Remember that 500 *mm* for main traverse is set for 12 o’clock position for circumferential traverse.
5. Click *Radial Traverse* to set the desired radial movement of probes. This program was designed to generate files to traverse the probes from “Tip” to “Hub”, however, the probes traverse in upward direction i.e., from “Hub” to “Tip”. Remember that 100 *mm* for radial traverse is set for “Hub” end of blade span, hence, if the total desired radial movement of probes is 65 *mm*, the probes move from 100 *mm* (Hub end) to 46 *mm* (Tip end).

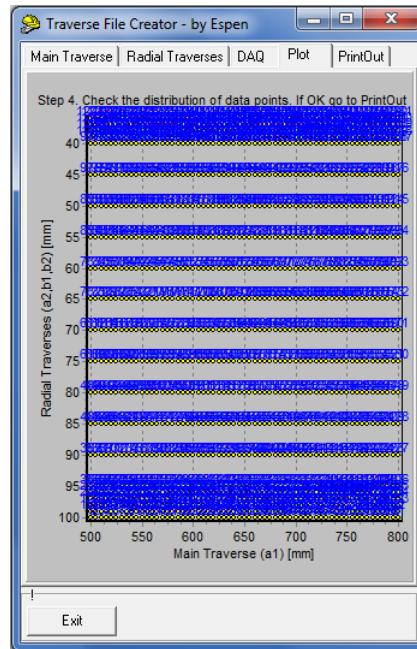


Fig. 77.: Plot showing test-grid generated from *GenFile* program

6. The general practice for setting radial movement of probes is to have a fine grid near hub and tip region and relatively coarse grid in the mid region. The default values in Fig. 76 show that radial traverse has 1 mm step size for both hub and tip region whereas, step size of 5 mm for mid section.
7. Now, go to *DAQ* tab and create the test file by clicking *CreateBtn*.
8. A plot of generated script file can be checked by clicking *Plot* tab (Fig. 77).
9. Generated test script file can be checked and then saved to desired location by choosing the *PrintOut* tab.
10. REMEMBER: Make sure to check the sequence of commands for radial movement of probes in generated test script file. Refer Table VIII to check the correct sequence of radial movement for the probes:

Table VIII.: Correct sequence of radial movement for probes

Sl. No.	Traversing UP (from HUB to TIP)	Traversing DOWN (from TIP to HUB)
1	A-2	B-2
2	B-1	B-1
3	B-2	A-2

11. Fig. 78 shows an example of a traverse plot followed by the test script code. Here, the probe is traversed circumferentially from 500 *mm* to 700 *mm* with step size of 100 *mm* whereas, radial traverse has a step size of 1 *mm* from 100 *mm* to 98 *mm* and then with a step size of 3 *mm* to end at 92 *mm*. Note the last four lines and change in sequence done manually to return the probes back to 100 *mm* (Hub end) and 500 *mm* (12 o'clock position).

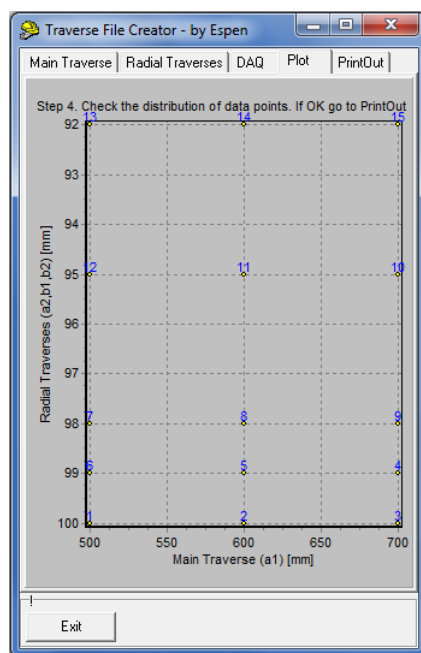


Fig. 78.: Example plot generated from *GenFile* program

Listing I.1: Example of Test script

```
a,2,100,0,0
b,1,100,0,0
b,2,100,0,0
a,1,500,100,2000
a,1,600,100,2000
a,1,700,100,2000
a,2,99,0,0
b,1,99,0,0
b,2,99,0,0
a,1,700,100,2000
a,1,600,100,2000
a,1,500,100,2000
a,2,98,0,0
b,1,98,0,0
b,2,98,0,0
a,1,500,100,2000
a,1,600,100,2000
a,1,700,100,2000
a,2,95,0,0
b,1,95,0,0
b,2,95,0,0
a,1,700,100,2000
a,1,600,100,2000
a,1,500,100,2000
a,2,92,0,0
b,1,92,0,0
b,2,92,0,0
a,1,500,100,2000
a,1,600,100,2000
a,1,700,100,2000
a,1,500,0,0
b,2,100,0,0
b,1,100,0,0
a,2,100,0,0
```


APPENDIX D

CONNECTION MAPS

Figures 79-83 show the connection maps for all the channels used for data acquisition.

Five-Hole Probes						
Station #	Hole #	Tubing #	Scanner #	Channel #	Pressure Rating of Transducer	Column # in RAW DATA File
Station-3	1	1	Scanner-3 (200.200.1.24)	1	2.5 PSI	38
	2	2		2	2.5 PSI	39
	3	3		3	2.5 PSI	40
	4	4		4	2.5 PSI	41
	5	5		5	2.5 PSI	42
Station-4	1	1	Scanner-4 (200.200.1.26)	1	5 PSI	54
	2	2		2	5 PSI	55
	3	3		3	5 PSI	56
	4	4		4	5 PSI	57
	5	5		5	5 PSI	58
Station-5	1	1	Scanner-4 (200.200.1.26)	6	5 PSI	59
	2	2		7	5 PSI	60
	3	3		9	5 PSI	62
	4	4		10	5 PSI	63
	5	5		11	5 PSI	64

Fig. 79.: Connection map for 5-hole Probes

Station-1						
Circumferential Position	Radial Position	Tubing #	Scanner #	Channel #	Pressure Rating of Transducer	Column # in RAW DATA File
@ 2:00	Hub	1	Scanner-1 (200.200.1.22)	2	10" WC	7
	Hub-Mid	2		4	10" WC	9
	Tip-Mid	3		6	10" WC	11
	Tip	4		8	10" WC	13
@ 4:00	Hub	1		10	10" WC	15
	Hub-Mid	2		12	10" WC	17
	Tip-Mid	3		14	10" WC	19
	Tip	4		16	10" WC	21
@ 8:00	Hub	1		9	10" WC	14
	Hub-Mid	2		11	10" WC	16
	Tip-Mid	3		13	10" WC	18
	Tip	4		15	10" WC	20
@ 10:00	Hub	1		1	10" WC	6
	Hub-Mid	2		3	10" WC	8
	Tip-Mid	3		5	10" WC	10
	Tip	4		7	10" WC	12

Station-7							
Circumferential Position	Radial Position	Tubing #	Scanner #	Channel #	Pressure Rating of Transducer	Column # in RAW DATA File	
@ 2:00	Hub	1	Scanner-5 (200.200.1.25)	2	5 PSI	71	
	Hub-Mid	2		4	5 PSI	73	
	Tip-Mid	3		6	5 PSI	75	
	Tip	4		8	5 PSI	77	
@ 4:00	Hub	1		9	5 PSI	78	
	Hub-Mid	2		11	5 PSI	80	
	Tip-Mid	3		13	5 PSI	82	
	Tip	4		15	5 PSI	84	
@ 8:00	Hub	1		10	5 PSI	79	
	Hub-Mid	2		12	5 PSI	81	
	Tip-Mid	3		14	5 PSI	83	
	Tip	4		16	5 PSI	85	
@ 10:00	Hub	1		Scanner-6 (200.200.1.27)	9	5 PSI	94
	Hub-Mid	2		Scanner-6 (200.200.1.27)	10	5 PSI	95
	Tip-Mid	3		Scanner-6 (200.200.1.27)	15	5 PSI	100
	Tip	4		Scanner-4 (200.200.1.26)	8	5 PSI	61

Fig. 80.: Connection map for Rakes (Total Pressure)

Station-1						
Circumferential Position	Radial Position	Tubing #	Scanner #	Channel #	Pressure Rating of Transducer	Column # in RAW DATA File
@ 12:30	-	1	Scanner-2 (200.200.1.57)	1	10" WC	22
@ 3:30	-	2		2	10" WC	23
@ 6:30	-	3		3	10" WC	24
@ 9:30	-	4		4	10" WC	25

Station-2						
Circumferential Position	Radial Position	Tubing #	Scanner #	Channel #	Pressure Rating of Transducer	Column # in RAW DATA File
@ 1:00	-	5	Scanner-2 (200.200.1.57)	9	10" WC	30
@ 4:00	-	6		10	10" WC	31
@ 7:00	-	7		11	10" WC	32
-	-	-	-	-	-	-

Station-6						
Circumferential Position	Radial Position	Tubing #	Scanner #	Channel #	Pressure Rating of Transducer	Column # in RAW DATA File
@ 2:00	-	9	Scanner-6 (200.200.1.27)	11	5 PSID	96
@ 5:00	-	10	Scanner-4 (200.200.1.26)	14	5 PSID	67
@ 8:00	-	11		15	5 PSID	68
@ 11:00	-	12		16	5 PSID	69

Station-7						
Circumferential Position	Radial Position	Tubing #	Scanner #	Channel #	Pressure Rating of Transducer	Column # in RAW DATA File
@ 2:30	-	13	Scanner-6 (200.200.1.27)	14	5 PSID	99
@ 5:30	-	14		16	5 PSID	101
@ 8:30	-	15	Scanner-4 (200.200.1.26)	13	5 PSID	66
@ 11:30	-	16	Scanner-6 (200.200.1.27)	12	5 PSID	97

Fig. 81.: Connection map for Casing-taps (Static Pressure)

Venturi - Inlet						
Circumferential Position	Radial Position	Tubing #	Scanner #	Channel #	Pressure Rating of Transducer	Column # in RAW DATA File
@ 10:30	-	6	Scanner-7 (200.200.1.58)	14	5 PSI	115
@ 4:30	-	8		12	5 PSI	113
@ 1:30	-	9		11	5 PSI	112
@ 7:30	-	7		15	5 PSI	116

Venturi - Throat						
Circumferential Position	Radial Position	Tubing #	Scanner #	Channel #	Pressure Rating of Transducer	Column # in RAW DATA File
@ 6:00	-	1	Scanner-7 (200.200.1.58)	5	5 PSI	106
@ 9:00	-	2		16	5 PSI	117
@ 3:00	-	3		7	5 PSI	108
@ 12:00	-	4		8	5 PSI	109

Fig. 82.: Connection map for Venturi

T-Rings					
Station #	Tubing #	Scanner #	Channel #	Pressure Rating of Transducer	Column # in RAW DATA File
Station-3	1	Scanner-3 (200.200.1.24)	13	2.5 PSI	50
Station-4	2	Scanner-3 (200.200.1.24)	14	2.5 PSI	51
Station-5	3	Scanner-6 (200.200.1.27)	13	5 PSI	98

Fig. 83.: Connection map for T-rings

APPENDIX E

MATLAB CODES

There are three MATLAB codes attached in this section and their description is as follows:

1. **Code to plot all channels with time history from raw data:** This code is named as *Plotrawdata_FINAL.m* and prompts the user to choose the raw data file and generates plots as shown in Fig. 84
2. **Code to plot and generate a text file for summary of averages from all channels:** Once *Summary_n_Graph_FINAL.m* code is run, the user gets a set of plots as shown in Fig. 85.
3. **Code to automatically acquire weather data for any date and time:** This code (*Gather_weather_conditions_FINAL.m*) is used to gather weather data for any city, on any date at any time. The code prompts the user to enter the desired details in a window (Fig. 86a) and generates text files along with a plot for quick reference (Fig. 86b).

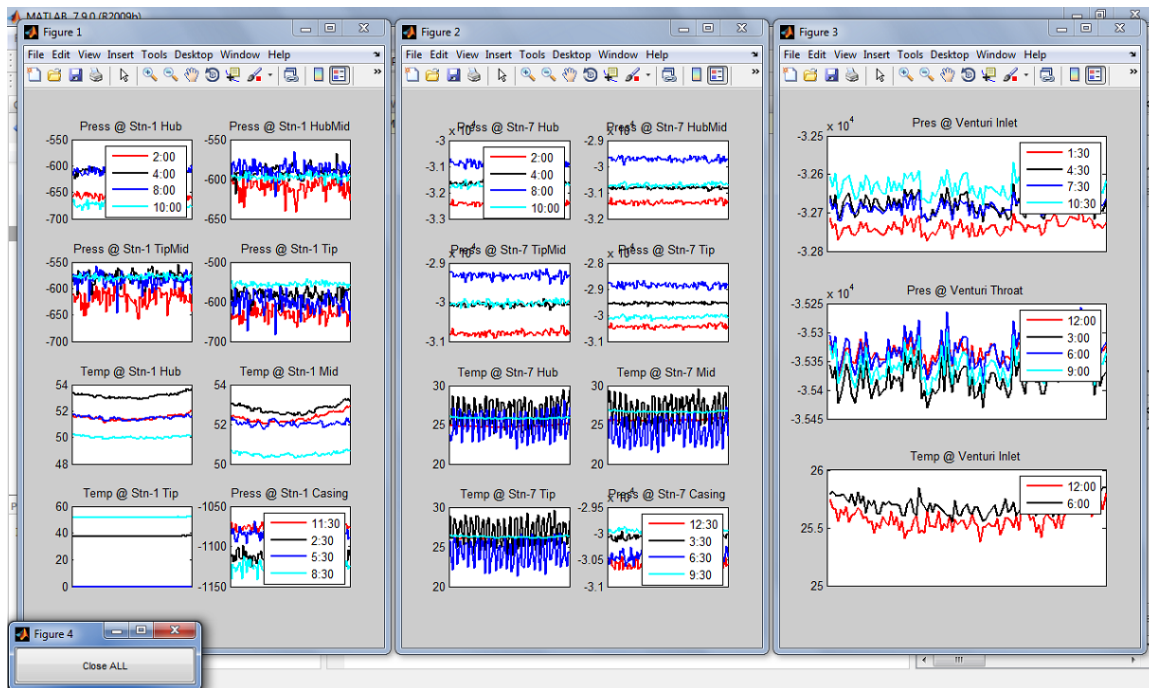


Fig. 84.: Plot of all channels from raw data with time history

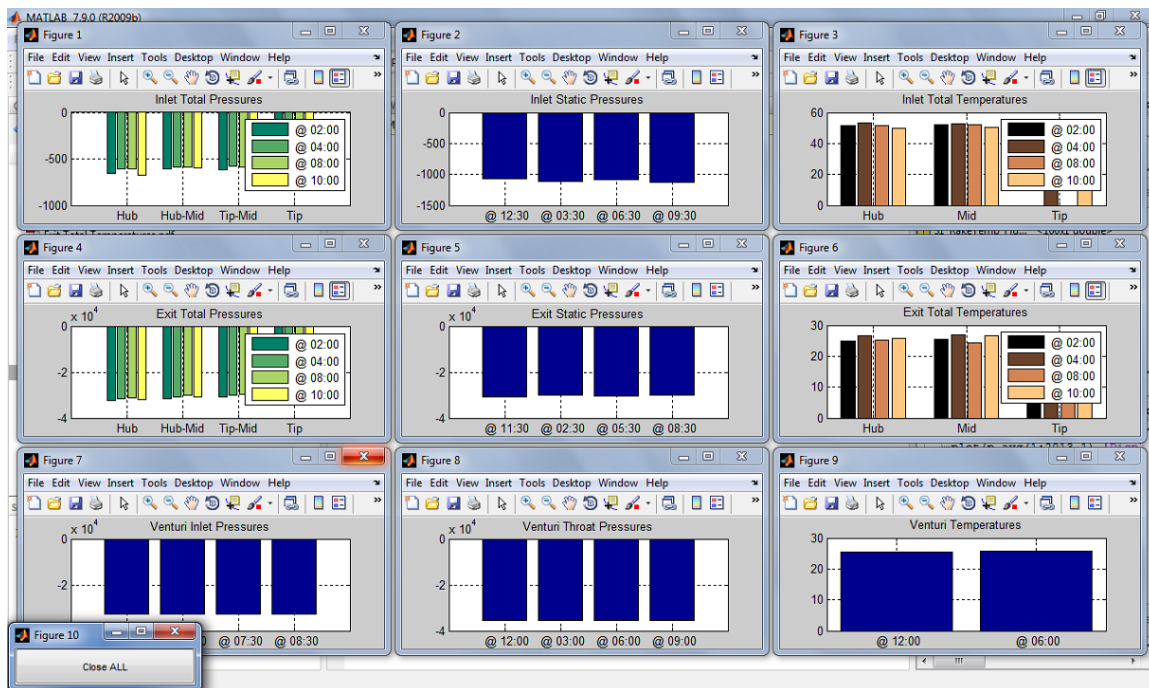


Fig. 85.: Plot showing averages of all channels from raw data

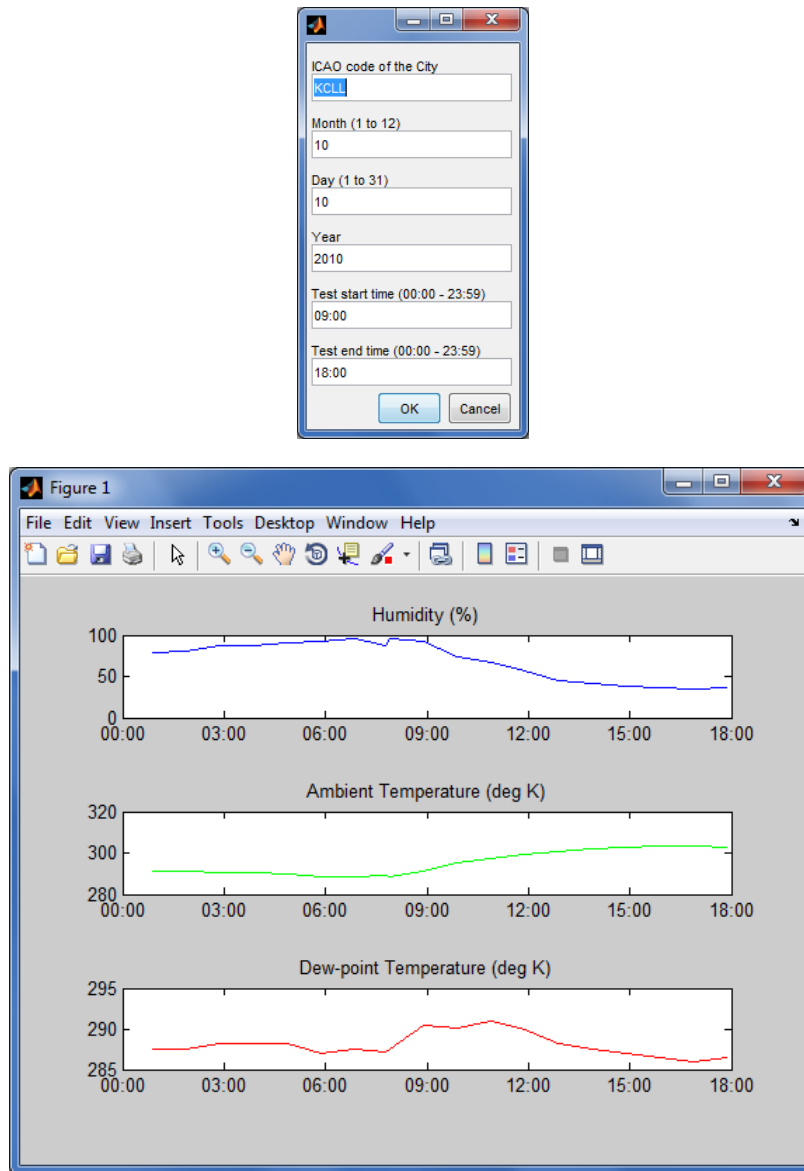


Fig. 86.: Input and output windows from Matlab code for weather data

Listing I.2: MATLAB code *Plotrawdata_FINAL.m*

```

1  %This code was written to provide a quick visual feedback
    to the user about the values of all the channels being
    acquired in the raw data file with a time history.
2  %
3  %REMEMBER: This code assumes that User has used same
    connection map as given along with this code in the
    THESIS Report.
4  %
5  %AUTHOR: Kapil Sharma
6
7  clc;
8  clear all;
9  [input_file,input_path] = uigetfile('*.dat','Select the
    Raw data-file from Turbo.vi');
10 fileToRead1=strcat(input_path,input_file);
11 importrawdata(fileToRead1);
12
13 %%%%%%%%%%%%%%%%%%%%%%%%%%%%%%%%%%%%%%%%%%% Inlet Total Pressures
14 S1_Rake_Hub_2=data(:,7);
15 S1_Rake_Hub_4=data(:,15);
16 S1_Rake_Hub_8=data(:,14);
17 S1_Rake_Hub_10=data(:,6);
18
19 S1_Rake_HubMid_2=data(:,9);
20 S1_Rake_HubMid_4=data(:,17);
21 S1_Rake_HubMid_8=data(:,16);
22 S1_Rake_HubMid_10=data(:,8);
23
24 S1_Rake_TipMid_2=data(:,11);
25 S1_Rake_TipMid_4=data(:,19);
26 S1_Rake_TipMid_8=data(:,18);
27 S1_Rake_TipMid_10=data(:,10);
28
29 S1_Rake_Tip_2=data(:,13);
30 S1_Rake_Tip_4=data(:,21);
31 S1_Rake_Tip_8=data(:,20);
32 S1_Rake_Tip_10=data(:,12);
33
34 %%%%%%%%%%%%%%%%%%%%%%%%%%%%%%%%%%%%%%%%%%% Inlet Static Pressures
35 S1_Casing_1230=data(:,22);
36 S1_Casing_330=data(:,23);
37 S1_Casing_630=data(:,24);
38 S1_Casing_930=data(:,25);
39
40 %%%%%%%%%%%%%%%%%%%%%%%%%%%%%%%%%%%%%%%%%%% Inlet Temperatures
41 S1_RakeTemp_Hub_2=data(:,151);
42 S1_RakeTemp_Hub_4=data(:,142);
43 S1_RakeTemp_Hub_8=data(:,145);
44 S1_RakeTemp_Hub_10=data(:,148);

```



```
45
46 S1_RakeTemp_Mid_2=data(:,152);
47 S1_RakeTemp_Mid_4=data(:,143);
48 S1_RakeTemp_Mid_8=data(:,146);
49 S1_RakeTemp_Mid_10=data(:,149);
50
51 S1_RakeTemp_Tip_2=data(:,153);
52 S1_RakeTemp_Tip_4=data(:,154);
53 S1_RakeTemp_Tip_8=data(:,147);
54 S1_RakeTemp_Tip_10=data(:,150);
55
56 %%%%%%%%%%%%%%%%%%%%%%%%%%%%%%%%%%%%%%%%%% Exit Total Pressures
57 S7_Rake_Hub_2=data(:,71);
58 S7_Rake_Hub_4=data(:,78);
59 S7_Rake_Hub_8=data(:,79);
60 S7_Rake_Hub_10=data(:,94);
61
62 S7_Rake_HubMid_2=data(:,73);
63 S7_Rake_HubMid_4=data(:,80);
64 S7_Rake_HubMid_8=data(:,81);
65 S7_Rake_HubMid_10=data(:,95);
66
67 S7_Rake_TipMid_2=data(:,75);
68 S7_Rake_TipMid_4=data(:,82);
69 S7_Rake_TipMid_8=data(:,83);
70 S7_Rake_TipMid_10=data(:,100);
71
72 S7_Rake_Tip_2=data(:,77);
73 S7_Rake_Tip_4=data(:,84);
74 S7_Rake_Tip_8=data(:,85);
75 S7_Rake_Tip_10=data(:,61);
76
77 %%%%%%%%%%%%%%%%%%%%%%%%%%%%%%%%%%%%%%%%%% Exit Static Pressures
78 S7_Casing_1130=data(:,97);
79 S7_Casing_230=data(:,99);
80 S7_Casing_530=data(:,101);
81 S7_Casing_830=data(:,66);
82
83 %%%%%%%%%%%%%%%%%%%%%%%%%%%%%%%%%%%%%%%%%% Exit Temperatures
84 S7_RakeTemp_Hub_2=data(:,139);
85 S7_RakeTemp_Hub_4=data(:,130);
86 S7_RakeTemp_Hub_8=data(:,133);
87 S7_RakeTemp_Hub_10=data(:,136);
88
89 S7_RakeTemp_Mid_2=data(:,140);
90 S7_RakeTemp_Mid_4=data(:,131);
91 S7_RakeTemp_Mid_8=data(:,134);
92 S7_RakeTemp_Mid_10=data(:,128);
93
94 S7_RakeTemp_Tip_2=data(:,141);
95 S7_RakeTemp_Tip_4=data(:,132);
```

```

96 S7_RakeTemp_Tip_8=data(:,129);
97 S7_RakeTemp_Tip_10=data(:,138);
98
99 %%%%%%%%%%%%%%%%%%%%%%%%%%%%%%%%%%%%%%%%%%% Venturi Inlet Pressures
100 Venturi_Inlet_130=data(:,112);
101 Venturi_Inlet_430=data(:,113);
102 Venturi_Inlet_730=data(:,116);
103 Venturi_Inlet_1030=data(:,115);
104
105 %%%%%%%%%%%%%%%%%%%%%%%%%%%%%%%%%%%%%%%%%%% Venturi Throat Pressures
106 Venturi_Throat_1200=data(:,109);
107 Venturi_Throat_300=data(:,108);
108 Venturi_Throat_600=data(:,106);
109 Venturi_Throat_900=data(:,117);
110
111 %%%%%%%%%%%%%%%%%%%%%%%%%%%%%%%%%%%%%%%%%%% Venturi Temperatures
112 Venturi_Temp_1200=data(:,158);
113 Venturi_Temp_600=data(:,157);
114
115 %%%%%%%%%%%%%%%%%%%%%%%%%%%%%%%%%%%%%%%%%%%
116 subplot(1,3,1);
117 %%%%%%%%%%%%%%%%%%%%%%%%%%%%%%%%%%%%%%%%%%%
118 subplot(4,2,1);
119 plot(S1_Rake_Hub_2,'r','LineWidth',2);
120 hold on
121 plot(S1_Rake_Hub_4,'k','LineWidth',2);
122 hold on
123 plot(S1_Rake_Hub_8,'b','LineWidth',2);
124 hold on
125 plot(S1_Rake_Hub_10,'c','LineWidth',2);
126 legend('2:00','4:00','8:00','10:00')
127 title('Press @ Stn-1 Hub')
128 set(gca,'XTick',[],'XTickLabel',[])
129 % set(gca,'YTick',[],'YTickLabel',[])
130
131 subplot(4,2,2);
132 plot(S1_Rake_HubMid_2,'r','LineWidth',2);
133 hold on
134 plot(S1_Rake_HubMid_4,'k','LineWidth',2);
135 hold on
136 plot(S1_Rake_HubMid_8,'b','LineWidth',2);
137 hold on
138 plot(S1_Rake_HubMid_10,'c','LineWidth',2);
139 title('Press @ Stn-1 HubMid')
140 set(gca,'XTick',[],'XTickLabel',[])
141 % set(gca,'YTick',[],'YTickLabel',[])
142
143 subplot(4,2,3);
144 plot(S1_Rake_TipMid_2,'r','LineWidth',2);
145 hold on
146 plot(S1_Rake_TipMid_4,'k','LineWidth',2);

```

```

147 hold on
148 plot(S1_Rake_TipMid_8,'b','LineWidth',2);
149 hold on
150 plot(S1_Rake_TipMid_10,'c','LineWidth',2);
151 title ('Press @ Stn-1 TipMid')
152 set(gca, 'XTick',[], 'XTickLabel',[])
153 % set(gca, 'YTick',[], 'YTickLabel',[])
154
155 subplot(4,2,4);
156 plot(S1_Rake_Tip_2,'r','LineWidth',2);
157 hold on
158 plot(S1_Rake_Tip_4,'k','LineWidth',2);
159 hold on
160 plot(S1_Rake_Tip_8,'b','LineWidth',2);
161 hold on
162 plot(S1_Rake_Tip_10,'c','LineWidth',2);
163 title ('Press @ Stn-1 Tip')
164 set(gca, 'XTick',[], 'XTickLabel',[])
165 % set(gca, 'YTick',[], 'YTickLabel',[])
166
167 subplot(4,2,5);
168 plot(S1_RakeTemp_Hub_2,'r','LineWidth',2);
169 hold on
170 plot(S1_RakeTemp_Hub_4,'k','LineWidth',2);
171 hold on
172 plot(S1_RakeTemp_Hub_8,'b','LineWidth',2);
173 hold on
174 plot(S1_RakeTemp_Hub_10,'c','LineWidth',2);
175 title ('Temp @ Stn-1 Hub')
176 set(gca, 'XTick',[], 'XTickLabel',[])
177 % set(gca, 'YTick',[], 'YTickLabel',[])
178
179 subplot(4,2,6);
180 plot(S1_RakeTemp_Mid_2,'r','LineWidth',2);
181 hold on
182 plot(S1_RakeTemp_Mid_4,'k','LineWidth',2);
183 hold on
184 plot(S1_RakeTemp_Mid_8,'b','LineWidth',2);
185 hold on
186 plot(S1_RakeTemp_Mid_10,'c','LineWidth',2);
187 title ('Temp @ Stn-1 Mid')
188 set(gca, 'XTick',[], 'XTickLabel',[])
189 % set(gca, 'YTick',[], 'YTickLabel',[])
190
191 subplot(4,2,7);
192 plot(S1_RakeTemp_Tip_2,'r','LineWidth',2);
193 hold on
194 plot(S1_RakeTemp_Tip_4,'k','LineWidth',2);
195 hold on
196 plot(S1_RakeTemp_Tip_8,'b','LineWidth',2);
197 hold on

```

```

198 plot(S1_RakeTemp_Tip_10,'c','LineWidth',2);
199 title ('Temp @ Stn-1 Tip')
200 set(gca, 'XTick',[], 'XTickLabel',[])
201 % set(gca, 'YTick',[], 'YTickLabel',[])
202
203 subplot(4,2,8);
204 plot(S1_Casing_1230,'r','LineWidth',2);
205 hold on
206 plot(S1_Casing_330,'k','LineWidth',2);
207 hold on
208 plot(S1_Casing_630,'b','LineWidth',2);
209 hold on
210 plot(S1_Casing_930,'c','LineWidth',2);
211 legend('11:30','2:30','5:30','8:30')
212 title ('Press @ Stn-1 Casing')
213 set(gca, 'XTick',[], 'XTickLabel',[])
214 % set(gca, 'YTick',[], 'YTickLabel',[])
215 %%%%%%%%%%%
216
217 %%%%%%%%%%%
218 subfigure(1,3,2);
219 %%%%%%%%%%%
220 subplot(4,2,1);
221 plot(S7_Rake_Hub_2,'r','LineWidth',2);
222 hold on
223 plot(S7_Rake_Hub_4,'k','LineWidth',2);
224 hold on
225 plot(S7_Rake_Hub_8,'b','LineWidth',2);
226 hold on
227 plot(S7_Rake_Hub_10,'c','LineWidth',2);
228 legend('2:00','4:00','8:00','10:00')
229 title ('Press @ Stn-7 Hub')
230 set(gca, 'XTick',[], 'XTickLabel',[])
231 % set(gca, 'YTick',[], 'YTickLabel',[])
232
233 subplot(4,2,2);
234 plot(S7_Rake_HubMid_2,'r','LineWidth',2);
235 hold on
236 plot(S7_Rake_HubMid_4,'k','LineWidth',2);
237 hold on
238 plot(S7_Rake_HubMid_8,'b','LineWidth',2);
239 hold on
240 plot(S7_Rake_HubMid_10,'c','LineWidth',2);
241 title ('Press @ Stn-7 HubMid')
242 set(gca, 'XTick',[], 'XTickLabel',[])
243 % set(gca, 'YTick',[], 'YTickLabel',[])
244
245 subplot(4,2,3);
246 plot(S7_Rake_TipMid_2,'r','LineWidth',2);
247 hold on
248 plot(S7_Rake_TipMid_4,'k','LineWidth',2);

```

```
249 hold on
250 plot(S7_Rake_TipMid_8,'b','LineWidth',2);
251 hold on
252 plot(S7_Rake_TipMid_10,'c','LineWidth',2);
253 title ('Press @ Stn-7 TipMid')
254 set(gca, 'XTick',[], 'XTickLabel',[])
255 % set(gca, 'YTick',[], 'YTickLabel',[])
256
257 subplot(4,2,4);
258 plot(S7_Rake_Tip_2,'r','LineWidth',2);
259 hold on
260 plot(S7_Rake_Tip_4,'k','LineWidth',2);
261 hold on
262 plot(S7_Rake_Tip_8,'b','LineWidth',2);
263 hold on
264 plot(S7_Rake_Tip_10,'c','LineWidth',2);
265 title ('Press @ Stn-7 Tip')
266 set(gca, 'XTick',[], 'XTickLabel',[])
267 % set(gca, 'YTick',[], 'YTickLabel',[])
268
269 subplot(4,2,5);
270 plot(S7_RakeTemp_Hub_2,'r','LineWidth',2);
271 hold on
272 plot(S7_RakeTemp_Hub_4,'k','LineWidth',2);
273 hold on
274 plot(S7_RakeTemp_Hub_8,'b','LineWidth',2);
275 hold on
276 plot(S7_RakeTemp_Hub_10,'c','LineWidth',2);
277 title ('Temp @ Stn-7 Hub')
278 set(gca, 'XTick',[], 'XTickLabel',[])
279 % set(gca, 'YTick',[], 'YTickLabel',[])
280
281 subplot(4,2,6);
282 plot(S7_RakeTemp_Mid_2,'r','LineWidth',2);
283 hold on
284 plot(S7_RakeTemp_Mid_4,'k','LineWidth',2);
285 hold on
286 plot(S7_RakeTemp_Mid_8,'b','LineWidth',2);
287 hold on
288 plot(S7_RakeTemp_Mid_10,'c','LineWidth',2);
289 title ('Temp @ Stn-7 Mid')
290 set(gca, 'XTick',[], 'XTickLabel',[])
291 % set(gca, 'YTick',[], 'YTickLabel',[])
292
293 subplot(4,2,7);
294 plot(S7_RakeTemp_Tip_2,'r','LineWidth',2);
295 hold on
296 plot(S7_RakeTemp_Tip_4,'k','LineWidth',2);
297 hold on
298 plot(S7_RakeTemp_Tip_8,'b','LineWidth',2);
299 hold on
```

```

300 plot(S7_RakeTemp_Tip_10,'c','LineWidth',2);
301 title ('Temp @ Stn-7 Tip')
302 set(gca, 'XTick',[], 'XTickLabel',[])
303 % set(gca, 'YTick',[], 'YTickLabel',[])
304
305 subplot(4,2,8);
306 plot(S7_Casing_1130,'r','LineWidth',2);
307 hold on
308 plot(S7_Casing_230,'k','LineWidth',2);
309 hold on
310 plot(S7_Casing_530,'b','LineWidth',2);
311 hold on
312 plot(S7_Casing_830,'c','LineWidth',2);
313 legend('12:30','3:30','6:30','9:30')
314 title ('Press @ Stn-7 Casing')
315 set(gca, 'XTick',[], 'XTickLabel',[])
316 % set(gca, 'YTick',[], 'YTickLabel',[])
317 %%%%%%%%%%%%%%%%%%%%%%%%%%%%%%%%%%%%%%%%%%%%%%%%%%%%%%%%%%%
318
319 %%%%%%%%%%%%%%%%%%%%%%%%%%%%%%%%%%%%%%%%%%%%%%%%%%%%%%%%%%%
320 subfigure(1,3,3);
321 %%%%%%%%%%%%%%%%%%%%%%%%%%%%%%%%%%%%%%%%%%%%%%%%%%%%%%%%%%%
322 subplot(3,1,1);
323 plot(Venturi_Inlet_130,'r','LineWidth',2);
324 hold on
325 plot(Venturi_Inlet_430,'k','LineWidth',2);
326 hold on
327 plot(Venturi_Inlet_730,'b','LineWidth',2);
328 hold on
329 plot(Venturi_Inlet_1030,'c','LineWidth',2);
330 legend('1:30','4:30','7:30','10:30')
331 title ('Pres @ Venturi Inlet')
332 set(gca, 'XTick',[], 'XTickLabel',[])
333 % set(gca, 'YTick',[], 'YTickLabel',[])
334
335 subplot(3,1,2);
336 plot(Venturi_Throat_1200,'r','LineWidth',2);
337 hold on
338 plot(Venturi_Throat_300,'k','LineWidth',2);
339 hold on
340 plot(Venturi_Throat_600,'b','LineWidth',2);
341 hold on
342 plot(Venturi_Throat_900,'c','LineWidth',2);
343 legend('12:00','3:00','6:00','9:00')
344 title ('Pres @ Venturi Throat')
345 set(gca, 'XTick',[], 'XTickLabel',[])
346 % set(gca, 'YTick',[], 'YTickLabel',[])
347
348 subplot(3,1,3);
349 plot(Venturi_Temp_1200,'r','LineWidth',2);
350 hold on

```

```
351 plot(Venturi_Temp_600, 'k', 'LineWidth', 2);
352 legend('12:00', '6:00')
353 title ('Temp @ Venturi Inlet')
354 set(gca, 'XTick', [], 'XTickLabel', [])
355 % set(gca, 'YTick', [], 'YTickLabel', [])
356 %%%%%%%%%%%%%%%%%%%%%%%%%%%%%%%%%%%%%%%%%%%%%%%%%%%%%%%%%%%
357
358 f = figure('MenuBar', 'none', 'Position', [10 50 200 40]);
359 h = uicontrol('Position', [1 2 200 40], 'String', 'Close
    ALL', 'Callback', 'uiresume(gcf)');
360 uiwait(gcf);
361 close all;
```

Listing I.3: MATLAB code *Summary_n_Graph_FINAL.m*

```

1  %This code was written to provide a quick visual feedback
    to the user about the average values of all the
    channels being acquired in the raw data file. The code
    also generates a text file of the summary of averages
    in the same directory where ths code is located.
2  %
3  %REMEMBER: This code assumes that User has used same
    connection map as given along with this code in the
    THESIS Report.
4  %
5  %AUTHOR: Kapil Sharma
6
7  clc;
8  clear all;
9  [input_file,input_path] = uigetfile('*.dat','Select the
    Raw data-file from Turbo.vi');
10 fileToRead1=strcat(input_path,input_file);
11 importrawdata(fileToRead1);
12
13 % Inlet Total Pressures
14 S1_Rake_Hub_2=data(:,7);
15 S1_Rake_Hub_4=data(:,15);
16 S1_Rake_Hub_8=data(:,14);
17 S1_Rake_Hub_10=data(:,6);
18 Avg_S1_Rake_Hub_2=mean(S1_Rake_Hub_2);
19 Avg_S1_Rake_Hub_4=mean(S1_Rake_Hub_4);
20 Avg_S1_Rake_Hub_8=mean(S1_Rake_Hub_8);
21 Avg_S1_Rake_Hub_10=mean(S1_Rake_Hub_10);
22
23 S1_Rake_HubMid_2=data(:,9);
24 S1_Rake_HubMid_4=data(:,17);
25 S1_Rake_HubMid_8=data(:,16);
26 S1_Rake_HubMid_10=data(:,8);
27 Avg_S1_Rake_HubMid_2=mean(S1_Rake_HubMid_2);
28 Avg_S1_Rake_HubMid_4=mean(S1_Rake_HubMid_4);
29 Avg_S1_Rake_HubMid_8=mean(S1_Rake_HubMid_8);
30 Avg_S1_Rake_HubMid_10=mean(S1_Rake_HubMid_10);
31
32 S1_Rake_TipMid_2=data(:,11);
33 S1_Rake_TipMid_4=data(:,19);
34 S1_Rake_TipMid_8=data(:,18);
35 S1_Rake_TipMid_10=data(:,10);
36 Avg_S1_Rake_TipMid_2=mean(S1_Rake_TipMid_2);
37 Avg_S1_Rake_TipMid_4=mean(S1_Rake_TipMid_4);
38 Avg_S1_Rake_TipMid_8=mean(S1_Rake_TipMid_8);
39 Avg_S1_Rake_TipMid_10=mean(S1_Rake_TipMid_10);
40
41 S1_Rake_Tip_2=data(:,13);
42 S1_Rake_Tip_4=data(:,21);

```



```

43 S1_Rake_Tip_8=data(:,20);
44 S1_Rake_Tip_10=data(:,12);
45 Avg_S1_Rake_Tip_2=mean(S1_Rake_Tip_2);
46 Avg_S1_Rake_Tip_4=mean(S1_Rake_Tip_4);
47 Avg_S1_Rake_Tip_8=mean(S1_Rake_Tip_8);
48 Avg_S1_Rake_Tip_10=mean(S1_Rake_Tip_10);
49
50 subfigure(3,3,1);
51 Inlet_Rake=[Avg_S1_Rake_Hub_2 Avg_S1_Rake_Hub_4
    Avg_S1_Rake_Hub_8 Avg_S1_Rake_Hub_10;
    Avg_S1_Rake_HubMid_2 Avg_S1_Rake_HubMid_4
    Avg_S1_Rake_HubMid_8 Avg_S1_Rake_HubMid_10;
    Avg_S1_Rake_TipMid_2 Avg_S1_Rake_TipMid_4
    Avg_S1_Rake_TipMid_8 Avg_S1_Rake_TipMid_10;
    Avg_S1_Rake_Tip_2 Avg_S1_Rake_Tip_4 Avg_S1_Rake_Tip_8
    Avg_S1_Rake_Tip_10];
52 bar(Inlet_Rake);
53 colormap(summer)
54 title('Inlet Total Pressures')
55 set(gca,'XTickLabel',{' Hub ' ;'Hub-Mid';'Tip-Mid';
    Tip '})
56 legend('@ 02:00', '@ 04:00', '@ 08:00', '@ 10:00')
57 grid on
58
59 % Inlet Static Pressures
60 S1_Casing_1230=data(:,22);
61 S1_Casing_330=data(:,23);
62 S1_Casing_630=data(:,24);
63 S1_Casing_930=data(:,25);
64 Avg_S1_Casing_1230=mean(S1_Casing_1230);
65 Avg_S1_Casing_330=mean(S1_Casing_330);
66 Avg_S1_Casing_630=mean(S1_Casing_630);
67 Avg_S1_Casing_930=mean(S1_Casing_930);
68
69 subfigure(3,3,2);
70 Inlet_Casing=[Avg_S1_Casing_1230 Avg_S1_Casing_330
    Avg_S1_Casing_630 Avg_S1_Casing_930];
71 bar(Inlet_Casing);
72 title('Inlet Static Pressures')
73 set(gca,'XTickLabel',{' @ 12:30'; '@ 03:30'; '@ 06:30';
    @ 09:30'})
74 grid on
75
76 %Inlet Temperatures
77 S1_RakeTemp_Hub_2=data(:,151);
78 S1_RakeTemp_Hub_4=data(:,142);
79 S1_RakeTemp_Hub_8=data(:,145);
80 S1_RakeTemp_Hub_10=data(:,148);
81 Avg_S1_RakeTemp_Hub_2=mean(S1_RakeTemp_Hub_2);
82 Avg_S1_RakeTemp_Hub_4=mean(S1_RakeTemp_Hub_4);
83 Avg_S1_RakeTemp_Hub_8=mean(S1_RakeTemp_Hub_8);

```

```

84 Avg_S1_RakeTemp_Hub_10=mean(S1_RakeTemp_Hub_10);
85
86 S1_RakeTemp_Mid_2=data(:,152);
87 S1_RakeTemp_Mid_4=data(:,143);
88 S1_RakeTemp_Mid_8=data(:,146);
89 S1_RakeTemp_Mid_10=data(:,149);
90 Avg_S1_RakeTemp_Mid_2=mean(S1_RakeTemp_Mid_2);
91 Avg_S1_RakeTemp_Mid_4=mean(S1_RakeTemp_Mid_4);
92 Avg_S1_RakeTemp_Mid_8=mean(S1_RakeTemp_Mid_8);
93 Avg_S1_RakeTemp_Mid_10=mean(S1_RakeTemp_Mid_10);
94
95 S1_RakeTemp_Tip_2=data(:,153);
96 S1_RakeTemp_Tip_4=data(:,154);
97 S1_RakeTemp_Tip_8=data(:,147);
98 S1_RakeTemp_Tip_10=data(:,150);
99 Avg_S1_RakeTemp_Tip_2=mean(S1_RakeTemp_Tip_2);
100 Avg_S1_RakeTemp_Tip_4=mean(S1_RakeTemp_Tip_4);
101 Avg_S1_RakeTemp_Tip_8=mean(S1_RakeTemp_Tip_8);
102 Avg_S1_RakeTemp_Tip_10=mean(S1_RakeTemp_Tip_10);
103
104 subfigure(3,3,3);
105 Inlet_RakeTemp=[Avg_S1_RakeTemp_Hub_2
    Avg_S1_RakeTemp_Hub_4 Avg_S1_RakeTemp_Hub_8
    Avg_S1_RakeTemp_Hub_10;Avg_S1_RakeTemp_Mid_2
    Avg_S1_RakeTemp_Mid_4 Avg_S1_RakeTemp_Mid_8
    Avg_S1_RakeTemp_Mid_10;Avg_S1_RakeTemp_Tip_2
    Avg_S1_RakeTemp_Tip_4 Avg_S1_RakeTemp_Tip_8
    Avg_S1_RakeTemp_Tip_10];
106 bar(Inlet_RakeTemp);
107 colormap(copper)
108 title('Inlet Total Temperatures')
109 set(gca,'XTickLabel',[' Hub ',' Mid ',' Tip '])
110 legend('@ 02:00', '@ 04:00', '@ 08:00', '@ 10:00')
111 grid on
112
113 % Exit Total Pressures
114 S7_Rake_Hub_2=data(:,71);
115 S7_Rake_Hub_4=data(:,78);
116 S7_Rake_Hub_8=data(:,79);
117 S7_Rake_Hub_10=data(:,94);
118 Avg_S7_Rake_Hub_2=mean(S7_Rake_Hub_2);
119 Avg_S7_Rake_Hub_4=mean(S7_Rake_Hub_4);
120 Avg_S7_Rake_Hub_8=mean(S7_Rake_Hub_8);
121 Avg_S7_Rake_Hub_10=mean(S7_Rake_Hub_10);
122
123 S7_Rake_HubMid_2=data(:,73);
124 S7_Rake_HubMid_4=data(:,80);
125 S7_Rake_HubMid_8=data(:,81);
126 S7_Rake_HubMid_10=data(:,95);
127 Avg_S7_Rake_HubMid_2=mean(S7_Rake_HubMid_2);
128 Avg_S7_Rake_HubMid_4=mean(S7_Rake_HubMid_4);

```

```

129 Avg_S7_Rake_HubMid_8=mean(S7_Rake_HubMid_8);
130 Avg_S7_Rake_HubMid_10=mean(S7_Rake_HubMid_10);
131
132 S7_Rake_TipMid_2=data(:,75);
133 S7_Rake_TipMid_4=data(:,82);
134 S7_Rake_TipMid_8=data(:,83);
135 S7_Rake_TipMid_10=data(:,100);
136 Avg_S7_Rake_TipMid_2=mean(S7_Rake_TipMid_2);
137 Avg_S7_Rake_TipMid_4=mean(S7_Rake_TipMid_4);
138 Avg_S7_Rake_TipMid_8=mean(S7_Rake_TipMid_8);
139 Avg_S7_Rake_TipMid_10=mean(S7_Rake_TipMid_10);
140
141 S7_Rake_Tip_2=data(:,77);
142 S7_Rake_Tip_4=data(:,84);
143 S7_Rake_Tip_8=data(:,85);
144 S7_Rake_Tip_10=data(:,61);
145 Avg_S7_Rake_Tip_2=mean(S7_Rake_Tip_2);
146 Avg_S7_Rake_Tip_4=mean(S7_Rake_Tip_4);
147 Avg_S7_Rake_Tip_8=mean(S7_Rake_Tip_8);
148 Avg_S7_Rake_Tip_10=mean(S7_Rake_Tip_10);
149
150 subfigure(3,3,4);
151 Exit_Rake=[Avg_S7_Rake_Hub_2 Avg_S7_Rake_Hub_4
            Avg_S7_Rake_Hub_8 Avg_S7_Rake_Hub_10;
            Avg_S7_Rake_HubMid_2 Avg_S7_Rake_HubMid_4
            Avg_S7_Rake_HubMid_8 Avg_S7_Rake_HubMid_10;
            Avg_S7_Rake_TipMid_2 Avg_S7_Rake_TipMid_4
            Avg_S7_Rake_TipMid_8 Avg_S7_Rake_TipMid_10;
            Avg_S7_Rake_Tip_2 Avg_S7_Rake_Tip_4 Avg_S7_Rake_Tip_8
            Avg_S7_Rake_Tip_10];
152 bar(Exit_Rake);
153 colormap(summer)
154 title('Exit Total Pressures')
155 set(gca,'XTickLabel',{' Hub ' ;'Hub-Mid';'Tip-Mid';'
    Tip '})
156 legend('@ 02:00', '@ 04:00', '@ 08:00', '@ 10:00')
157 grid on
158
159 % Exit Static Pressures
160 S7_Casing_1130=data(:,97);
161 S7_Casing_230=data(:,99);
162 S7_Casing_530=data(:,101);
163 S7_Casing_830=data(:,66);
164 Avg_S7_Casing_1130=mean(S7_Casing_1130);
165 Avg_S7_Casing_230=mean(S7_Casing_230);
166 Avg_S7_Casing_530=mean(S7_Casing_530);
167 Avg_S7_Casing_830=mean(S7_Casing_830);
168
169 subfigure(3,3,5);
170 Exit_Casing=[Avg_S7_Casing_1130 Avg_S7_Casing_230
              Avg_S7_Casing_530 Avg_S7_Casing_830];

```

```

171 bar(Exit_Casing);
172 title('Exit Static Pressures')
173 set(gca, 'XTickLabel', [' @ 11:30'; ' @ 02:30'; ' @ 05:30'; '
    @ 08:30'])
174 grid on
175
176 %Exit Temperatures
177 S7_RakeTemp_Hub_2=data(:,139);
178 S7_RakeTemp_Hub_4=data(:,130);
179 S7_RakeTemp_Hub_8=data(:,133);
180 S7_RakeTemp_Hub_10=data(:,136);
181 Avg_S7_RakeTemp_Hub_2=mean(S7_RakeTemp_Hub_2);
182 Avg_S7_RakeTemp_Hub_4=mean(S7_RakeTemp_Hub_4);
183 Avg_S7_RakeTemp_Hub_8=mean(S7_RakeTemp_Hub_8);
184 Avg_S7_RakeTemp_Hub_10=mean(S7_RakeTemp_Hub_10);
185
186 S7_RakeTemp_Mid_2=data(:,140);
187 S7_RakeTemp_Mid_4=data(:,131);
188 S7_RakeTemp_Mid_8=data(:,134);
189 S7_RakeTemp_Mid_10=data(:,128);
190 Avg_S7_RakeTemp_Mid_2=mean(S7_RakeTemp_Mid_2);
191 Avg_S7_RakeTemp_Mid_4=mean(S7_RakeTemp_Mid_4);
192 Avg_S7_RakeTemp_Mid_8=mean(S7_RakeTemp_Mid_8);
193 Avg_S7_RakeTemp_Mid_10=mean(S7_RakeTemp_Mid_10);
194
195 S7_RakeTemp_Tip_2=data(:,141);
196 S7_RakeTemp_Tip_4=data(:,132);
197 S7_RakeTemp_Tip_8=data(:,129);
198 S7_RakeTemp_Tip_10=data(:,138);
199 Avg_S7_RakeTemp_Tip_2=mean(S7_RakeTemp_Tip_2);
200 Avg_S7_RakeTemp_Tip_4=mean(S7_RakeTemp_Tip_4);
201 Avg_S7_RakeTemp_Tip_8=mean(S7_RakeTemp_Tip_8);
202 Avg_S7_RakeTemp_Tip_10=mean(S7_RakeTemp_Tip_10);
203
204 subfigure(3,3,6);
205 Exit_RakeTemp=[Avg_S7_RakeTemp_Hub_2
    Avg_S7_RakeTemp_Hub_4 Avg_S7_RakeTemp_Hub_8
    Avg_S7_RakeTemp_Hub_10;Avg_S7_RakeTemp_Mid_2
    Avg_S7_RakeTemp_Mid_4 Avg_S7_RakeTemp_Mid_8
    Avg_S7_RakeTemp_Mid_10;Avg_S7_RakeTemp_Tip_2
    Avg_S7_RakeTemp_Tip_4 Avg_S7_RakeTemp_Tip_8
    Avg_S7_RakeTemp_Tip_10];
206 bar(Exit_RakeTemp);
207 colormap(copper)
208 title('Exit Total Temperatures')
209 set(gca, 'XTickLabel', [' Hub '; ' Mid '; ' Tip '])
210 legend(' @ 02:00', ' @ 04:00', ' @ 08:00', ' @ 10:00')
211 grid on
212
213 %Venturi Inlet Pressures
214 Venturi_Inlet_130=data(:,112);

```

```

215 Venturi_Inlet_430=data(:,113);
216 Venturi_Inlet_730=data(:,116);
217 Venturi_Inlet_1030=data(:,115);
218 Avg_Venturi_Inlet_130=mean(Venturi_Inlet_130);
219 Avg_Venturi_Inlet_430=mean(Venturi_Inlet_430);
220 Avg_Venturi_Inlet_730=mean(Venturi_Inlet_730);
221 Avg_Venturi_Inlet_1030=mean(Venturi_Inlet_1030);
222
223 subfigure(3,3,7);
224 Venturi_Inlet=[Avg_Venturi_Inlet_130
                Avg_Venturi_Inlet_430 Avg_Venturi_Inlet_730
                Avg_Venturi_Inlet_1030];
225 bar(Venturi_Inlet);
226 title('Venturi Inlet Pressures')
227 set(gca,'XTickLabel',{' @ 01:30'; ' @ 04:30'; ' @ 07:30'; '
                @ 08:30'})
228 grid on
229
230 %Venturi Throat Pressures
231 Venturi_Throat_1200=data(:,109);
232 Venturi_Throat_300=data(:,108);
233 Venturi_Throat_600=data(:,106);
234 Venturi_Throat_900=data(:,117);
235 Avg_Venturi_Throat_1200=mean(Venturi_Throat_1200);
236 Avg_Venturi_Throat_300=mean(Venturi_Throat_300);
237 Avg_Venturi_Throat_600=mean(Venturi_Throat_600);
238 Avg_Venturi_Throat_900=mean(Venturi_Throat_900);
239
240 subfigure(3,3,8);
241 Venturi_Throat=[Avg_Venturi_Throat_1200
                 Avg_Venturi_Throat_300 Avg_Venturi_Throat_600
                 Avg_Venturi_Throat_900];
242 bar(Venturi_Throat);
243 title('Venturi Throat Pressures')
244 set(gca,'XTickLabel',{' @ 12:00'; ' @ 03:00'; ' @ 06:00'; '
                 @ 09:00'})
245 grid on
246
247 %Venturi Temperatures
248 Venturi_Temp_1200=data(:,158);
249 Venturi_Temp_600=data(:,157);
250 Avg_Venturi_Temp_1200=mean(Venturi_Temp_1200);
251 Avg_Venturi_Temp_600=mean(Venturi_Temp_600);
252
253 subfigure(3,3,9);
254 Venturi_Temp=[Avg_Venturi_Temp_1200 Avg_Venturi_Temp_600
                ];
255 bar(Venturi_Temp);
256 title('Venturi Temperatures')
257 set(gca,'XTickLabel',{' @ 12:00'; ' @ 06:00'})
258 grid on

```

```

259
260 % Uncomment following print commands to generate separate
      pdf files of
261 % the plots
262
263 % print -f1 -dpdf 'Inlet Total Pressures.pdf'
264 % print -f2 -dpdf 'Inlet Static Pressures.pdf'
265 % print -f3 -dpdf 'Inlet Total Temperatures.pdf'
266 % print -f4 -dpdf 'Exit Total Pressures.pdf'
267 % print -f5 -dpdf 'Exit Static Pressures.pdf'
268 % print -f6 -dpdf 'Exit Total Temperatures.pdf'
269 % print -f7 -dpdf 'Venturi Inlet Pressures.pdf'
270 % print -f8 -dpdf 'Venturi Throat Pressures.pdf'
271 % print -f9 -dpdf 'Venturi Temperatures.pdf'
272
273
274 f = figure('MenuBar','none','Position',[10 50 200 40]);
275 h = uicontrol('Position',[1 2 200 40], 'String','Close
      ALL','Callback','uiresume(gcf)');
276 uiwait(gcf);
277 close all;
278
279 str1=('Summary-');
280 y=length(input_file)-4;
281 str2=input_file(1:y);
282 str3=('.txt');
283 output_file=strcat(str1,str2,str3);
284 fid = fopen(output_file, 'w');
285 fprintf(fid, 'Average Inlet Total Pressure (Pascal) \n');
286 fprintf(fid, '\n Rake Hub @ 2:00      _____ %10.3f
      Column # 2', Avg_S1_Rake_Hub_2);
287 fprintf(fid, '\n Rake Hub @ 4:00      _____ %10.3f
      Column # 10', Avg_S1_Rake_Hub_4);
288 fprintf(fid, '\n Rake Hub @ 8:00      _____ %10.3f
      Column # 9', Avg_S1_Rake_Hub_8);
289 fprintf(fid, '\n Rake Hub @ 10:00     _____ %10.3f
      Column # 1', Avg_S1_Rake_Hub_10);
290 fprintf(fid, '\n');
291 fprintf(fid, '\n Rake Hub-Mid @ 2:00   _____ %10.3f
      Column # 4', Avg_S1_Rake_HubMid_2);
292 fprintf(fid, '\n Rake Hub-Mid @ 4:00   _____ %10.3f
      Column # 12', Avg_S1_Rake_HubMid_4);
293 fprintf(fid, '\n Rake Hub-Mid @ 8:00   _____ %10.3f
      Column # 11', Avg_S1_Rake_HubMid_8);
294 fprintf(fid, '\n Rake Hub-Mid @ 10:00  _____ %10.3f
      Column # 3', Avg_S1_Rake_HubMid_10);
295 fprintf(fid, '\n');
296 fprintf(fid, '\n Rake Tip-Mid @ 2:00   _____ %10.3f
      Column # 6', Avg_S1_Rake_TipMid_2);

```

```

297 fprintf(fid, '\n Rake Tip-Mid @ 4:00      _____ %10.3f
      Column # 14', Avg_S1_Rake_TipMid_4);
298 fprintf(fid, '\n Rake Tip-Mid @ 8:00      _____ %10.3f
      Column # 13', Avg_S1_Rake_TipMid_8);
299 fprintf(fid, '\n Rake Tip-Mid @ 10:00     _____ %10.3f
      Column # 5', Avg_S1_Rake_TipMid_10);
300 fprintf(fid, '\n');
301 fprintf(fid, '\n Rake Tip @ 2:00           _____ %10.3f
      Column # 8', Avg_S1_Rake_Tip_2);
302 fprintf(fid, '\n Rake Tip @ 4:00           _____ %10.3f
      Column # 16', Avg_S1_Rake_Tip_4);
303 fprintf(fid, '\n Rake Tip @ 8:00           _____ %10.3f
      Column # 15', Avg_S1_Rake_Tip_8);
304 fprintf(fid, '\n Rake Tip @ 10:00          _____ %10.3f
      Column # 7', Avg_S1_Rake_Tip_10);
305 fprintf(fid, '\n');
306 fprintf(fid, '
      %%%%%%%%%%%%%%%%%%%%%%%%%%%%%%%%%%%%%%%%%%%%%%%%%%%%%%%%%%\n');
307 fprintf(fid, '\n');
308
309 fprintf(fid, '\nAverage Inlet Static Pressure (Pascal) \n'
      );
310 fprintf(fid, '\n Tap @ 12:30             _____ %10.3f
      Column # 17', Avg_S1_Casing_1230);
311 fprintf(fid, '\n Tap @ 3:30             _____ %10.3f
      Column # 18', Avg_S1_Casing_330);
312 fprintf(fid, '\n Tap @ 6:30             _____ %10.3f
      Column # 19', Avg_S1_Casing_630);
313 fprintf(fid, '\n Tap @ 9:30             _____ %10.3f
      Column # 20', Avg_S1_Casing_930);
314 fprintf(fid, '\n');
315 fprintf(fid, '
      %%%%%%%%%%%%%%%%%%%%%%%%%%%%%%%%%%%%%%%%%%%%%%%%%%%%%%%%%%\n');
316 fprintf(fid, '\n');
317
318 fprintf(fid, '\nAverage Inlet Temperature (deg C) \n');
319 fprintf(fid, '\n Rake Hub @ 2:00         _____ %10.3f
      Column # 33', Avg_S1_RakeTemp_Hub_2);
320 fprintf(fid, '\n Rake Hub @ 4:00         _____ %10.3f
      Column # 24', Avg_S1_RakeTemp_Hub_4);
321 fprintf(fid, '\n Rake Hub @ 8:00         _____ %10.3f
      Column # 27', Avg_S1_RakeTemp_Hub_8);
322 fprintf(fid, '\n Rake Hub @ 10:00        _____ %10.3f
      Column # 30', Avg_S1_RakeTemp_Hub_10);
323 fprintf(fid, '\n');
324 fprintf(fid, '\n Rake Mid @ 2:00         _____ %10.3f
      Column # 34', Avg_S1_RakeTemp_Mid_2);
325 fprintf(fid, '\n Rake Mid @ 4:00         _____ %10.3f
      Column # 25', Avg_S1_RakeTemp_Mid_4);

```

```

326 fprintf(fid, '\n Rake Mid @ 8:00      _____ %10.3f
      Column # 28', Avg_S1_RakeTemp_Mid_8);
327 fprintf(fid, '\n Rake Mid @ 10:00     _____ %10.3f
      Column # 31', Avg_S1_RakeTemp_Mid_10);
328 fprintf(fid, '\n');
329 fprintf(fid, '\n Rake Tip @ 2:00      _____ %10.3f
      Column # 35', Avg_S1_RakeTemp_Tip_2);
330 fprintf(fid, '\n Rake Tip @ 4:00      _____ %10.3f
      Column # 36', Avg_S1_RakeTemp_Tip_4);
331 fprintf(fid, '\n Rake Tip @ 8:00      _____ %10.3f
      Column # 29', Avg_S1_RakeTemp_Tip_8);
332 fprintf(fid, '\n Rake Tip @ 10:00     _____ %10.3f
      Column # 32', Avg_S1_RakeTemp_Tip_10);
333 fprintf(fid, '\n');
334 fprintf(fid, '
      %%%%%%%%%%%%%%%%%%%%%%%%%%%%%%%%%%%%%%%%%%%%%%%%%%%%%%%%%%\n');
335 fprintf(fid, '\n');
336
337 fprintf(fid, '\nAverage Exit Total Pressure (Pascal) \n');
338 fprintf(fid, '\n Rake Hub @ 2:00      _____ %10.3f
      Column # 66', Avg_S7_Rake_Hub_2);
339 fprintf(fid, '\n Rake Hub @ 4:00      _____ %10.3f
      Column # 73', Avg_S7_Rake_Hub_4);
340 fprintf(fid, '\n Rake Hub @ 8:00      _____ %10.3f
      Column # 74', Avg_S7_Rake_Hub_8);
341 fprintf(fid, '\n Rake Hub @ 10:00     _____ %10.3f
      Column # 89', Avg_S7_Rake_Hub_10);
342 fprintf(fid, '\n');
343 fprintf(fid, '\n Rake Hub-Mid @ 2:00     _____ %10.3f
      Column # 68', Avg_S7_Rake_HubMid_2);
344 fprintf(fid, '\n Rake Hub-Mid @ 4:00     _____ %10.3f
      Column # 75', Avg_S7_Rake_HubMid_4);
345 fprintf(fid, '\n Rake Hub-Mid @ 8:00     _____ %10.3f
      Column # 76', Avg_S7_Rake_HubMid_8);
346 fprintf(fid, '\n Rake Hub-Mid @ 10:00    _____ %10.3f
      Column # 90', Avg_S7_Rake_HubMid_10);
347 fprintf(fid, '\n');
348 fprintf(fid, '\n Rake Tip-Mid @ 2:00     _____ %10.3f
      Column # 70', Avg_S7_Rake_TipMid_2);
349 fprintf(fid, '\n Rake Tip-Mid @ 4:00     _____ %10.3f
      Column # 77', Avg_S7_Rake_TipMid_4);
350 fprintf(fid, '\n Rake Tip-Mid @ 8:00     _____ %10.3f
      Column # 78', Avg_S7_Rake_TipMid_8);
351 fprintf(fid, '\n Rake Tip-Mid @ 10:00    _____ %10.3f
      Column # 95', Avg_S7_Rake_TipMid_10);
352 fprintf(fid, '\n');
353 fprintf(fid, '\n Rake Tip @ 2:00      _____ %10.3f
      Column # 72', Avg_S7_Rake_Tip_2);

```



```

354 fprintf(fid, '\n Rake Tip @ 4:00          _____ %10.3f
      Column # 79', Avg_S7_Rake_Tip_4);
355 fprintf(fid, '\n Rake Tip @ 8:00          _____ %10.3f
      Column # 80', Avg_S7_Rake_Tip_8);
356 fprintf(fid, '\n Rake Tip @ 10:00         _____ %10.3f
      Column # 56', Avg_S7_Rake_Tip_10);
357 fprintf(fid, '\n');
358 fprintf(fid, '
      %%%%%%%%%%%%%%%%%%%%%%%%%%%%%%%%%%%%%%%%%%%%%%%%%%%%%%%%%%\n');
359 fprintf(fid, '\n');
360
361 fprintf(fid, '\nAverage Exit Static Pressure (Pascal) \n')
      ;
362 fprintf(fid, '\n Tap @ 11:30             _____ %10.3f
      Column # 92', Avg_S7_Casing_1130);
363 fprintf(fid, '\n Tap @ 2:30              _____ %10.3f
      Column # 94', Avg_S7_Casing_230);
364 fprintf(fid, '\n Tap @ 5:30              _____ %10.3f
      Column # 96', Avg_S7_Casing_530);
365 fprintf(fid, '\n Tap @ 8:30              _____ %10.3f
      Column # 61', Avg_S7_Casing_830);
366 fprintf(fid, '\n');
367 fprintf(fid, '
      %%%%%%%%%%%%%%%%%%%%%%%%%%%%%%%%%%%%%%%%%%%%%%%%%%%%%%%%%%\n');
368 fprintf(fid, '\n');
369
370 fprintf(fid, '\nAverage Exit Temperature (deg C) \n');
371 fprintf(fid, '\n Rake Hub @ 2:00             _____ %10.3f
      Column # 21', Avg_S7_RakeTemp_Hub_2);
372 fprintf(fid, '\n Rake Hub @ 4:00             _____ %10.3f
      Column # 12', Avg_S7_RakeTemp_Hub_4);
373 fprintf(fid, '\n Rake Hub @ 8:00             _____ %10.3f
      Column # 15', Avg_S7_RakeTemp_Hub_8);
374 fprintf(fid, '\n Rake Hub @ 10:00            _____ %10.3f
      Column # 18', Avg_S7_RakeTemp_Hub_10);
375 fprintf(fid, '\n');
376 fprintf(fid, '\n Rake Mid @ 2:00             _____ %10.3f
      Column # 22', Avg_S7_RakeTemp_Mid_2);
377 fprintf(fid, '\n Rake Mid @ 4:00             _____ %10.3f
      Column # 13', Avg_S7_RakeTemp_Mid_4);
378 fprintf(fid, '\n Rake Mid @ 8:00             _____ %10.3f
      Column # 16', Avg_S7_RakeTemp_Mid_8);
379 fprintf(fid, '\n Rake Mid @ 10:00            _____ %10.3f
      Column # 10', Avg_S7_RakeTemp_Mid_10);
380 fprintf(fid, '\n');
381 fprintf(fid, '\n Rake Tip @ 2:00             _____ %10.3f
      Column # 23', Avg_S7_RakeTemp_Tip_2);
382 fprintf(fid, '\n Rake Tip @ 4:00             _____ %10.3f
      Column # 14', Avg_S7_RakeTemp_Tip_4);

```

```

383 fprintf(fid, '\n Rake Tip @ 8:00      _____ %10.3f
      Column # 11', Avg_S7_RakeTemp_Tip_8);
384 fprintf(fid, '\n Rake Tip @ 10:00     _____ %10.3f
      Column # 20', Avg_S7_RakeTemp_Tip_10);
385 fprintf(fid, '\n');
386 fprintf(fid, '
      %%%%%%%%%%%%%%%%%%%%%%%%%%%%%%%%%%%%%%%%%%%%%%%%%%%%%%%%%%\n');
387 fprintf(fid, '\n');
388
389 fprintf(fid, '\nAverage Venturi Pressure (Pascal) \n');
390 fprintf(fid, '\n Venturi Inlet @ 1:30     _____ %10.3f
      Column # 107', Avg_Venturi_Inlet_130);
391 fprintf(fid, '\n Venturi Inlet @ 4:30     _____ %10.3f
      Column # 108', Avg_Venturi_Inlet_430);
392 fprintf(fid, '\n Venturi Inlet @ 7:30     _____ %10.3f
      Column # 111', Avg_Venturi_Inlet_730);
393 fprintf(fid, '\n Venturi Inlet @ 10:30    _____ %10.3f
      Column # 110', Avg_Venturi_Inlet_1030);
394 fprintf(fid, '\n');
395 fprintf(fid, '\n Venturi Throat @ 12:00----- %10.3f
      Column # 104', Avg_Venturi_Throat_1200);
396 fprintf(fid, '\n Venturi Throat @ 3:00      _____ %10.3f
      Column # 103', Avg_Venturi_Throat_300);
397 fprintf(fid, '\n Venturi Throat @ 6:00      _____ %10.3f
      Column # 101', Avg_Venturi_Throat_600);
398 fprintf(fid, '\n Venturi Throat @ 9:00      _____ %10.3f
      Column # 112', Avg_Venturi_Throat_900);
399 fprintf(fid, '\n');
400 fprintf(fid, '
      %%%%%%%%%%%%%%%%%%%%%%%%%%%%%%%%%%%%%%%%%%%%%%%%%%%%%%%%%%\n');
401 fprintf(fid, '\n');
402
403 fprintf(fid, '\nAverage Venturi Temperature (deg C) \n');
404 fprintf(fid, '\n Venturi Temp @ 12:00     _____ %10.3f
      Column # 40', Avg_Venturi_Temp_1200);
405 fprintf(fid, '\n Venturi Temp @ 6:00      _____ %10.3f
      Column # 39', Avg_Venturi_Temp_600);
406
407 fclose(fid);

```

Listing I.4: MATLAB code *Gather_weather_conditions_FINAL.m*

```

1  %This code was written to gather weather conditions for
    any date, time and city. The user just needs to enter
    the ICAO code for desired city and choose the date and
    time duration to get the output as graphs for quick
    visual reference and various text files as described
    below:
2  %
3  %1) H.txt: Contains two columns:
4  %           "Time"           "Humidity(%)"
5  %
6  %2) T_n_D.txt: This file gives:
7  %   "Time"  "Ambient Temperature(K)" "Dew Point
    Temperature(K)"
8  %
9  %3) tio.txt and weather.txt: This files are not of any
    use and can be deleted.
10 %
11 %AUTHOR: Kapil Sharma
12
13 clc;
14 clear all;
15
16 % Prompt for user input for City code along with day and
    month of the year
17 d=datevec(datetime(date));
18
19 prompt={'ICAO code of the City', 'Month (1 to 12)', 'Day
    (1 to 31)', 'Year', 'Test start time (00:00 - 23:59)',
    'Test end time (00:00 - 23:59)'};
20 defans={'KCLL', num2str(d(2)), num2str(d(3)), num2str(d
    (1)), '09:00', '18:00'};
21 fields = {'city_code', 'month', 'day', 'year', 'test_start'
    , 'test_end'};
22 options.Resize='on';
23 options.WindowStyle='normal';
24 options.Interpreter='tex';
25 info = inputdlg(prompt, '', 1, defans, 'on');
26 if ~isempty(info) %see if user hit cancel
27     info = cell2struct(info, fields);
28     city_code = info.city_code;
29     month = info.month;
30     day = info.day;
31     year = info.year;
32     test_start = info.test_start;
33     test_end = info.test_end;
34 end
35
36 % Create a String of the URL
37 str1=('http://www.wunderground.com/history/airport/');

```

```

38 str2=('/DailyHistory.html?req_city=NA&req_state=NA&
    req_statename=NA&format=20');
39 str3=('/');
40 str4=('0');
41 str5=(':');
42 url=strcat(str1,city_code,str3,year,str3,month,str3,day,
    str2);
43
44 % Access data from the Internet and write it to a file
    called "weather.txt"
45 urlwrite(url,'weather.txt');
46
47 % Read time, temperature, dew point and humidity from "
    weather.txt"
48 fid = fopen('weather.txt');
49 C = textscan(fid,'%s %f %f %d %*[\n]', 'Delimiter',' ',' '
    headerLines', 2);
50 fclose(fid);
51
52 time=C{1};
53 temp=(C{2}-32).*(5/9)+273.15;
54 dew=(C{3}-32).*(5/9)+273.15;
55 humidity=C{4};
56 rows=size(temp);
57
58 % Save time in a file called "tio.txt"
59 fid = fopen('tio.txt', 'w');
60 for ii=1:rows(1)-1,
61     fprintf( fid, '%s \n',time{ii});
62 end
63 fclose(fid);
64
65 % Separate time into 2 columns of hh:mm and AM/PM
66 fid = fopen('tio.txt');
67 dummy = textscan(fid,'%s %s', 'Delimiter',' ');
68 fclose(fid);
69
70 % Combine time into 1 column as a single string of hh:mm
    AM/PM
71 y=strcat(dummy{1},dummy{2});
72
73 % Convert the time into a vector of 6 columns and get hh
    and mm
74 k=datevec(y);
75 p=datevec(test_start);
76 q=datevec(test_end);
77 hh_start=num2str(p(4));
78 mm_start=p(5);
79 hh_end=num2str(q(4));
80 mm_end=q(5);

```

```

81 hh=cellstr(num2str(k(:,4)));
82 mm=cellstr(num2str(k(:,5)));
83
84 % Add Zero in front of minutes with single digits
85 if mm_start<10
86     u=num2str(mm_start);
87     mm_start=strcat(str4,u);
88 else
89     mm_start=num2str(mm_start);
90 end
91 if mm_end<10
92     u=num2str(mm_end);
93     mm_end=strcat(str4,u);
94 else
95     mm_end=num2str(mm_end);
96 end
97
98 t_start=strcat(hh_start,mm_start);
99 t_end=strcat(hh_end,mm_end);
100 a=str2num(t_start);
101 b=str2num(t_end);
102
103 for ii=1:rows(1)-1,
104     l=str2num(mm{ii});
105     if l<10
106         ll=num2str(l);
107         mm{ii}=strcat(str4,ll);
108     end
109 end
110
111 time_24_colon=strcat(hh,str5,mm);
112 time_24=strcat(hh,mm);
113
114 % Save 1. Time, Temperature and Dew point in "T.n.D.txt"
115 %     2. Time and Humidity in "H.txt"
116 fid1 = fopen('T.n.D.txt','w');
117 fid2 = fopen('H.txt','w');
118 for ii=1:rows(1)-1
119     c=str2num(time_24{ii});
120     if c>a && c<b
121         fprintf(fid1,'%s %10.2f %10.2f \n',time_24_colon
122             {ii}, temp(ii), dew(ii));
123         fprintf(fid2,'%s\t%10.2f\n',time_24{ii},
124             humidity(ii));
125     end
126 end
127 fclose(fid1);
128 fclose(fid2);

```

```
129 for ii=1:rows(1)-1,
130     z{ii}=strcat(year,month,day,'T',hh{ii},mm{ii},'00');
131     RH(ii)=humidity(ii);
132     T_C(ii)=temp(ii);
133     D_C(ii)=dew(ii);
134 end
135 zz=datetime(datevec(z,'yyyymmddTHHMMSS'));
136
137 subplot(3,1,1);
138 plot(zz,RH);
139 datetick('x','HH:MM');
140 title('Humidity (%)');
141
142 subplot(3,1,2);
143 plot(zz,T_C,'g');
144 datetick('x','HH:MM');
145 title('Ambient Temperature (deg K)');
146
147 subplot(3,1,3);
148 plot(zz,D_C,'r');
149 datetick('x','HH:MM');
150 title('Dew-point Temperature (deg K)');
```

APPENDIX F

INSTRUCTIONS FOR TURBINE START-UP

- Check the oil level indicators (Fig. 87) on both sides of compressor.



Fig. 87.: Oil level indicator for compressor

- The breaker for variable frequency controller is located outside of the test cell and must be switched “ON” now.
- Open the test-cell window.
- Start the cooling water for dynamometer with a pressure of 20 psi.
- Turn dynamometer “ON” from the main power supply box of *Froude Consine*(Fig. 88) located inside the test cell. Switch is on the side of the box.



Fig. 88.: Power supply box for dynamometer



Fig. 89.: Controller for dynamometer

- Press green colored “✓” button on the dynamometer controller (Fig. 89) to ensure dynamometer is engaged. Set desired rpm output as 600 rpm and lock the controller at this value.
- Use *SetZero* program from the desktop to zero all pressure transducers. The program icon looks as Fig. 90.
- Switch “ON” the variable frequency controller (Fig. 91) and set desired frequency output to 15 Hz before pressing the black “Start” button on this controller.

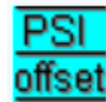


Fig. 90.: Icon for SetZero program



Fig. 91.: Variable frequency controller for compressor

- At this point, turbine rotor starts moving. Wait for sometime before taking down a log of all temperatures along with torque and power in the “Log Book”.
- Now, move to a frequency of 30 Hz by turning the knob on compressor controller in clockwise direction. The compressor frequency should be increased very slowly, a quick increase can lead to the grease getting sucked out of back bearing, resulting in a catastrophic failure.
- The engine speed can be taken up to 1200 rpm at this point of time. Don’t forget to lock the dynamometer controller every time a change to engine speed is made.
- Keep a check on venturi temperature and if it is close to the dew-point, turn “ON” heater (Fig. 92) and adjust desired temperature so as to have a margin of about $5^{\circ}C$ between venturi and dew point temperature.
- IMPORTANT: DO NOT TURN THE HEATER “ON” FOR COMPRESSOR FREQUENCY BELOW 30 Hz .
- From this point on, take a log at every step while increasing the compressor frequency (increments of 5 Hz) and engine speed (increments of 600 rpm) to desired values for start of actual test.



Fig. 92.: Heater controller

APPENDIX G

INSTRUCTIONS TO SHUTDOWN THE TURBINE

- Completely turn the knob of variable frequency controller counter-clockwise to set the reference output frequency to 0 *Hz*.
- IMMEDIATELY set the heater temperature to 0°C and then turn heater “OFF” before switching the handle for electrical breaker to “OFF” position.
- Wait for the compressor frequency to become 0 *Hz* and then switch the variable frequency controller “OFF”.
- Now, slowly and gradually set the engine speed to 200 *rpm* and then wait for the engine speed reach 0 *rpm* by itself.
- Switch “OFF” the main power supply box of the dynamometer.
- Close the test-cell window.
- Switch “OFF” the electrical breaker for compressor outside test-cell.
- Allow the dynamometer to cool down by waiting for 10 *mins.* before closing butterfly valve for water supply to dynamometer.

VITA

Name: Kapil Sharma

Address: Texas A&M University, Department of Mechanical Engineering,
3123 TAMU, College Station, TX 77843-3123

Email: kapil.s.aggie@gmail.com

Education: Bachelor of Engineering, Mechanical Engineering, May 2004
National Institute of Technology Karnataka, Surathkal, India

Master of Science, Mechanical Engineering, May 2011
Texas A&M University, College Station, TX